THESIS REPORT
Ph.D.

SYSTEMS
RESEARCH
CENTER

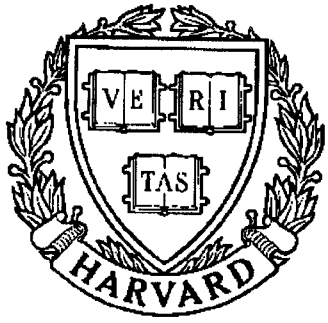

Supported by the National Science Foundation Engineering Research Center Program (NSFD CD 8803012), the University of Maryland, Harvard University, and Industry

Analysis of Surface Quality in Machining of Metals and Advanced Ceramics

by T-W. Hwang
Advisor: G.M. Zhang

Ph.D. 92-21

Abstract

Title of Dissertation: Analysis of Surface Quality in Machining of Metals and Advanced Ceramics

Tsu-Wei Hwang, Doctor of Philosophy, 1992

Dissertation directed by: Assistant Professor Guangming Zhang
Department of Mechanical Engineering &
Institute for Systems Research

Of all the processes used to shape metals, it is machining in which the conditions of operation are most varied. Good dimensional accuracy and surface quality from machining processes should be maintained such that the product's function and customer's satisfaction are assured. On the other hand, advanced ceramics have emerged as an important class of materials with uses in a variety of high performance applications such as aerospace, engines, and cutting tools. Many of these applications require the machining of ceramic component surfaces with tight dimensional accuracy and surface finish.

Among the many of possible causes which can tarnish the machined surface quality, the most important ones, such as tool vibration and elastoplastic deformation, are identified. This research is, therefore, focused on the analyses of these identified factors in order to have a better understanding of their roles

in the surface texture formation process during machining, which in turn can improve the efficiency and quality of machining processes.

The irregularities of a machined surface due to random tool vibration are investigated through a Markov-chain based stochastic approach. The dynamic characteristics of the metal cutting processes, especially the variation of material properties such as the microhardness, are modeled as a Markov-chain type random excitation source to introduce the random tool motion during machining.

An updated Lagrange method is applied for the analysis of elastoplastic deformation observed on machined surfaces. A three dimensional finite element model is built to simulate a single-point metal cutting process. The results of the analysis could be applied as a surface texture modification model to enhance the accuracy of the prediction of a machined surface texture.

By combining the aforementioned analytical work, a computer-based surface topography simulator, which can predict the surface topography formed under a given machining process, is developed. Experimental work is also performed to verify the results predicted by the simulator.

The study of machining of advanced ceramics (such as aluminum oxide and DICOR) is focused on the fundamental material removal mechanisms during machining. Based on the study, a cost-effective, chemical-assisted novel machining process is proposed to improve the surface quality.

Analysis of Surface Quality in Machining of Metals and Advanced Ceramics

by

Tsu-Wei Hwang

Dissertation submitted to the Faculty of the Graduate School
of the University of Maryland in partial fulfillment
of the requirements for the degree of
Doctor of Philosophy
1992

Advisory Committee:

Assistant Professor Guangming Zhang, Chairman/Advisor
Professor James Dally
Professor Andre Tits
Associate Professor William Walston
Professor Jackson Yang

Dedication

To my parents, my wife and my adorable son

Acknowledgements

I wish to express sincere appreciation to my dissertation advisor, Dr. Guangming Zhang. Without his encouragement, support and guidance, this work would never be possible. Special thanks are also given to all members of our research group for spending their time and energy in helping me with the experiments.

I gratefully appreciate the advice and comments provided by the members of my advisory committee, Drs. James Dally, Andre Tits, William Walston, and Jackson Yang. The help from Dr. Mohamed Abdelhamid is also acknowledged.

Most of all, I would like to express my deepest appreciation to the love and encouragement of my wife and parents.

Contents

List of Tables

List of Figures

Nomenclature

b_i: state transition probability from state $i+1$ to i

d_i: duration of occurrence at state i

d_{i_j}: j^{th} duration of occurrence at state i

dq: average slope (or rms slope) of a measured surface profile

$\boldsymbol{f}(d_i)$: discrete probability density function of d_i

f: feed rate

m: number of subdivisions in the cutting speed direction

n: number of subdivisions in the feed direction

number of teeth in a cutter

n_s: number of samples in one revolution

p_{g_j}: probability of j^{th} group distribution for assignment

p_{ij}: state transition probability from state i to state j

$[p]$: transition probability matrix

q_t: observed event at time t

r: cutter radius of an end mill

r_{kl}: state ratio within the k, l^{th} subdivision

$\overline{r}$: mean of the state ratios

t_r: tool nose radius

$y(x)$: deviations of a surface profile from mean line at location x

C_e: end cutting edge angle

C_s: side cutting edge angle

D: workpiece (feature) diameter

K_i: number of occurrences of state i

K_{obs}: total number of observations in a state map

K_s: unit cutting force

L: sampling length

M: equivalent mass of a machine tool strucutre

N: number of states

PTV: peak-to-valley value

Q: an observation sequence

R_a: roughness average value

R_q: root mean squared value

R_t: peak-to-valley value

S_i: the i^{th} state

S_m: peak spacing average

ϵ_{cr}: critical equivalent plastic strain

ϵ_i: initial state probability of state i

ϵ_p^{eq}: equivalent plastic strain

$\dot{\epsilon}$: total strain rate for elastoplastic deformation

$\dot{\epsilon}_e$: elastic part of the total strain rate

$\dot{\epsilon}_p$: plastic part of the total strain rate

μ_{g_j}: j^{th} group mean microhardness value

μ_i: mean microhardness value in the i^{th} cross-section

ν: overlapping factor

π_i: long-term fraction of state i observed in a state map

$\rho(r)$: correlation coefficient function

σ_M^{eq}: equivalent *von Mises* stress

σ_{g_j}: j^{th} group standard deviation of microhardness

σ_i: standard deviation of microhardness in the i^{th} cross-section

σ_r: standard deviation of the state ratios

σ_{PTV}: standard deviation of PTV

σ_{R_a}: standard deviation of R_a

σ_{R_q}: standard deviation of R_q

θ: cutting force angle

ξ: damping coefficient

Π: a matrix consisting of π_i's

Γ: a matrix consisting of $1 - p_{ii}$'s

Chapter 1

Introduction

1.1 Motivation and Background

The ever increasing competition in the marketplace is forcing the industries to seriously evaluate the design and manufacturing of their products. Surface quality and dimensional accuracy, which are the major concerns for machined components, should be well controlled such that the product's function as well as customers' satisfaction are assured.

Traditional quality control programs for manufacturing industry depend on the limitations of the machining processes involved as well as the arbitrary and discrete opinions of designer, operator, and inspector which, all too often, do not coincide. The resultant problems become apparently acute as the demand for a shortened product cycle time, reduced waste, and consistent, high level of quality has increased in the past decade to keep pace with the marketplace competition. This also has become more evident with the new advances in machining processes (such as cell type machine centers) and applications of new materials (such as advanced ceramic and metal matrix composite materials).

Unfortunately, there are few signs that the numbers of components machined or the money expended on machining are being reduced. Machining is still the cheapest way to make very many shapes and is likely to continue to be so for many years. The further evolution of the machining technology to higher standards of efficiency and accuracy is of great importance to industry generally.

Progress in the technology of machining is achieved by the ingenuity and experiment, the intuition, logical thought of many practitioners engaged in the arts of machining. People in the industry are all constantly probing to find answers to new problems created by the necessity to machine novel materials, to reduce costs, to increase rates of material removal, and to achieve greater precision or surface finish. However competent they can be, they would not feel that they can solve the problems if they had not had deeper knowledge of what was happening at the cutting edge of the tool.

The cutting process happens in a very small volume of material around the cutting edge that determines the performance of tools, the machinability of materials, and quality of the machined surfaces. During cutting, the interface between tool and work material is largely inaccessible to observation, but indirect evidence concerning tool vibration, tool wear, stresses, metal flow and temperatures between the said interface could be estimated through analytical or experimental methods.

In machining, surface roughness as well as size of the machined part must be brought within a desired tolerance. Even when a finishing process such as grinding, honing or lapping is applied later, the surface roughness due to machining should be as small as possible to save finishing time. From the tribological point of view, certain surface textures are more favorable than others.

To produce such surface textures it requires the knowledge of the tool-work interactions during machining.

Metal cutting process has been studied extensively for a long time. Due to the complexity of the process, it is extremely difficult to have a general model which can interpret the mechanism of what's going on between a cutting tool and the material being cut. The formation of a machined surface, as mostly observed from a single-point cutting process (such as turning), may at least be affected by three major causes [Shaw 84]:

1. The geometry of cutting tool and cutting parameter settings which forms the basic shape of a machined surface or the *nominal machined surface*,

2. Vibration or chattering of the machine tool caused by the dynamic cutting force variation during machining, which superposes the trace of tool tip vibratory motion on the nominal machined surface, and

3. The elastoplastic interactions between the tool-workpiece interface, which will not only deform the material but also keep residual stresses in the machined parts.

Results from previous research have revealed that the tool geometry and machining parameters are the main factors relating to the formation of the deterministic part of the surface texture. By providing precise spindle and feed mechanisms, the deterministic part of the tool path errors can be well controlled during machining. However, formation of the surface irregularities caused by random tool vibration and elastoplastic deformation have not been well understood.

A recent study indicated that the randomly distributed material properties, such as hardness, in the workpiece is one of the major sources which can cause

the random tool vibration during machining [Zh 86]. Interest has been stirred to establish a mapping function between the variability of standard material properties and the formation of surface irregularities through the evaluation of the random tool motion during machining. A quantitative evaluation of the stochastic portion of the tool path error still remains to be investigated.

The elastoplastic deformation process observed on the machined surface contributes to another portion of the surface irregularities. However, the basic mechanism of the elastoplastic process occurred on the tool-workpiece interface is not clearly understood yet because of the complex phenomena observed on the interface. The research in this area has drawn the most attention from those who have attempted analyses of machining. Their contributions have provided a foundation for the understanding of the basic mechanism of metal cutting processes. But problems still exist since most of the research works performed are only for orthogonal cutting processes, a simplified model which is not aimed at depicting the elastoplastic deformation process observed on the machined surface. As a result, further investigation of the elastoplastic deformation process based on a more realistic model is needed.

On the other hand, the use of advanced ceramics has increased as the mechanical components for high-performance application require superior material properties. Research has been done on several aspects [Br. 86, Bu. 74], such as new material development, property evaluation, the optimum design of components and strength reliability analysis, etc... In addition to these aspects, the importance of the machinability of ceramic materials has increased for economic and technological reasons, as pointed out by King et al [KiWh 66]. However, the high cost of machining due to the brittleness and hardness of ceramic materials

has been the major barrier to the widespread introduction of advanced structural ceramics. Therefore, the search for cost-effective machining processes is critical if the use of advanced ceramic materials for general engineering applications is expected to become popular.

1.2 Scope of the Study

The major concern of this research is to gain the knowledge for improving the surface quality of machined components. Efforts are directed toward the analysis of material removal mechanisms observed in the machining of metal and advanced ceramics. Topics such as the work material properties, elastic-plastic recovery and deformation processes, development of a computer-aided surface texture simulator and tribological interactions with emphasis on chemo-assisted machining of advanced ceramics are investigated. The results of the study should lead to a more accurate modeling of material removal mechanisms during machining processes.

Other than this chapter, there are six other chapters in this thesis. The contents of each chapter are summarized as follows:

- Chapter Two: Literature Review

  This chapter gives an overview for the relevant works in this research. Definitions of terms often used in the machining science are also provided for explaining the problems encountered in this field.

- Chapter Three: Stochastic Modeling for the Characterization of Random Tool Motion during Machining

This work presents the development of a new stochastic approach to characterize the random tool motion during machining. The complexity of the cutting mechanism is represented by a random excitation system related to the physical properties of the material being machined. A Markov-chain based stochastic approach is developed to model the random tool motion as the response of a machining system under the random excitation. In considering a turning operation, a concept of group distributions is introduced to characterize the global effect on the cutting force due to the variation of a certain material property. A model of segment excitation is used to describe its micro function within an individual revolution. A distribution pattern observed in the material property is represented by a transition model. The simulation of random tool motion during machining resembles the generation of Markov chains. Microstructure analysis and image process are used to collect data, calculate relevant statistics, and estimate the system parameters specified in the developed stochastic model.

- Chapter Four: Analysis of Elastoplastic Deformation Observed on the Machined Surfaces

  This work presents a non-linear quasi-static analysis of the elastoplastic interaction observed between a single-point cutting tool and the workpiece material being cut. An updated Lagrange method is applied to solve the large strain elastoplastic deformation problem using a three dimensional finite element model which could simulate a single-point metal cutting process. The effects of tool geometry and cutting parameter settings on

the elastoplastic deformation of machined surfaces are investigated through the analysis. The results of this analysis can be applied as a surface texture modification model to enhance the accuracy of a computer-aided surface texture generation system, an important part for the computer-integrated manufacturing.

- Chapter Five: Development of a Computer Simulator to Dynamically Visualize the Surface Texture Formed during Machining

  This work integrates the previous two research topics as well as the machine tool structure to dynamically simulate the surface texture formed during machining. A framework is presented to consolidate the model based material removal mechanisms during metal cutting. Case studies through both computer simulations and experiments are performed to verify the validity of the developed models, which form the framework of the simulator. Descriptions of experimental works are also presented to show how the microstructural analyses of work materials are performed, how the cutting forces are measured, and how the machined surfaces are characterized.

- Chapter Six: Study of the Material Removal Mechanisms in Machining of Advanced Ceramics

  Experimental study of the machining of advanced ceramic materials is presented in this work. The cutting force during machining is measured by a force transducer; and the surface finish is inspected by a profilometer. Scanning electron microscope (SEM) is used to study the mechanism of the surface formation in microscale. Special attention is paid to the investiga-

tion of chemo-mechanical effects of using different types of cutting fluids on those performance measures of interest. Results from this study provide rich information on the cutting mechanisms during the machining of advanced ceramic materials and the effect of tribological interactions occurred at the interface between the cutting tool and work material. Through the factorial design of experiments, the effects of cutting parameters on the finished surface quality can also be examined. Such information is very helpful for compiling a machinability database for the machining of advanced ceramic materials.

- Chapter Seven: Conclusions and Recommendations

  This chapter summarizes the dissertation and gives suggestions for future work in this research area.

Chapter 2

Literature Review

2.1 Introduction

This chapter provides a comprehensive survey of literature related to the surface finish in machining of metal and ceramic materials. Definitions of an engineering surface are presented in the next section. Each part is also divided into subsections to further explain the definitions of terms and models with advantages and disadvantages applied in the research of this field.

2.2 Surface Texture - Defining an Engineering Surface

In this section, the definitions of surface finish as well as the topics related to the surface finish are discussed. As a standard, turning is chosen as the machining process to clarify the discussion.

In designing an engineering component, it is important to specify the degree of surface quality desired on the component. The surfaces produced by machin-

ing and other methods of manufacturing are generally irregular and complex. Of practical importance are the geometric irregularities generated by the machining method. These are defined by height, spacing and direction, and other random characteristics not of a geometric nature. The general term employed to define these surface irregularities is called *Surface Texture* or *Surface Topography* which forms the pattern of the surface. A typical machined surface, such as the one shown in Fig. 2.1a, has a combination of roughness, waviness, lay and flaws. The roughness with its typical roughness height and roughness spacing represents the most closely spaced peaks and valleys. It is usually produced by the combination of the tool's geometry, feed rate and many other sources during cutting. The waviness results from such factors as deflections of the machine or work, chattering, or cutting tool runout. It consists of more widely spaced irregularities upon which the roughness is superimposed. Lay is a result of the production method used; it determines the direction of the predominant surface pattern. Surfaces produced by machining processes ordinarily have a strong lay pattern; that is, they are unidirectional. Flaws, on the other hand, are irregularities scattered at places without a predetermined pattern. They include cracks, scratches, holes, etc. The surface texture is usually assessed by taking a sampling length or trace at an angle perpendicular to the lay direction on the surface. The traces taken from a surface are also called *surface profiles.*

The most common measures of the primary surface texture are known as arithmetic average (AA or roughness average, R_a) and the root-mean-square roughness (R_q) [ANSI 85]. They describe the deviation of the surface roughness

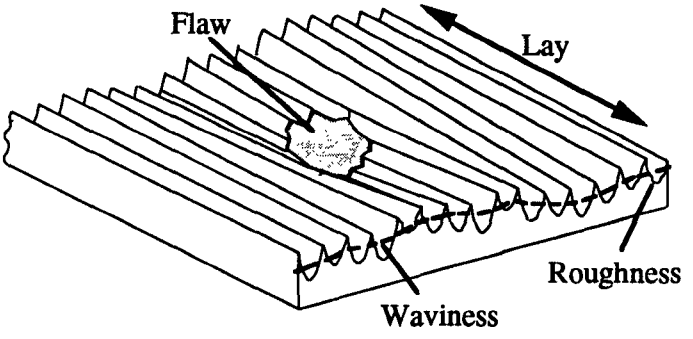

a. Surface Texture to Show Roughness, Waviness, Lay and Flaws

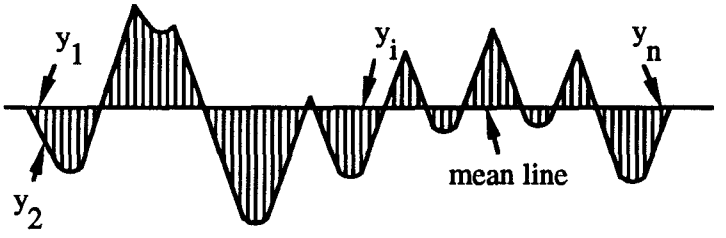

$$R_a \cong \frac{1}{n}\sum_{i=1}^{n} |y_i| \qquad R_q \cong \sqrt{\frac{1}{n}\sum_{i=1}^{n} y_i^2} \qquad dq \cong \sqrt{\frac{1}{n}\sum_{i=1}^{n}\left[\frac{|y_{i+1} - y_i|}{\Delta x}\right]^2}$$

b. Evaluation of Surface Roughness Average, Root Mean Squared Values and Averaged Slope

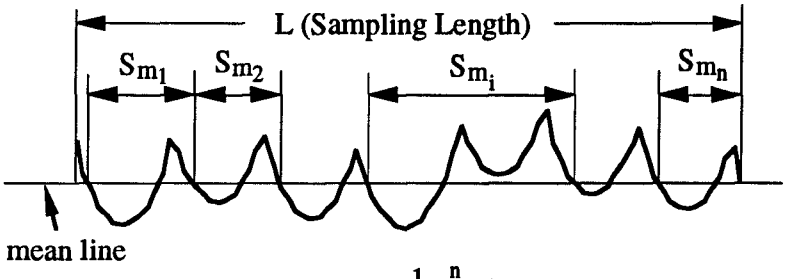

$$S_m = \frac{1}{n}\sum_{i=1}^{n} S_{m_i}$$

c. Evaluation of Peak Spacing

Figure 2.1: Defining an Engineering Surface

from a mean line or centerline and are defined by the following equations.

$$R_a = \frac{1}{L}\int_0^L |y(x)|\,dx \tag{2.1}$$

and

$$R_q = \left(\frac{1}{L}\int_0^L y^2(x)dx\right)^{\frac{1}{2}} \tag{2.2}$$

where L is the sampling length, and y's are the deviations from the mean line at locations along the x direction on which the trace was taken (see Fig. 2.1b). In general, the lower the R_a or R_q of a surface, the smoother the surface.

Other than R_a and R_q, there are a great variety of surface quality indices. Many of them have been developed to characterize the function of surfaces for particular applications [Bi 85]. In fact, more than 50 indices have been defined for industrial use and many of them appear in national standards as well. These indices may be classified into four categories: height indices, wavelength indices, hybrid indices, and statistical functions [Th 82].

- Height Indices: These are measures of the vertical characteristics of the surface deviations. R_a and R_q are typical indices in this category. Other indices like *Peak-to-Valley* (*PTV* or R_t), *Skewness* (R_{sk}) and *Kurtosis* (R_{ku}) are also common.

- Wavelength Indices: These are measures of the horizontal characteristics of the surface deviations. The spacings or wavelengths of the peaks and valleys of a surface are often characteristic of the process that formed the surface, such as the shot size for a blasted surface, the grit size of a grinding wheel or the feed of a tool. A typical wavelength index, recognized as stan-

dard by the International Organization for Standardization (ISO) [ISO 84], is the peak spacing, S_m. It is defined for a surface profile as the average spacing between two successive negative going crossings of the mean line (see Fig. 2.1c).

- Hybrid Indices: These are a combination of height and wavelength indices. Slope (dq) and curvature are two examples since they combine the concepts of height deviation and lateral displacement. The definition for dq is

$$dq = \sqrt{\frac{\sum_{i=1}^{N} [y_i'(x)]^2}{N}} \tag{2.3}$$

where $y_i'(x)$ is the derivative of the profile measured from the mean line at the i^{th} sample point along the x direction on which the trace was taken.

- Statistical Functions: More information of a surface profile may be obtained from statistical functions such as those used in connection with random process theory and time series analysis [Na 71, BePi 71]. Four important statistical functions are the amplitude density function (or height distribution), the bearing area curve, the autocorrelation function, and the power spectrum density. The definitions and applications of these functions are described in several works [BePi 71, Na 71, Th 82].

2.3 Composition of Surface Texture Formed in Metal Cutting

Based on the previous study of surface texture formed in metal cutting, a machined surface is generally formed due to the following sources [Mash 88, Sa 63, SeBa 77, Shaw 84]:

- the geometry of cutting tool and cutting parameter settings,
- built-up edge effect,
- vibration or chattering of the cutting tool structure,
- the elastoplastic deformation on the machined surface, and
- tool wear effect.

Each of these effects is discussed in the following sections.

2.3.1 Geometrical Effect on Surface Roughness

In a turning operation, the component of surface roughness due to tool nose geometry and cutting parameters, such as feed and depth of cut, may be readily calculated. Figure 2.2 shows a plan view of a conventional turning operation with *feed marks* left behind on the finished surface.

Figure 2.3 shows an enlarged view of the tool tip defined by three quantities:

- tool nose radius ($t_r = \overline{OT}$),
- end-cutting edge angle (C_e), and
- side-cutting edge angle or lead angle (C_s).

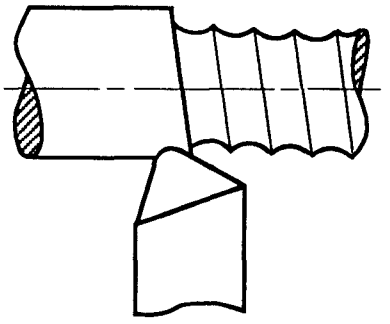

Figure 2.2: Plan View of a Conventional Turning Process with Feed Marks

If the tool nose radius is large compared with the feed, the surface will be generated by the nose radius alone (Case I in Fig. 2.3). Most of the finish machining operations fall into this case. From the geometry it is obvious that the ideal peak-to-valley value in this case is

$$R_t = \overline{OT} - \overline{OU} = t_r^2 - (t_r^2 - f^2/4)^{\frac{1}{2}} \cong \frac{f^2}{8t_r}, \text{ if } f < 2t_r \sin C_e. \qquad (2.4)$$

If the feed is larger than $2t_r \sin C_e$ (Case II in Fig. 2.3), the ideal peak-to-valley value will be [Sa 63]

$$R_t = t_r(1 - \cos C_e + F \cos C_e - \sin C_e \sqrt{2F - F^2}) \qquad (2.5)$$

where $F = f \sin C_e / t_r$.

Equation 2.4 shows that the ideal surface roughness decreases with a decrease in the feed rate or increase in the tool nose radius and is independent of the depth of cut and cutting speed. A real machined surface roughness produced by turning will usually exceed the ideal roughness due to other effects such as

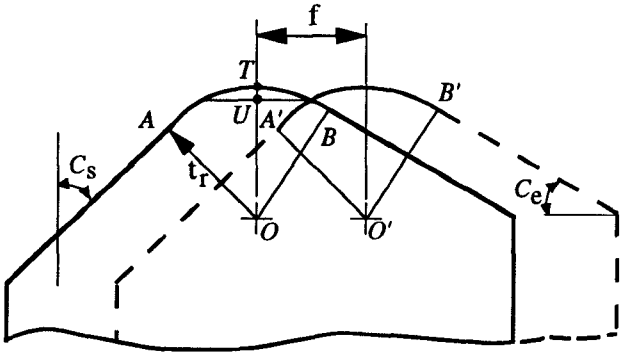

$$f < 2\,t_r \sin C_e$$

Case I: Two Noses Intersect

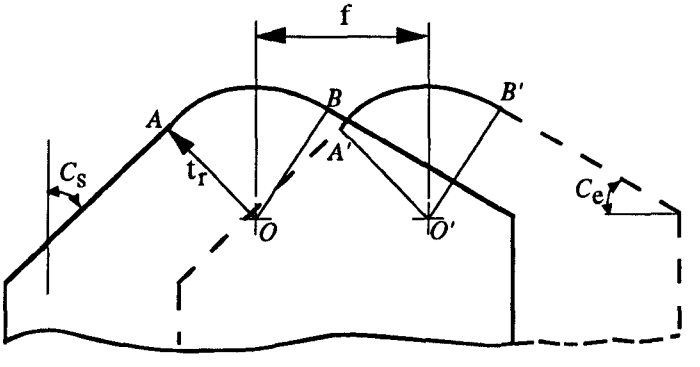

$$2\,t_r \sin C_e < f < t_r \left[\sin C_e + \cos C_s + (\cos C_e - \sin C_s)\cot C_e\right]$$

Case II: Tool Nose Intersects a Cutting Edge

Figure 2.3: Evaluation of the Theoretical Peak-to-Valley Value

built-up edge, tool vibration, elastoplastic deformation and tool wear. These effects will be discussed in the following sections.

Martellotti [Ma 41] has derived the following expression for the peak-to-valley value in a milling operation.

$$R_t = \frac{f^2}{8[r \pm (fn/\pi)]} \tag{2.6}$$

where f is the feed per tooth, r is the cutter radius, and n is the number of teeth in the cutter. The plus sign pertains to up-milling while the negative sign is for down-milling. This equation was found to be in good agreement with measured values by Martellotti if the run-out of the spindle was held to a very low value.

2.3.2 Effect of Built-Up Edge on Surface Finish

A built-up edge (BUE) forms on the tool face at a relative low cutting speed when cutting such common materials as steel and aluminum. There is no built-up edge at very low cutting speed (say $V = 0.3\ m/min$) since the temperature on the face of the chip is not sufficient to cause the chip surface to behave in a ductile manner. With an increase in cutting speed the chip metal in contact with the chip face becomes ductile and the resulting plastic flow on the chip face causes strain hardening and a further increase in the force tending to anchor the chip to the tool. When the bonding force between chip and tool exceeds the shear strength of the metal in the material body of the chip, at some particularly weak point near the tool face, the BUE forms. It causes poor surface finish.

The BUE causes an increase in the rake angle which in turn causes a decrease in the magnitude of the resultant force on the tool and a clockwise rotation of

the resultant force vector as shown in Fig. 2.4. As the BUE grows forward it will usually grow downward too, causing the surface to be undercut. When the BUE becomes large the resultant force loads the BUE as a cantilever and eventually the moment at the base of the BUE becomes sufficient to pry it loose. The BUE then passes off partly with the chip and partly on the finished surface. The growth and rapid breakage of the BUE cause a jagged surface on the machined part, which is the characteristic of the BUE component of surface roughness.

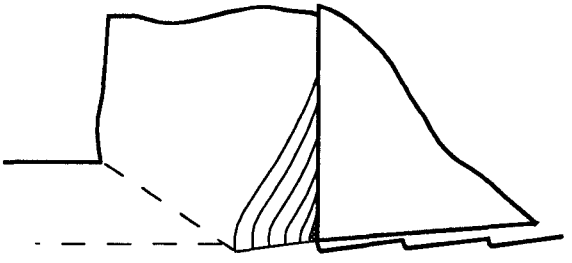

Figure 2.4: Formation of the Built-up Edge

Based on the observation from cutting tests, there is a *critical cutting speed* for disappearance of the built-up edge [NaIn 56]. Sata [Sa 63] summarized the critical cutting speed under various conditions:

1. The critical cutting speed remains unchanged with varying depth of cut except at very small depths of cut where the critical cutting speed is slightly larger.

2. The tool material has little effect on the critical cutting speed.

3. With an increase in the feed rate, the critical cutting speed is reduced.

4. With an increase in the rake angle of tool, the critical cutting speed is reduced.

5. When cutting several kinds of steel, a lower critical cutting speed is obtained for harder materials. In other words, brittle metals do not form BUE.

In general, the size of the built-up edge can be controlled by increasing the cutting speed to a value higher than the critical cutting speed, a common practice on the shop floor. Therefore, high cutting speed is chosen for all of the cutting tests in this research to reduce the effect of built-up edge on the assessment of machined surfaces.

2.3.3 Effect of Tool Vibration on Surface Finish

Tool motion during machining can be decomposed into two parts, kinematic and vibratory motions. The kinematic motion of the tool during machining is determined by the cutting parameter settings as discussed in Section 2.3.1. Tool vibration is caused by the generated cutting force, which excites the tool structure to vibrate during machining. It is obvious that tool vibration generates irregularities on a machined surface.

Study of tool vibration has been extensive, and mathematical models to analyze the dynamic response of machining operation are readily available [Me 65, Tl 78]. However, little work has been done to develop an approach which can link the surface texture generation and cutting dynamics together. Especially, the random vibrations of the cutting tool during machining have been observed and become a major difficulty in establishing the relationship between surface finish and cutting conditions [NaWu 77, PaRe 81, Sa 63]. Some authors suggested that the random distribution of crystal defects or non-unique slip-line field in the shear

zone might be the source of random excitation system during machining [De 79, PaRe 81]. Unfortunately, no mathematical models are reported to describe the random excitation system observed during machining.

Until recently, a study of random tool motion due to the variability of material properties, such as the hardness variation in the workpiece material to be cut, has shed the light on the research of quantitatively evaluating the random tool motion during machining. Zhang [Zh 86] introduced the concept of sample variance theory, which was originally developed by chemical scientists for characterizing chemical mixing [Dan 52, ScBr 74, Tu 81], to mathematically model the nonhomogeneity of material properties in the workpiece as a random excitation source during machining.

This approach states that the random force variation observed during machining is mainly originated from the nonhomogeneity of the micro-hardness distribution inside the material being cut. During machining, if a soft or hard spot comes into contact with the cutting tool, a sudden impulsive force is produced at the cutting tool tip. This impulsive force results in the vibration of tool and a change in the depth of cut, which in turn changes the cutting force. This fluctuation in the cutting force can either diminish with time or be capable of supplying energy to the system to sustain the vibration. It has been shown that if the machining process is stable, the nonhomogeneity of material property will essentially produce a random cutting force in the machining process [KwAl 68]. This random excitation source is treated as a normally distributed statistical model in terms of the material hardness. The mean hardness of this normal distribution model is the same as that of the population mean, which can be estimated by the samples taken from the workpiece material through standard

microstructural analysis. The variation level of the random excitation source, or the sample variance (σ_s^2), is then evaluated by employing the sample variance theory [ZhKa 90], which is closely related to the cutting parameter settings (feed, depth of cut and cutting speed).

Based on the approach, it is found that:

1. The smaller the feed, the higher the variation level of the random excitation source which drives the tool during machining.

2. The smaller the feed, the weaker the basic pattern of the roughness profile. Therefore, the theoretical prediction of any surface quality indices (R_a, R_t), which are only based on the geometric shape of the tool and feed, will become meaningless.

The most significant contribution of this work is that it provides a quantitative evaluation method to study and control the stochastic portion of tool vibration as well as the surface roughness.

The derivation of the variance of the random excitation source depends on the correlation coefficient function and the sample geometrical shape function. The correlation coefficient function is evaluated based on an assumption that all the microhardness distribution along the longitudinal direction is identical on each cross-section of the workpiece material. This assumption would be acceptable if statistically there is no significant difference in the size and shape of the microstructures between the cross-sectional areas along the longitudinal direction. However, this assumption sometimes may not be valid when certain materials do have a different microstructure distribution from one cross-section to another along the longitudinal direction, such as those usually found in rolled bar stocks.

2.3.4 Elastoplastic Interaction on the Tool-Workpiece Interface

It is perceived that contact deformation of the workpiece and tool material, both elastic and plastic, develops during machining (Fig. 2.5). The deformations of the material being cut in the zone of contact with the cutting edge depend on the machining conditions (feed, depth of cut, speed), tool geometry and workpiece material properties [Mash 88, Sa 63]. Although the influence of the elastoplastic deformation on surface finish is not so important for medium cutting conditions (e.g., feed rate of 0.2 mm/rev), it cannot be ignored in the case of finish or precision turning. However, the basic mechanism of the elastoplastic process occurred on the tool-workpiece interface is not clearly understood yet because of the complex phenomena involved in metal cutting.

Studies of recrystallization show that plastic deformation occuring below the newly machined surface is strongly dependent on the cutting tool rake angle [BlRa 70]. Studies on two-phase alloys containing hard second phase particles (typical of high strength alloys) show that micro-void formation must occur severely in plastic deformation due to the punching out of prismatic dislocation loops at the particle-matrix interface [Bur 67]. However, the influence of mechanical properties of work material on the elastoplastic deformation have not been identified.

It may be observed from many tests that work hardened material and brittle material sustain little elastoplastic deformation on the surface finish after machining [Sa 63]. It is also interesting to find that increasing the cutting speed will decrease the plastic deformation observed. The possible explanation

for this phenomenon is that the higher the cutting speed, the less the time available for plastic deformation in the surface layer of the work material [Sa 63]. Unfortunately, there is no further study for the elastoplastic deformation on machined surfaces. It is also apparent that it is extremely difficult to develop a closed form solution for explaining the elastoplastic deformation process due to the complexity of the machining process. Therefore, numerical techniques, such as the finite element method, may be good alternatives for solving such a problem.

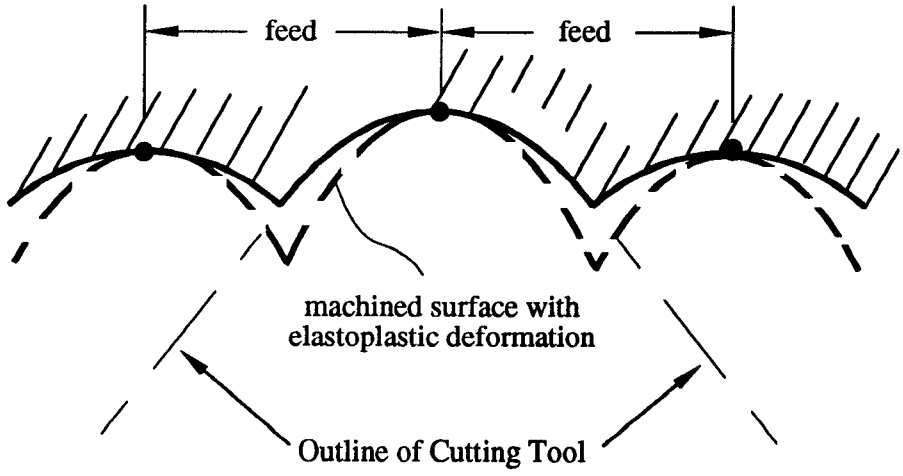

Figure 2.5: Effect of Elastoplastic Deformation on Surface Roughness

2.3.5 Effect of Tool Wear on Surface Finish

As pointed out by researchers [Pe 60, So 59], tool wear is also an important factor that influences the real surface roughness. It has been observed that the R_a vs. cutting time curve has the same general shape as the conventional wear land vs. cutting time curve [Shaw 84]. In other words, as tool wear proceeds,

the peak value of roughness increases and finally irregular peaks appear due to vibration [Lo. 89].

The increase of the roughness is due to the concentrated groove wear formed at the trailing edge of the tool. In finish cutting, small grooves develop along the feed direction on the cutting edge of tools which have small end cutting edge angles. There will usually be a single groove on the side cutting edge but may have several smaller grooves on the end cutting edge spaced at a distance equal to the feed. The number of grooves increases with decrease in the end cutting edge angle and with an increase in time. Pekelharing [Pe 60] has found that groove formation occurs at a decreasing rate at cutting speeds below 200 m/min. At higher speeds (or temperatures) the rate appears to be constant.

On the other hand, when the tool is worn, its effect on the cutting force variation can sometimes cause severe chattering during machining. As a strategy to control the effect of tool wear on machined surface quality, it is suggested that the tool wear process be treated as an *abnormal variation* to the machining process. This strategy, therefore, allows us to *temporarily exclude* the tool wear process from the *natural variation* during machining such as the nonhomogeneity of material properties in the workpiece [ZhHw 90a].

Chapter 3

A Stochastic Modeling for the Characterization of Random Tool Motion during Machining

3.1 Introduction

This chapter presents the development of a new stochastic approach to characterize random tool motion during machining. The complexity of cutting mechanism is represented by a random excitation system related to physical properties of the material being machined. A Markov-chain based stochastic approach is developed to model the random tool motion as the response of a machining system under the random excitation. In considering a turning operation, a concept of group distributions is introduced to characterize the global effect on the cutting force due to the variation of a certain material property. A model of segment excitation is used to describe its micro function within an individual revolution. A distribution pattern observed in the material property

is represented by a transition model. The simulation of random tool motion during machining resembles the generation of Markov chains. Microstructure analysis and image process are used to collect data, calculate relevant statistics and estimate the system parameters specified in the developed stochastic model. The developed stochastic model can be effectively used to simulate the random tool motion and to learn rich information on the performance measures of interest such as machining accuracy and finish quality. The new approach represents a major advance to create a fundamental scientific basis for the realization of a reliable and effective prediction system for information processing in sensor-based manufacturing.

3.2 Background

Computer integrated manufacturing systems have emerged in response to the requirements for great flexibility, productivity, and high quality of the product. As the computer technology advances, the manufacturing industry is now seeking a higher degree of production automation.

Sensor-based manufacturing leads to a new direction in the technological development. Instead of relying on intelligent human operators on the shop floor, sensing devices are intended to on-line collect signals related to the machining performance. Through signal processing, interpreters detect the process abnormalities, and built-in controllers take actions to return the process to a normal state. In this regard, mathematical modeling of random tool motion will be a necessity to ensure the sensitivity of monitoring systems to improve the machining precision, efficiency, and product quality. Great efforts have been

devoted to the discovery of quantitative descriptions of random tool motion. This statistical approach characterized by the development of a dynamic data system (DDS) was proposed in the 1970s [Pa. 80]. Discrete stochastic models, such as AR and ARMA models, are used to identify the transfer function of the physical system which is subject to random tool excitation. However, these models are in general used to describe stationary stochastic signals. For the application to model random tool motion which is a non-stationary time-varying process, these models are not suited and effective. Therefore, there exists a substantial distance towards the general adoption of these methods simply because of the complexity of manufacturing environments.

The hidden Markov model is a powerful tool in describing non-stationary time-varying process [RabJu 86]. It has been successfully applied to the modeling, processing, and recognition of speech signals which is well-known to be highly non-stationary. Due to the similarities between the speech signal and the random tool motion signal, the concept of Markov chain may serve as a theoretical foundation to initiate the modeling of random tool motion during machining.

In this chapter a new and stochastic approach is formulated for an analytical evaluation of random tool motion during machining. The developed approach consists of three statistical models to capture the dynamic characteristics of the cutting environment. For a turning operation a group distribution model is used to imitate the cutting process during one revolution as an assignment of known stochastic processes. For an assigned process, a normal distribution model is used to represent the random excitation system with mean and variance as its two parameters characterizing its average and variation levels. A transition model

is used to recognize possible patterns or inherent correlations of the tool motion between consecutive revolutions.

In the next section, the basic methodology of applying the Markov-chain model to characterize the random excitation source during machining is described. Procedure to identify the state transition probability matrix, which is the key for modeling the transition pattern of microstructures observed in the workpiece material, is discussed in detail afterward. A case study through both experiments and computer simulations is provided to demonstrate the application of using the proposed approach to study the finish quality of machined surfaces caused by random tool motion. Results from the experiments and computer simulations are presented for verification of the proposed approach. Summary of this chapter is presented in the final section.

3.3 Basic Methodology

3.3.1 Concept of Random Tool Motion

During a machining operation, the cutting tool moves along a path defined by the kinematic motion of the machine tool which is determined by the cutting parameters. In the case of a turning operation, spiral tool paths are most common. In addition to the kinematic motion, the cutting tool vibrates about its moving path in small magnitudes. Close examination suggests that tool vibration be of random nature and should be dealt with stochastically.

It has been well known that the built-up edge, tool wear, and unevenly distributed material properties (such as microhardness) are the major sources of

observed random tool motion. Among these sources, the random tool motion caused by the built-up edge can be controlled by increasing the cutting speed, a common practice on the shop floor. It is believed that random tool motion becomes severe as tool wear progresses during machining; and at the same time, the non-uniform distribution of hardness in the material being cut beats the cutting tool in a random manner. However, to distinguish between the effect of tool wear and the effect due to the distribution of material properties on random tool motion seems extremely difficult although not impossible.

As a strategy to control the random tool vibration, in this research we treat the random tool motion caused by tool wear as an *abnormal variation* to the machining process, and the random tool motion caused by other sources except tool wear as the *natural variation* to the machining process. This strategy, therefore, suggests that the unevenly distributed material properties become the main source for introducing the *natural* random tool motion if a high cutting speed is used for diminishing the effects due to the phenomenon of the built-up edge. In the following sections the physical meaning of the unevenly distributed material property, such as microhardness, related to the random tool motion during machining, and the stochastic modeling of this relation are discussed.

3.3.2 Dynamic Characteristics of the Cutting Environment

From the cutting dynamics point of view, it is beneficial if we treat the cutting process as a sampling process in which the cutting tool meets a series of small samples of the workpiece material (as illustrated in Fig. 3.1). Each of

the small samples (or blocks) in Fig. 3.1 may possess distinct characteristics in its microstructure. The cutting force generated in this process then varies in a random nature as the microhardness value of each of the samples varies. As a result, the random variation of the cutting force introduces random tool vibration during machining. Accordingly, it is necessary to identify the characteristics of the cutting environment embedded in the microstructures of workpiece material.

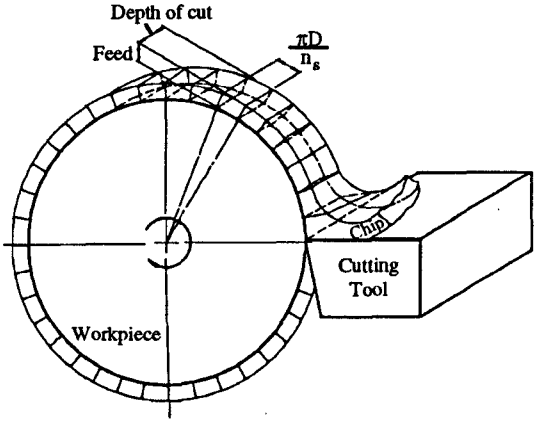

Figure 3.1: Cutting Process as a Sampling Process

As a first attempt to model the cutting dynamics in microscale, microstructural analysis of the workpiece material should be performed. Figure 3.2a shows the micro-photographs of four representative samples taken from different cross-sections of a rolled AISI 1020 steel bar. The photographs were then scanned and digitized as bitmap files (pictures in Fig. 3.2 are actually bitmaps). The ferrite structures (bright part or 0's in the bitmap file) and pearlite structures (dark part or 1's in the bitmap file), which are much harder than the ferrite, are clearly shown in the photographs.

It can be proven that the microhardness distributed within each cross-section tends to be a normal distribution [ZhKa 90] (as also shown in Fig. 3.2a). More-

over, depending on the microstructures along the bar, the said distributions for different cross-sections may be statistically different from (or similar to) each other as those shown in the group 1 or group 2 of Fig. 3.2a. If the microstructures are homogeneously distributed along the steel bar, the difference of microstructures among the cross-sections may not be sensed by the cutting tool when it passes along the bar with a preset feed rate during machining. In this case, a single (normal) distribution will be sufficient for modeling the microhardness distribution in the entire workpiece material.

However, if a sample was taken from the longitudinal direction of the bar, such as the one shown in Fig. 3.2b, the microstructures will be quite different from those shown in Fig. 3.2a. It is obvious that the pearlite structures in Fig. 3.2b tend to be distributed as stripes with certain pattern along the longitudinal direction of the bar which were formed during fabrication by the rolling process. As a result, when the tool passes from one revolution to the next, the cutting force generated will also possess a similar pattern which is then transmitted to the cutting tool in a form of vibration.

Based on the above observation, when the tool is cutting around one revolution of the material, a specific distribution which is applied statistically to estimate the microhardness of each blocks in the cross-section should be assigned. As the tool moves to the next revolution of the material, a distribution which may or may not be the same as the previous one should also be assigned. The assignment of these distributions is discussed in the next section. On the other hand, when the microhardness of each small block around one revolution, which is next to the previous one, is to be assigned based on the current distribution, it has to simultaneously follow the transition pattern as observed in the longitudinal

direction of the material. It should be pointed out that the cutting parameter settings (e.g., feed rate, depth of cut, and spindle speed) will have significant effects on the determination of the statistics for the microstructures distributed in the material (both in the cross-sectional and longitudinal directions). These issues will be covered in detail in the following sections.

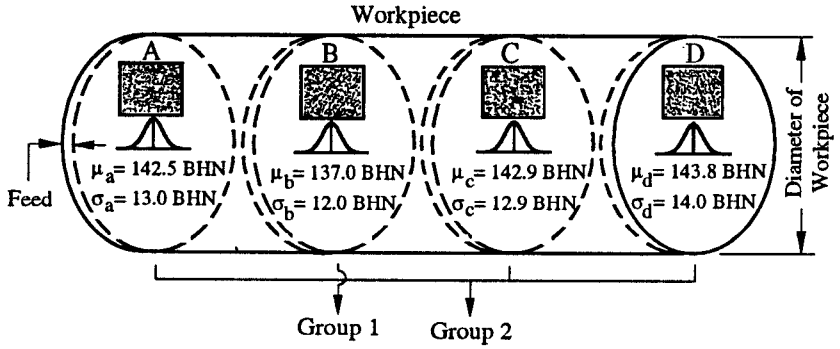

a. Microstructures from Different Cross-Sections

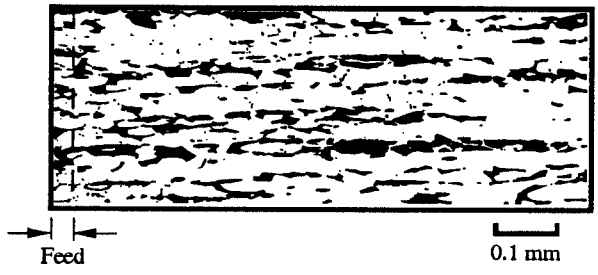

b. Microstructures from Longitudinal Direction

Figure 3.2: Microstructures from an AISI 1020 Steel Bar

3.3.3 A Stochastic Approach to Simulate the Micro Cutting Dynamics

Assignment of Group Distributions

As mentioned earlier, it is perceivable that the microhardness in different cross-sections of the same material has different distributions. For example, if we take ten samples from ten different cross sections of a steel bar, it is very likely that each sample has a different mean (μ_i, $i = 1, 2, ..., 10$) and variance (σ_i^2, $i = 1, 2, ..., 10$) of microhardness distributions. However, among the differences between means and variances some may have significance, some may not, from a statistical point of view. If we perform the significance tests on means, the ten distributions could be statistically 'grouped' into groups under certain criterion. Each group may then be characterized by a new mean and variance based on the statistics of the members in each group.

Figure 3.3 presents such a case that the distributions of ten samples were divided into three groups with their new means (μ_{g_j}, $j = 1, 2, 3$) and variances ($\sigma_{g_j}^2$, $j = 1, 2, 3$). These three distributions are called *Group Distributions.* Therefore, one can choose any of the three group distributions to re-characterize the original ten samples as well as any other samples from different cross-sections of the same steel bar. Beside the mean and variance, the probability of each group distribution (p_{g_j}), such that any cross section within the material will be characterized by the distribution, could also be estimated. For example, in Fig. 3.3 three out of ten samples are grouped as distribution one; hence, the probability that distribution one will occur in any cross section is 0.3. For clarity, we use different background shadings to represent different group distributions as

shown in Fig. 3.3. It is emphasized that these group distributions are determined by the microstructural analysis of the workpiece material which is technically feasible. Therefore, if there is enough information from the microstructural analysis, the group distributions can be determined as a known property of the material. Based on the said group distribution probabilities, one can then assign the group distributions to the consecutive cross-sections (it can be done by using a random number generator) which will be encountered by the cutting tool during machining (as shown in Fig. 3.3).

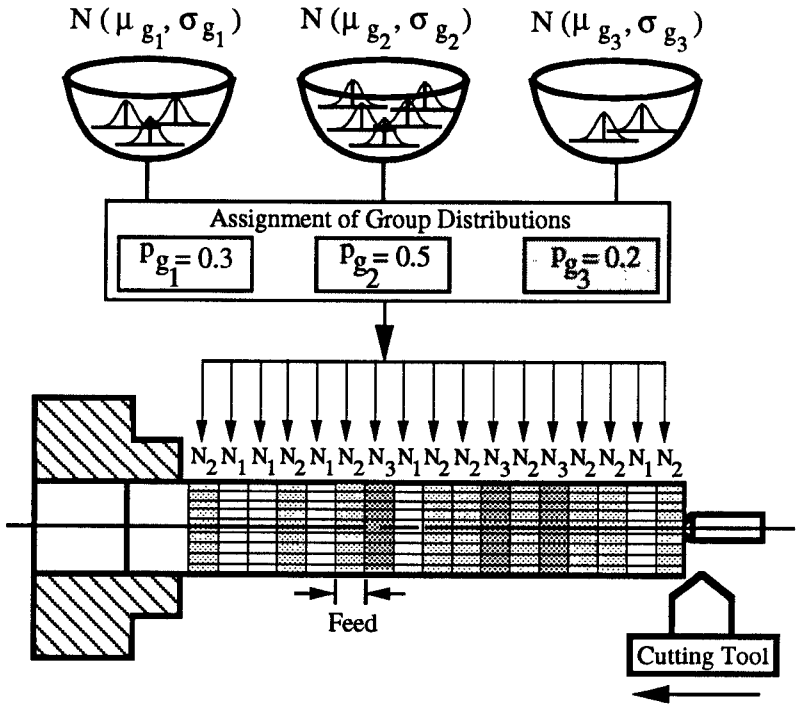

Figure 3.3: Assignment of Group Distributions to Each Segment

Segment Model for Single Revolutions

After the assignment of group distributions to each of the cross sections, it is intuitive that one can then determine the microhardness of each block within a

specific revolution (or *segment*) as previously shown in Fig. 3.1. For example, if the first revolution is assigned by group distribution two, the microhardness of each block in this revolution can be directly determined by the mean and variance of the group distribution two (since it is a normal distribution). Therefore, it is possible to determine the microhardness of each block in any other segments of the material in the same fashion.

As observed earlier, there exists a certain pattern in the microstructures along the longitudinal direction of the steel bar. In other words, there is an underlying correlation between the consecutive segments. This pattern has to be identified before the microhardness in the blocks of consecutive segments can be further assigned. This issue is discussed in the next section.

Transition Model for Pattern Recognitions

Research in the speech recognition process by applying the basic theory of Markov chains [RabJu 86] has provided the insight to this work as how to model the pattern of microstructures as seen in Fig. 3.2b. With a good model, we can predict the outcome and learn as much as possible via simulation of the process. How does one apply the Markov chains as a tool to model the transition pattern encountered during a machining process? We need first to understand the basic mechanism of Markov chains. A brief description and definitions of a Markov chain are presented as follows.

Consider a system which may be described at any time as being in one of a set of mutually exclusive states $(S_1, S_2, ..., S_N)$. According to a set of probabilistic rules, the system may, at certain discrete instants of time, undergo *changes of state* (or *state transition*). One could number the particular event of a time

instant $(q_1, q_2, ..., q_t)$ at which transitions may occur. A Markov chain or discrete-state Markov process is a random process $\{q_t, t = 1, 2, ...\}$ that takes on a finite or countable number of states (e.g., $S_1, S_2, ..., S_N$) and satisfies the following condition:

$$P(q_t = S_j | q_{t-1} = S_i, q_{t-2} = S_k, ..., q_1 = S_m) = P(q_t = S_j | q_{t-1} = S_i) \qquad (3.1)$$

for all $t > 0$ and all possible states (say, N of them) [Dr 67]. In other words, a Markov chain is a discrete random process in which the next state entered depends only on the current state, but not on the previous states. The transitions between states are governed by a set of state transition probabilities $\{p_{ij}\}$, where p_{ij} is the probability of going directly from state i to state j as i and j vary over all possible states, or

$$p_{ij} = P(q_t = S_j | q_{t-1} = S_i) = P(S_j | S_i), \ \forall \ i, j \in [1, N]; \ p_{ij} \text{ independent of } t \qquad (3.2)$$

with the following properties

$$p_{ij} \geq 0 \text{ and } \sum_{j=1}^{N} p_{ij} = 1, \ \forall \ i \in [1, N] \qquad (3.3)$$

It is often convenient to display these transition probabilities as members of a square matrix, i.e.,

$$[p] = \begin{bmatrix} p_{11} & p_{12} & \cdots & p_{1N} \\ p_{21} & p_{22} & \cdots & p_{2N} \\ \cdots & \cdots & \cdots & \cdots \\ p_{N1} & p_{N2} & \cdots & p_{NN} \end{bmatrix} \tag{3.4}$$

As a simple example, a two-state ($N = 2$) Markov process with a 2×2 transition probability matrix:

$$[p] = \begin{bmatrix} p_{11} & p_{12} \\ p_{21} & p_{22} \end{bmatrix}$$

is demonstrated here. Suppose that a coin tossing experiment is performed, and a sequence of observations are given; e.g., an observed sequence of the outcome would be $Q = \{S_1, S_1, S_2, S_2, S_1\}$, where S_1 stands for heads and S_2 stands for tails. It is desired to determine the probability of Q if the model is given (namely, it follows Eqs. 3.2 and 3.3). This probability can be expressed as

$$\begin{aligned} P(Q|Model) &= P(\{S_1, S_1, S_2, S_2, S_1\}|Model) \\ &= P(S_1)P(S_1|S_1)P(S_2|S_1)P(S_2|S_2)P(S_1|S_2) \\ &= \epsilon_1 p_{11} p_{12} p_{22} p_{21} \end{aligned}$$

where the notation

$$\epsilon_i = P(q_1 = S_i), \ \forall \, i \in [1, N] \tag{3.5}$$

stands for the initial state probabilities (it is usually set to 1) [RabJu 86, Ro 83].

It is also important to find out what the probability would be if a known state

keeps in that state for exactly d observations [RabJu 86]. This probability can be evaluated as the probability of the observation sequence $Q = \{q_1 = S_i, q_2 = S_i, \ldots, q_{d_i} = S_i, q_{d_i+1} = S_{j,j\neq i}\}$, given the model, which is

$$P(Q|Model, q_1 = S_i) = (p_{ii})^{d_i-1}(1 - p_{ii}) = \boldsymbol{f}(d_i) \tag{3.6}$$

The quantity $\boldsymbol{f}(d_i)$ is the discrete probability density function of duration d in state i. Therefore, the expected number of observations (duration) in a state conditioned on starting in that state is

$$E(d_i) = \sum_{d_i=1}^{\infty} d_i \boldsymbol{f}(d_i) = \sum_{d_i=1}^{\infty} d_i (p_{ii})^{d_i-1}(1 - p_{ii}) = \frac{1}{1 - p_{ii}}, \ \forall\, i \in [1, N]. \tag{3.7}$$

As long as the state transition probabilities $\{p_{ij}, \ \forall\, i, j \in [1, N]\}$ are defined, the pattern existing in the microstructures along the longitudinal direction of the steel bar can be recovered. Suppose that a two state Markov process (assuming that state one possesses the softest microhardness distribution) is given as the transition model, and a sample block of the first revolution has been identified being under state one. Then the state of a neighboring sample block in the second revolution which is just next to the first one can be determined based on the transition probabilities of p_{1j}, $j = 1, 2$. For example, if the transition probability from state one to itself, p_{11}, is 0.8, and the transition probability from state one to state two, p_{12}, is 0.2 (recall Eq. 3.3), the next state will most likely be still under state one. This work can be easily done by using a random number generator.

From the proposed stochastic approach, the relation between the microstructures of workpiece material and the random tool motion could be studied through computer simulation. This study could then serve as a tool for us to learn more about the random nature of a machining process. Before doing so, it is imperative to develop a method for identifying the parameters of the transition model, i.e., the states and transition probability matrix. Such a method is presented in the next section.

3.4 Identification of the Transition Model Parameters

The states and state transition probabilities are important to model a Markov process. This section will present a method about how to identify them from an observed image of microstructures of the workpiece material similar to the one shown in Fig. 3.2b.

3.4.1 Determination of State Boundaries and States

Suppose that the cutting parameter settings, such as feed and cutting speed in a turning process, are given. The image in Fig. 3.2b can be divided into subdivisions along both the longitudinal (feed) and vertical (cutting) directions based on the settings. For example, the microstructures shown in Fig. 3.4a are divided into six subdivisions along the longitudinal direction and two subdivisions along the vertical direction (based on the cutting parameter settings). Since the image is stored as a bitmap file (0's and 1's), one can calculate the ratio of the number

of black pixels (hard spots) to the total number of pixels in each subdivision. We call this a *state ratio* and is defined as

$$r_{kl} = \frac{\textit{Number of Black Pixels within the } (k,l)\textit{th Subdivision}}{\textit{Total Number of Pixels within the } (k,l)\textit{th Subdivision}},\ k \leq m,\ l \leq n. \tag{3.8}$$

where m is the number of subdivisions in the cutting speed direction, and n is the number of subdivisions in the feed direction. The purpose of evaluating these ratios is to determine the *state* of each subdivision associated with the hardness variation within the given image area. If the number of states is determined in advance (the number of states could be two, three, four, or even more), the *state* of individual subdivisions can be determined based on the *state ratios.*

To fix the idea, a map of *state ratios*, calculated in each subdivision based on Eq. 3.8, is shown in Fig. 3.4b. The mean ($\overline{r}$) and standard deviation (σ_r) of these ratios can also be evaluated. It is true that if the number of observations (i.e., the total number of subdivisions in the image) is very large, the distribution of *state ratios* will tend to be a normal distribution.

From the above distribution, the *state ratios* are then divided into regions based on the number of states to be considered. The boundaries of each region can be determined by using the 3σ criteria; i.e., a) divide the ratios between $[\overline{r}-3\sigma_r, \overline{r}+3\sigma_r]$ by N (the number of states) and call this number dr $(= 6\sigma_r/N)$; b) the boundaries will be $(-\infty,\ \overline{r} - 3\sigma_r + dr]$, $(\overline{r} - 3\sigma_r + dr,\ \overline{r} - 3\sigma_r + 2dr]$,..., and $(\overline{r} + 3\sigma_r - dr,\ +\infty)$.

Suppose that the number of states of the hardness variation is two, the hardness of each subdivision can be either at state I (soft) or state II (hard). Therefore, any ratio in the map which is smaller than the mean value ($\overline{r}$) can

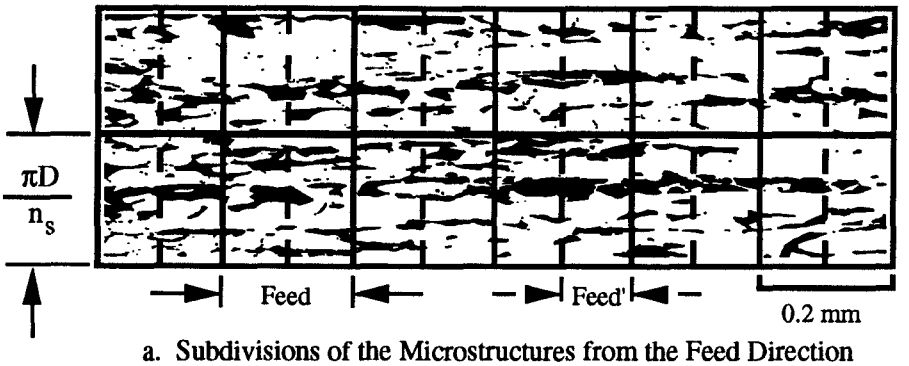

a. Subdivisions of the Microstructures from the Feed Direction

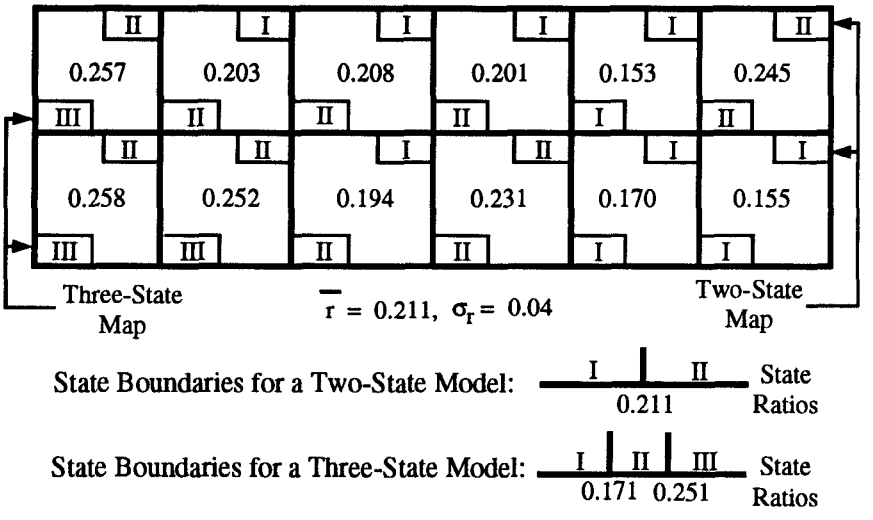

b. State Ratios and State Maps associated with Feed = 0.2 mm

Figure 3.4: Determination of State Boundaries and State Maps

be assigned at state *I*, and those larger than the mean value can be assigned at state *II*. In other words, the mean value of the ratios is the *state boundary* for a two-state model. The upper-right corners of each subdivision in Fig. 3.4b shows the states after they are assigned. This specific assignment of states is called a *state map*. The state map of a three-state model is also shown in Fig. 3.4b (lower-left corners) for comparison.

It is obvious that if the cutting parameters (feed or speed) are changed, the *state ratios* (and hence the state map) will also be changed. For example, if the

feed rate is reduced by one half, the same image will have more subdivisions (as those divided by dashed lines in Fig. 3.4a). Thus, the pixels in each subdivision will be different, and the *state ratios* as well as the state maps will also be different.

3.4.2 Estimation of Transition Probability Matrix, $[p]$

Two-State Markov Process

How can one evaluate the transition probabilities or the transition probability matrix $[p]$ from the observed state map? It is clear from Eq. 3.7 that as long as the expected duration of a state i is estimated, the probability for transition from state i to itself can be estimated by

$$\hat{p}_{ii} = 1 - \frac{1}{\hat{E}(d_i)}. \tag{3.9}$$

The evaluation of $\hat{E}(d_i)$ can be done by a) counting the number of occurrences of state i (It should be noted that an occurrence of state i is defined as the continuous observation of staying at state i without changing to any other states.) and b) counting the duration of each occurrence of state i observed from the state map; i.e.,

$$\hat{E}(d_i) = \frac{\sum_{j=1}^{K_i} d_{i_j}}{K_i} \tag{3.10}$$

where d_{i_j} is the j^{th} duration of occurrence at state i and K_i is the number of occurrences of state i. For example, there are three occurrences of state I in the map of Fig. 3.4b (i.e., $K_1 = 3$). The duration of each occurrence can also be

counted; i.e.,

$$d_{i_1} = Length(I, I, I, I) = 4,\ d_{i_2} = Length(I) = 1,\ d_{i_3} = Length(I, I) = 2$$

where $i = 1$ (at state I). Therefore, the estimated expectation of duration at state I from the observation is

$$\hat{E}(d_1) = \frac{d_{1_1} + d_{1_2} + d_{1_3}}{Number\ of\ occurrences\ of\ state\ I} = \frac{4+1+2}{3} = \frac{7}{3}$$

The meaning of the above number (7/3) is that the expected duration of staying in state I is about 2.3 (feeds) in the feed direction. The probability for transition from state I to itself is then calculated from Eq. 3.9:

$$\hat{p}_{11} = 1 - \frac{1}{\hat{E}(d_1)} = \frac{4}{7}$$

Similarly, there are four occurrences of state II in the map of Fig. 3.4 ($K_2 = 4$). The estimated expectation of duration at state II from the observation is

$$\hat{E}(d_2) = \frac{d_{2_1} + d_{2_2} + d_{2_3} + d_{2_4}}{Number\ of\ occurrences\ of\ state\ II} = \frac{1+1+2+1}{4} = \frac{5}{4};$$

therefore,

$$\hat{p}_{22} = 1 - \frac{1}{5/4} = \frac{1}{5}.$$

It is obvious that from Eq. 3.3 the transition probabilities of $\hat{p}_{12}$ and $\hat{p}_{21}$ can also be estimated. Therefore, the estimated transition probability matrix of this

two-state Markov process based on the image given in Fig. 3.4a is

$$[\hat{p}] = \begin{bmatrix} 4/7 & 3/7 \\ 4/5 & 1/5 \end{bmatrix}.$$

N-State Markov Process (N > 2)

If the number of states is not two but three, four, or even more, how does one estimate the transition probability matrix? Based on the state map of a three-state Markov process (Fig. 3.4b), and following the calculations similar to that of the two-state model, the estimated expectation of duration at state *I, II,* and *III* are

$$\hat{E}(d_1) = \frac{1+2}{2} = 1.5,\ \hat{E}(d_2) = \frac{3+1+2}{3} = 2.0,\ \text{and}\ \hat{E}(d_3) = \frac{1+2}{2} = 1.5,$$

respectively. Therefore, from Eq. 3.9, we can estimate the following transition probabilities:

$$\hat{p}_{11} = 1 - \frac{1}{\hat{E}(d_1)} = \frac{1}{3},\ \hat{p}_{22} = 1 - \frac{1}{\hat{E}(d_2)} = \frac{1}{2},\ \text{and}\ \hat{p}_{33} = 1 - \frac{1}{\hat{E}(d_3)} = \frac{1}{3}.$$

Since the transition probabilities of p_{ii}'s have been estimated, the problem now is how to estimate other transition probabilities, $p_{ij,j\neq i}$, in the $[p]$ matrix.

Suppose that each state can only change to its neighboring states or to itself (e.g., state i can only change to state $i+1$, $i-1$, or i), the transition probability

matrix will have a form as follows

$$[p] = \begin{bmatrix} p_{11} & 1-p_{11} & 0 & 0 & \ldots & 0 \\ b_1 & p_{22} & 1-p_{22}-b_1 & 0 & \ldots & 0 \\ 0 & b_2 & p_{33} & 1-p_{33}-b_2 & \ldots & 0 \\ \ldots & \ldots & \ldots & \ldots & \ldots & \ldots \\ 0 & \ldots & 0 & b_{N-2} & p_{N-1\,N-1} & 1-p_{N-1\,N-1}-b_{N-2} \\ 0 & \ldots & \ldots & 0 & 1-p_{NN} & p_{NN} \end{bmatrix} \tag{3.11}$$

where b_i, $i = 1, 2, ..., N-2$, are the probabilities for transition from state $i+1$ to state i. This type of transition pattern is sometimes referred as the *birth and death* Markov process [Ch 67]. It is obvious that the estimation of above $[p]$ is much easier than the estimation of Eq. 3.4 since only the b_i's are to be determined in the above $[p]$ matrix. Actually, based on the observed microstructures of the workpiece material, this type of transition seems the most favorable for our purpose.

To determine the b_i's, a stationary distribution of the (N) states, $\underline{\pi} = [\pi_1\, \pi_2 \ldots \pi_N]$ where π_i is the 'long-term fraction' of state i observed in the state map (e.g., Fig. 3.4b), should be first defined, and it should satisfy the matrix equation [Ch 67]

$$\underline{\pi} = \underline{\pi}[p]. \tag{3.12}$$

The π_i's can be estimated by

$$\hat{\pi}_i = \frac{\sum_{j=1}^{K_i} d_{i_j}}{K_{obs}} \tag{3.13}$$

where d_{i_j} is the j^{th} duration of occurrence at state i, K_i is the number of occurrences of state i, and K_{obs} is the total number of observations in the state map (i.e., the number of subdivisions in the cutting speed direction, m, times the number of subdivisions in the feed direction, n). For example, from the state map of Fig. 3.4b, the estimated π_i's are

$$\hat{\pi}_1 = \frac{d_{1_1} + d_{1_2}}{\textit{Total Number of Observations in the State Map}} = \frac{1+2}{2 \times 6} = \frac{1}{4},$$

similarly,

$$\hat{\pi}_2 = \frac{3+1+2}{2 \times 6} = \frac{1}{2}, \text{ and } \hat{\pi}_3 = \frac{1+2}{2 \times 6} = \frac{1}{4}.$$

From Eq. 3.12, one can manipulate the matrix equation such that b_i's can be evaluated based on the linear regression method. The derivation of b_i's is explained in the Appendix A. After solving the b_1 (=1/4) in this three-state model, the transition probability matrix is

$$[\hat{p}] = \begin{bmatrix} 1/3 & 2/3 & 0.0 \\ 1/4 & 1/2 & 1/4 \\ 0.0 & 2/3 & 1/3 \end{bmatrix}.$$

3.5 Case Study

A turning operation of machining an AISI 1020 steel bar with diameter of 72 mm and length of 300 mm was studied to verify the developed stochastic approach for modeling the random tool vibration during machining. The study consists of both the experimental work and computer simulations. They are discussed in this section.

3.5.1 Experimental Work

To verify the basic methodology developed for studying the micro cutting dynamics, experiments were carried out and the experimental results were compared with the results from computer simulation. The experimental work consists of:

1. Microstructural analysis (see Appendix B): This analysis provides the information regarding the microhardness distributions in the workpiece material, as discussed in previous sections. Samples taken from the steel bar were polished and etched for taking microphotographs under an optical microscope or a scanning electron microscope. Pictures of each sample were then scanned and image data files were stored. Statistical analysis was performed on the image files to get the related statistics for further calculation.

2. Machining tests: The machining of the AISI 1020 steel bar was performed on a CNC (computer numerical controlled) lathe with the following settings:

   - Cutting data: feed=0.23 mm/rev, depth of cut=0.5 mm, spindle speed=470 rpm (the built-up edge was insignificant at this speed).
   - Cutting tool: nose radius=0.6 mm, rake angle=0°, lead angle=20°.
   - Cutting fluid: none.
   - Cutting time: less than one minute (no tool wear was observed).

3. Measurement of surface profiles: The surface roughness along the feed direction (axial direction of the steel bar) was measured using a Talysurf

surface profilometer. Twenty five surface profiles were taken in parallel with a $0.2mm$ interval inside a rectangular area of $4.8 \times 4.0\, mm^2$ to form a surface topography as the one shown in Fig. 3.5a. A representative surface profile from the experiment is shown in Fig. 3.5b. The measured surface roughness indices, such as the roughness average values (R_a), root mean squared values (R_q), peak to valley values (R_t), and the standard deviation of each of them are listed in Table 3.1.

3.5.2 Computer Simulations

From the basic methodology described in Section 3.3.3, computer programs were written to simulate the micro cutting dynamics. The programs were all written using the FORTRAN 77 language and compiled on a Unix based operating environment. They are portable to any system with a FORTRAN 77 compiler (except that a graphics display module is device dependent). The main structure of the programs is based on the analysis of cutting dynamics which will be discussed in detail in Chapter 5.

The statistical approach mentioned in Section 3.3.3 is coded as subroutines and appended to the original programs. The same cutting parameter settings as chosen in the experiment, the digitized images from samples of the material, and the group distributions, are read as input data files. In this study three group distributions were estimated from the microstructural analysis; they are: $\mu_{g_1} = 110.0$ BHN, $p_{g_1} = 0.2$, $\mu_{g_2} = 143.0$ BHN, $p_{g_2} = 0.5$, $\mu_{g_3} = 165.0$ BHN, $p_{g_3} = 0.3$, and the standard deviations are the same ($\sigma_{g_{j,j=1,2,3}} = 12.0$ BHN). The state transition probability matrix is then estimated. The assignment of group

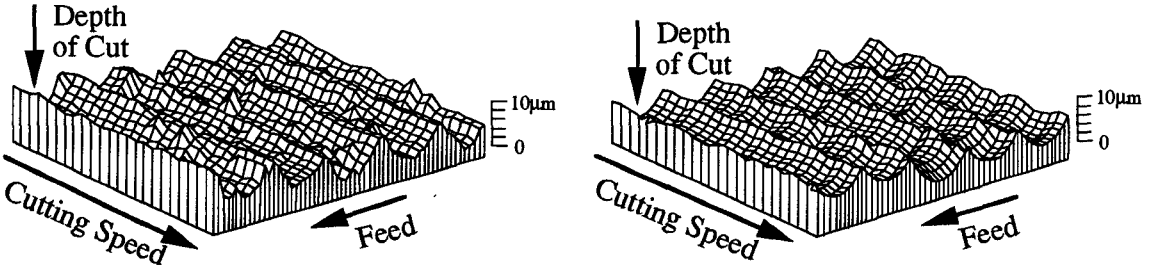

Measured Surface Topography

Simulated Surface Topography (Case 1)

a. Surface Topographies from Experiment and Computer Simulation

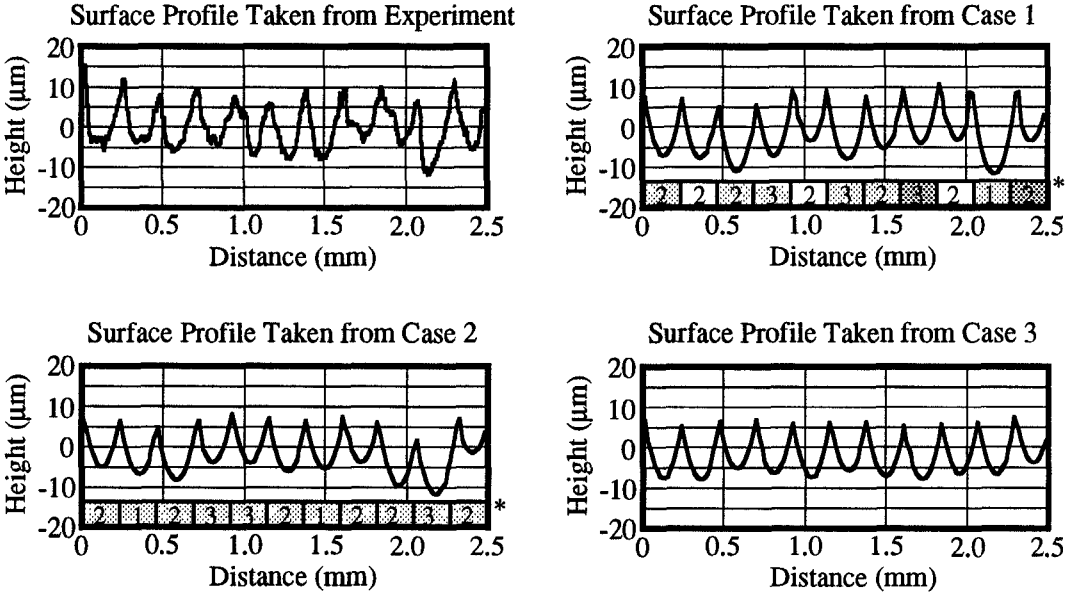

* The background shading of each block and the number inside it represent the assigned group distribution (recall Fig. 3.3) and its state associated with each feed, respectively.

b. Surface Profiles from Experiment and Computer Simulation

Figure 3.5: Surface Topographies and Profiles from Experiment and Simulation

distributions, the prediction of segment microhardness values and state map of the first revolution, assignment of the state maps of consecutive revolutions (or segments), and prediction of the microhardness values of all segments are then carried out one after another. As long as the microhardness values of each revolution are available, they are stored as one of the input data files for the evaluation of dynamic random tool motion. We call this set of input data as *Case 1.*

In order to see the effects of different microstructures on the random tool motion and simulated surface topographies, two other sets of microstructural models are also used (recall Section 2.2). The characteristics of these two input sets are:

- *Case 2:* Instead of assigning group distributions to each segment, only one normal distribution (μ_g = 143.0 BHN, σ_g = 12.0 BHN) is applied as the segment model in this case, and the transition model is still kept to simulate the pattern along the longitudinal direction. This case assumes that the microhardness distribution in one cross section of the material is similar to that of any other cross section.

- *Case 3:* This case assumes that the distribution of microhardness in the entire workpiece material is characterized by a single normal distribution and there is even no transition pattern along the longitudinal direction [ZhKa 90]. For example, we can heat treat a steel bar to spheroidize the pearlite structure into a matrix of soft, machinable ferrite structure [As 84]. Thus, the transition pattern existed along the longitudinal direction is destroyed and microstructures are almost homogeneously distributed as a

single distribution in this case.

The cutting force, dynamic response of tool vibration, surface profiles, and surface topography are part of the outputs available from the computer simulation. To check the validity of the proposed models, we compare the surface profiles and surface quality indices with experimental results (since they also represent the outcome of a machining process). A simulated surface topography from *Case 1* is shown in Fig. 3.5a. From the three cases of simulation, representative surface profiles along the feed direction are also shown in Fig. 3.5b. Based on the simulated surface profiles, we can then evaluate the surface roughness indices as those listed in Table 3.1.

3.6 Discussion of Results

A qualitative comparison is made by first looking at the two surface topographies shown in Fig. 3.5a. The common characteristics are the waviness of the surface texture along the cutting speed direction which is caused by tool vibration and the arc chain pattern which is caused by the tool motion along the feed (or longitudinal) direction. By comparing the surface profiles shown in Fig. 3.5b, it is found that profiles from *Case 1* and *2* are closer to the profile from the experiment because the height variations of profiles from *Case 1, 2*, and experiment are more prominent than that from *Case 3*. This can be explained by the transition pattern observed in the steel bar which is considered during simulation in *Case 1* and *2* but not in *Case 3*. The difference between *Case 1* and *2* is not easy to tell from the profiles. However, it is anticipated that the height variation of *Case 1*, where three group distributions are used, is more

prominent than that of *Case 2*, where only one distribution exists (refer to the shaded bars of *Case 1* and *2* in Fig. 3.5b). This qualitative comparison suggests that the validity of proposed models is very promising.

Table 3.1: Comparison of the Surface Roughness Indices

Units in μm	Experiment	*Case 1*	*Case 2*	*Case 3*
$\overline{R_a}$	4.20	4.05	3.95	3.95
σ_{R_a}	0.32	0.17	0.10	0.13
$\overline{R_q}$	5.04	4.96	4.81	4.83
σ_{R_q}	0.44	0.20	0.12	0.14
$\overline{R_t}$	20.28	17.09	16.56	16.58
σ_{R_t}	1.70	0.74	0.91	0.87

A quantitative comparison is done by comparing the surface roughness indices between the measured and simulated surface profiles. As listed in Table 3.1 that the simulation results from *Case 1* are well matched with those from the experiment. For instance, the mean values of R_a, R_q, and R_t from the measured surface are 4.20 μm, 5.04 μm, and 20.28 μm; and those from *Case 1* are 4.05 μm, 4.96 μm, and 17.09 μm, respectively. The significance tests on means were carried out to see the statistical difference between the mean values of surface indices. It turned out that the differences in R_a and R_q are statistically insignificant (it is 95% confident to say so) between those from *Case 1* and those from the experiment. Similarly, if tests were carried out for *Case 2* and *Case 3*, the R_a and R_q's of both cases are statistically different from that of the experiment. This comparison, therefore, provides a much stronger evidence that *Case 1* is the most likely situation happened during the machining of the AISI 1020 steel bar as performed in the experiment. It is, however, very interesting to observe that the R_t values from all simulation cases do not match that from the experiment. This relates to an elastoplastic interaction between the material

and cutting tool and will be discussed in Chapter 4.

To some extent, the above quantitative comparison has shown that through the proposed stochastic models (*Case 1*) and computer simulation, we can almost reconstruct the finished surface texture obtained from a turning process. On the other hand, the random tool motion during machining can also be characterized by the proposed stochastic approach if the nonhomogeneous material hardness distribution is considered as the most significant source to cause random excitation during machining.

3.7 Summary

A stochastic approach to characterize the random tool motion during machining has been proposed. It is based on the Markov-chain theory to characterize the non-stationary and time-varying signal process. The *group distributions*, *segment model*, and *transition model* are proposed to quantitatively evaluate the random tool motion caused by a random excitation related to microstructures of the workpiece material being cut. A method has also been developed to determine the states and state transition probabilities defined in the transition model. Results from experiments confirm the predictions obtained from computer simulations. It is believed that this research may become an essential part to quantify the random tool vibration during machining, a task which nowadays seems difficult but critical for developing a sensor-based machining system to improve the quality and productivity in the manufacturing industry.

Chapter 4

Analysis of Elastoplastic Deformation Observed on the Machined Surfaces

4.1 Introduction

This chapter presents a non-linear quasi-static analysis of the elastoplastic interaction observed between a single-point cutting tool and the workpiece material being cut. An updated Lagrange method is applied to solve the large strain elastoplastic deformation problem using a three-dimensional finite element model which simulates a single-point metal cutting process. The effects of cutting parameter settings on the elastoplastic deformation of machined surfaces are investigated through the analysis.

It is clear that surface quality as well as dimensional accuracy are important for the functional requirements of many engineering components and interfaces. It is also evident that the quality of a machined surface is closely related to the machining process used for producing the part. Therefore, understanding of the mechanism of surface texture formation during machining is compulsory to

improve the quality of machined parts.

Metal cutting processes have been studied extensively for a long time. Due to the complexity of the material removal process, it is extremely difficult to have a general model which can interpret the various mechanism taking place at the contact region of the cutting tool and the material being cut. The formation of a machined surface, as mostly observed from a single-point cutting process (such as turning), may at least be affected by three major causes (refer to Section 2.3): a) the geometry of cutting tool and cutting parameter settings which form the basic shape of a machined surface or the *nominal machined surface*, b) vibration or chattering of the machine tool, caused by the dynamic cutting force variation during machining, which superimposes the trace of tool tip vibratory motion on the nominal machined surface, and c) the elastoplastic interaction between the tool-workpiece interface, which will not only deform the material but also keep residual stresses inside the machined parts.

It is obvious that both tool vibration and elastoplastic deformation will cause the irregularities observed on a machined surface. Study of the stability of a machine tool structure to suppress the tool vibration during machining has been very promising in reducing the surface irregularities caused by tool vibration [TlAn 83]. However, the basic mechanism of the elastoplastic process occurred on the tool-workpiece interface has not yet been clearly understood. The research in this area has drawn the most attention from those who have attempted analyses of machining. For example, most of the research is based on the study of the orthogonal cutting process [ErMe 41]. Their contributions have provided a foundation for the understanding of the basic mechanism of metal cutting processes.

The computer advancement and the development of numerical methods have provided powerful tools for doing research in machining processes. Finite element method is the most prominent one among them. The first finite element analysis for metal cutting was due to Klamecki [Kl 73] who treated the incipient chip formation process using a three-dimensional model. However, the model used did not examine the formation of a machined surface. Ever since, many other finite element models have been proposed by researchers [Ta. 74, UsSh 82, St. 83, Iw. 84, StCa 85, CaSt 88, Lin 91, Ko. 91]. Unfortunately, all of these models dealt with orthogonal cutting only, which assumes a plane-strain condition for the workpiece material being machined (see Fig. 4.1), and they were not aimed at explaining the formation of surface texture during machining. Therefore, it is evident that further study of the finite element model and analysis procedure are necessary to reveal the mechanism of surface texture formed during machining.

There are two major objectives of this research: 1) to have a better understanding of the mechanism of surface texture formation during machining through the study of the elastoplastic deformation observed on the machined surfaces; and 2) to develop a surface texture modification model which can enhance the accuracy of a computer-aided surface texture simulator for the quality control of machined surfaces. In the next section, behavior of the tool-workpiece interface observed under the cutting action is studied. The procedure to analyze such a cutting process using a three-dimensional finite element model is discussed in detail afterwards. A case study to check the validity of the finite element model is presented where results from this analysis are compared with those from the turning of AISI 1020 steel bars and 6061-T6 aluminum alloy bars. Results and implications of this research are discussed and followed by the

summary.

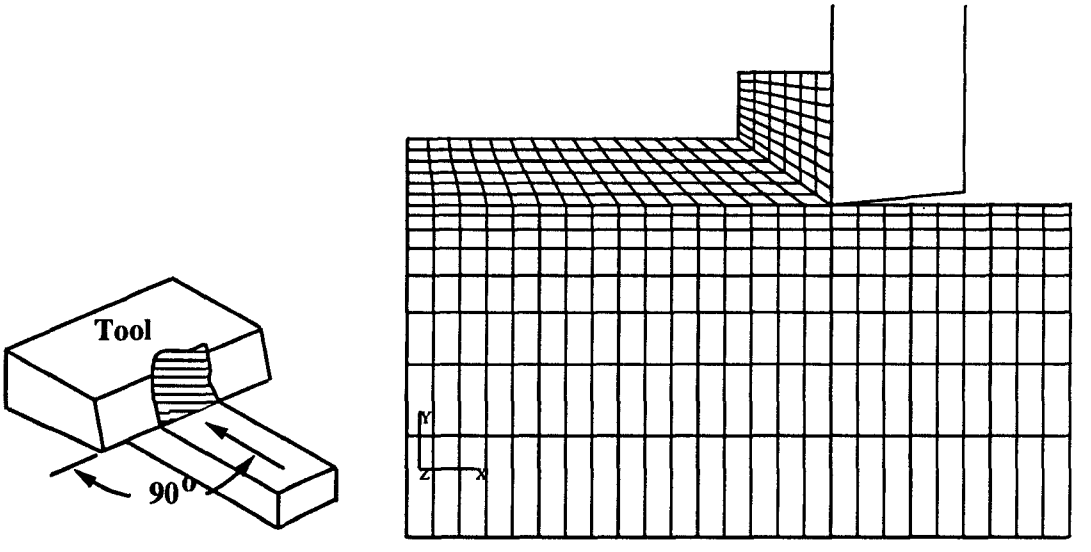

(a) Orthogonal Cutting (b) Finite Element Mesh for Orthogonal Cutting

Figure 4.1: Orthogonal Cutting Process and Its Finite Element Model

4.2 Investigation of the Tool-Workpiece Contact Area

Traditionally, the movement of the work material and the chip across the faces around the edge of a tool has been treated as a classical friction action where *frictional forces* tend to restrain the chip movement on the tool rake face. However, close studies of the tool-workpiece interface have revealed that this friction action is not what really happened for most metal cutting conditions (especially at high cutting speed) [Tr 91].

Under loading conditions in engineering sliding contact problems, the *real*

contact area is very small, often less than one hundredth of the *apparent area* of the contact surfaces. The frictional force is that required to break the bonding force between the molecules on the two *real contact* surfaces. This frictional force is proportional to the normal force between the two surfaces. However, when the normal force on the tool-chip interface is increased to such an extent (as in metal cutting) that the real area of contact is a large proportion of the *apparent contact* area due to plastic deformation, the force required to move one body over another is the frictional force needed to shear the weaker of the two materials across the whole contact area. This force is independent of the normal force when cutting at high speed, but is directly proportional to the area of contact, a relationship totally opposed to that of classical friction theory [BoTa 54].

Figure 4.2 shows examples of the *real* contact area under three different normal forces. In Fig. 4.2a, the normal force is the smallest; and the *real* contact area (at points A, B and C) is far less than the apparent contact area. As shown in Fig. 4.2b, when the normal force increases so does the *real* contact area (at points A', B' and C'). When the normal force is extremely large, the two surfaces are forced almost in complete contact as in Fig. 4.2c. Consequently, the friction force is no longer independent of the contact area as discussed above.

To better understand the mechanism occurring at the tool-work interface, knowledge of the distribution of the stresses is essential. It has been shown that in metal cutting the shaping of the new work surface is formed by fracture under shearing process [Ka. 83]. When ductile metals and alloys are being cut, the shearing process is plastically strained. In other words, plastic strain is an essential aspect of metal cutting. The amount of strain, which varies greatly on the tool-work contact area or beneath it, depends on the material properties,

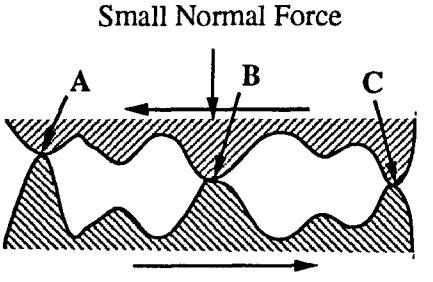

(a) Sliding Contact under Small Normal Force

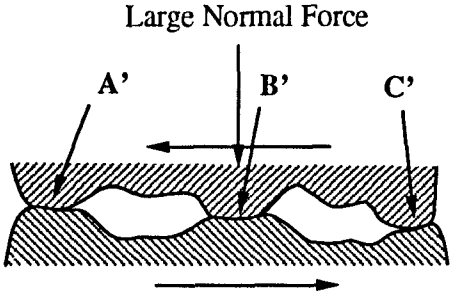

(b) Sliding Contact under Large Normal Force

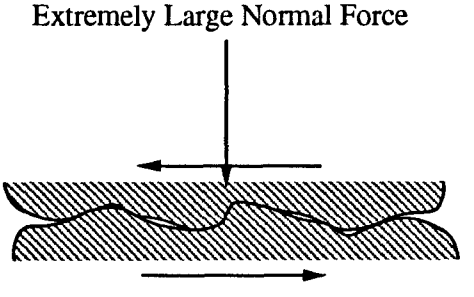

(c) Sliding Contact under Extremely Large Normal Force

Figure 4.2: Examples of Sliding Contact under Different Normal Forces

tool geometry, and cutting conditions.

Based on the observation from Trent [Tr 91], when cutting at high speed, the just-formed chip tends to stick to the tool rake face. On the tool flank face, the workpiece material underneath the tool edge is tracked by the tool edge as the tool moves across the newly formed surface. A three dimensional view of a single-point cutting process is schematically shown in Fig. 4.3 where a very hard cutting tool with a nose radius (R) moves into a *crescent* shaped uncut chip cross section (determined by the tool geometry and cutting parameter settings) of the workpiece material. The material just in front of the cutting tool edge experiences a large compressive stress and, therefore, is pushed back with large strain. When the cutting edge pushes further, it leads to the fracture of the work material, and chip separates from the workpiece along the cutting edge.

It is perceived that the contact deformation of the workpiece and tool material, both elastic and plastic, develops during machining. Because the hardness of the workpiece material is relatively low with respect to the hardness of the tool material, the contact deformation is mostly on the workpiece side. Depending on the stress distributed on the contact area, plastic deformation is superior to elastic deformation due to the high pressure exerted by the cutting tool at certain points of the workpiece surface and its sub-layer elements. A severe work hardening of the workpiece develops when the tool moves across the contact area during machining. As a result, these points will sustain the tool path trajectory with little distortion caused by the recovery of the plastic deformation. On the other hand, those points on the surface exerted by lower cutting pressure present elastic deformation. The recovery from the elastic deformation is more significant at these points as the cutting tool travels along the surface. Consequently,

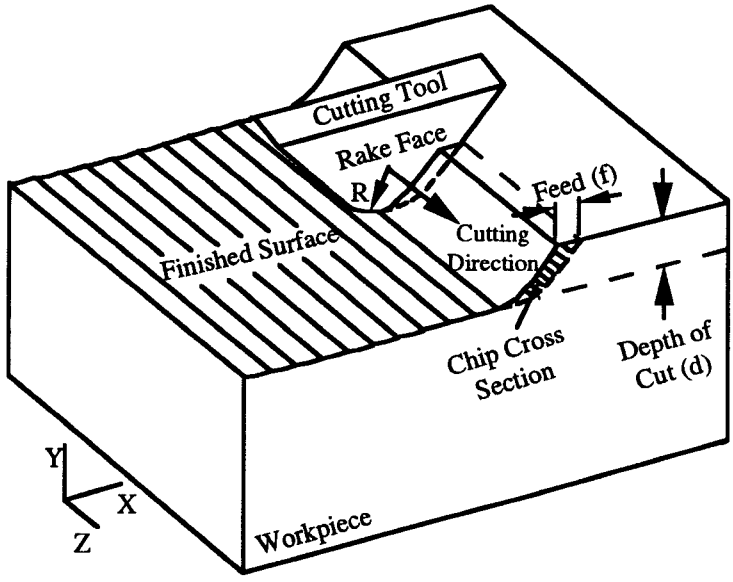

Figure 4.3: Three-Dimensional Representation of a Single-Point Cutting Process

the surface is somewhat distorted due to the elastic-plastic deformation in the recovery process.

Observations of the temperature effect on the stress-strain distribution in the tool-work and tool-chip interfaces have also been made by researchers. It is well known that most of the heat resulting from the work done on the shear plane to form the chip remains in the chip and is carried away with it, while a small amount but variable percentage is conducted into the workpiece and raises its temperature [Kr 66, Shaw 84, Tr 91]. Figure 4.4 shows that the cutting tool has the highest temperature distribution and the workpiece has the lowest temperature distribution under different cutting speed. On the other hand, the temperature effect on the chip tends to be compensated by the effects due to the strain rate increased under the same cutting condition as has been observed by researchers [Shaw 84, Tr 91]. Actually, the temperature effect tends to have more effect on the tool life than on the workpiece [Tr 91]. If the cutting temperature is properly controlled during cutting process (e.g., using cutting fluid to dissipate the heat generated during machining), it can be treated as a non-dominant factor in the elastoplastic deformation process on the machined workpiece material [Lin 91].

From the above investigation of the tool-workpiece interface, it becomes apparent that the development of a closed form solution to explain the elastoplastic deformation process observed on the machined surface is extremely difficult due to the complex deformation phenomena. Therefore, numerical techniques, such as the finite element method, may provide a good alternative for solving such a problem. Since our purpose is to investigate the effects of elastoplastic deformation process on the machined surfaces, this research is aimed at de-

veloping a three-dimensional finite element model which can account for the essential features observed in the metal cutting processes and can provide closer approximation to the actual deformed shape of a machined surface. In the following sections, the effects of different cutting conditions (feed rate and depth of cut) on the deformation process are also examined by a three-dimensional finite element model.

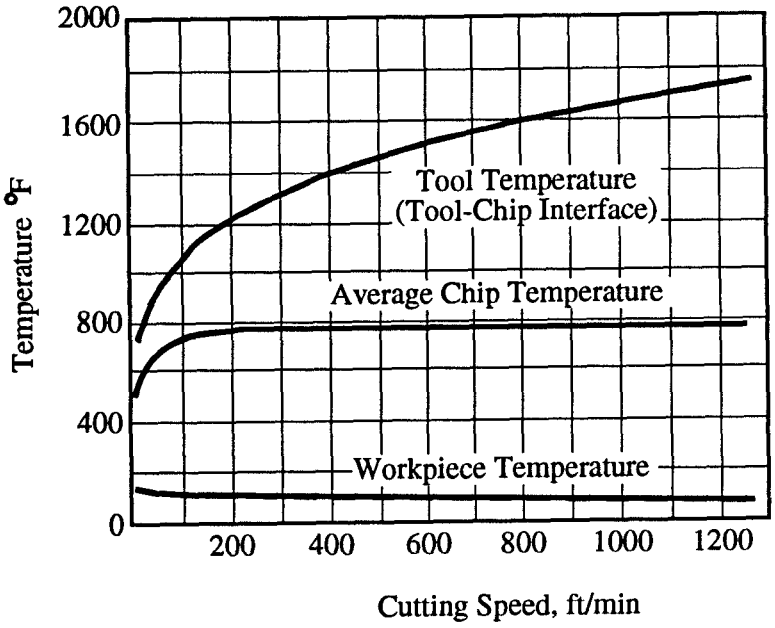

Figure 4.4: A Typical Temperature Distribution in Metal Cutting (from [Kr 66])

4.3 Three-Dimensional Finite Element Modeling

4.3.1 Major Features and Assumptions of the Model

Based on the need from the investigation mentioned in the previous Section, a three-dimensional finite element mesh is generated as shown in Fig. 4.5. The major features and assumptions of the generated meshes are:

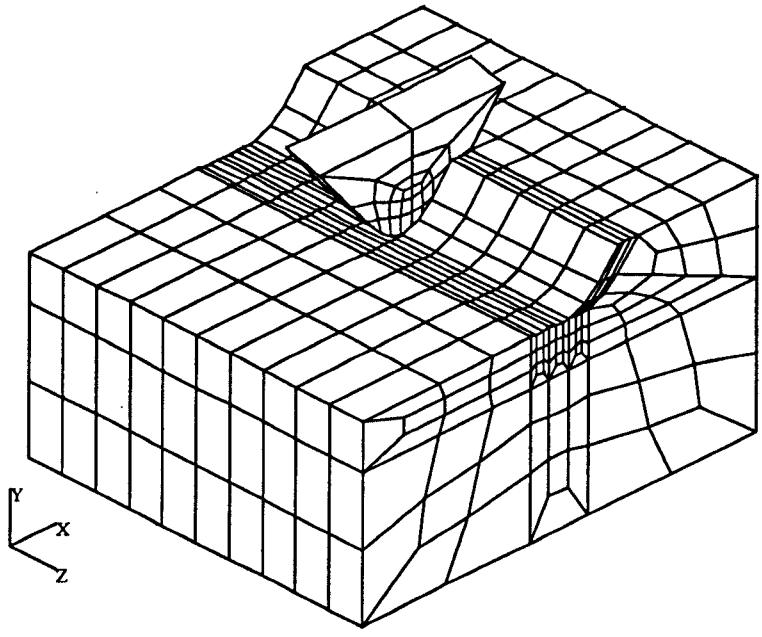

Figure 4.5: Three-Dimensional Finite Element Model

1. The tool material is treated as a rigid body moving across the workpiece material along a predefined tool path. Most of the cutting tool materials used for machining have much higher hardness values than those of the workpiece materials. For example, the hardness of a tungsten carbide tool

insert is usually in the range of (1800 - 3200 BHN) compared with that of a low carbon steel workpiece material which is around 140 BHN. It is reasonable to make such an assumption (tool is a rigid body) that the computer resource can be reserved for other features without sacrificing the accuracy of calculation.

2. In Fig. 4.5, there are 885 isoparametric, eight-node three-dimensional brick type of elements in the workpiece material model and 30 extra elements for simulating the rigid tool insert. The size of the element is based on a criterion such that the aspect ratio (e.g., the ratio of the larger dimension, say in the X direction, to the smaller dimension, say in the Y direction, of an element) of each element should not exceed a fixed upper limit [MARC 91]. Among the 885 elements, the interested area is near the tool path as shown in the middle part of the model. Therefore, finer meshes are necessary in this area to take the surface deformation during cutting into account.

3. Except the surface on top of the workpiece model, the nodes on the bounding surfaces of the workpiece are constrained in all the six degrees of freedom. This can be viewed as if a chunk of the workpiece, on which the tool is passing by, is *extracted* from its surrounding material. It is a common practice to assume that the boundaries of this chunk, *remote* from the tool-work interface, can be treated as deformation free when the material is being cut [ZiGo 74]. As shown in Fig. 4.5, the size of this chunk, depending on the geometry and size of the tool-work contact area, is chosen to be $4.69\,mm$ in the X direction, $2.48\,mm$ in the Y direction,

and $4.00\,mm$ in the Z direction, which can account for the cases applied in this study.

4. Adhesion occurred on tool-chip interface is assumed for the analysis. As mentioned earlier that the most important conclusion from the observation of the tool-work contact area is that the tool-chip interface may be under adhesion condition instead of friction if high cutting speed is used. This assumption yields that when the cutting tool moves across the workpiece, the contact between the tool and material is dominated by the normal force exerted on the interface of the tool and chip. This condition can be simulated by a special *contact* option under the finite element solution phase as will be discussed later.

5. As discussed in Section 4.2, the temperature effect can be excluded from this analysis since most of the concern is related to its effect on cutting tool life rather than on the workpiece material [Tr 91]. By disregarding the temperature effect, it alleviates the needs to a) find out the relation between the temperature variation and the stress-strain curve for different materials, and b) build a temperature distribution model in the cutting zone, a tedious and, in most of the cases, an inaccurate or even contradictory estimation, for the analysis under the desired cutting conditions [Kr 66, Shaw 84].

6. The tool wear and built-up edge are assumed to be insignificant under the cutting conditions applied in this analysis. For example, if the time period for cutting is restricted to be less than a fraction of a minute, the tool wear will become insignificant [Shaw 84, Tr 91]. On the other hand,

if the cutting speed is set high enough, the size of the built-up edge will actually become small and even diminished during machining [Sa 63]. As a justification for these assumptions, the machining tests performed in this work were confined to obey these phenomena.

4.3.2 Modeling of Elastoplastic Deformation in the Cutting Zone

If the effect of plastic flow on the cutting process is to be considered, the material property of the workpiece should include the information beyond the elastic region which is also necessary for the nonlinear stress-strain finite element analysis. The workpiece materials being used in this study are AISI 1020 steel and 6061-T6 aluminum alloy. Based on the available test data [Alloy 75, Boy 87], the true stress-strain relation of an AISI 1020 steel as well as the modulus of elasticity and the Poisson's ratio are given. The numerical data of the stress-strain relation of AISI 1020 steel in the *plastic* region is listed in Table 4.1. Similar information for 6061-T6 aluminum alloy is also available [Alloy 75, Ha 84].

Table 4.1: Equivalent Plastic Stress-Strain Relation of AISI 1020 Carbon Steel

Equivalent Plastic Strain	Stress (GPa)
0	248.7
0.0049	257.6
0.0083	272.6
0.0132	296.5
0.0183	323.5
0.0283	359.5
0.0383	389.4
0.0483	415.6

Since the problem defined in this research involves the large strain analysis of elastoplastic deformation, the constitutive laws have to be carefully determined. An *updated Lagrangian* type formulation is chosen for this analysis since it is more suitable for solving this type of problems [CaSt 88]. In this formulation, the total strain rate for an elastic-plastic material is separated into an elastic and a plastic part:

$$\dot{\epsilon} = \dot{\epsilon_e} + \dot{\epsilon_p}. \tag{4.1}$$

The above equation can be further manipulated, as those presented by Hutchinson [Hu 73] and Wang, et al.[WaBu 78], to account for the presence of three major nonlinearities in the problem, i.e., geometric nonlinearities (large bending effects), material nonlinearities, as present in the usual constitutive equations, and constitutive nonlinearities (large strain effects). If the large deformations are incompressible in the plastic region, which is usually the case for metal plasticity, the constitutive equation can be modified from an non-symmetric one to a symmetric one [Na. 81]. The solution for the rate equations can be transformed into incremental equations which could be solved through most of the numerical methods, such as the Newton-Raphson iteration, quasi-Newton iteration, conjugate gradient method, etc. However, the disadvantage of such a process to obtain a solution is the limited increment size due to accuracy and stability requirements. In other words, the computational time will become a burden due to the small increments of each iteration cycle.

From the investigation of the tool-work contact interaction, it is true that the plastic strain developed in the workpiece during machining is determined by the advancement of the cutting tool. When the tool moves along the tool path, it

forces the undeformed chip to deform. When the plastic strain in the workpiece reaches a critical point, chip separates from the workpiece, and it must involve the fracture at the vicinity around the tool tip [Ox 89]. As a result, the chip and workpiece should be handled separately as this occuring. A special option called *tying condition* which *ties* the nodes on the undeformed chip and those on the workpiece material is applied for this purpose. Initially, the nodes on the interface of the undeformed chip and workpiece are constrained together in all the degrees of freedom. When a certain separation condition is reached, the constraints just in front of the tool tip are released to allow the nodes on the chip side to separate from those on the workpiece side. On the other hand, when the just formed chip is *adhered* to the rake face of the tool, a new *tying condition* is applied on the tool-chip interface until the strain in the chip is beyond a certain limit, and the *tying condition* on the tool-chip interface is then released. The tool is then moved along the path with a small stepsize which is chosen to be one hundredth of the size of an element to insure the stability and accuracy of the solution.

How does one determine when the chip should separate from the workpiece, and when the chip should separate from the tool? Basically, there are two criteria to apply: the distance tolerance criterion [UsSh 82, Ko. 91], and the critical plastic strain criterion [CaSt 88]. The distance tolerance depends on the size of the element and has to be small enough such that the gap in front of the tool tip and the error on the steady-state response in the calculation are minimum. However, it is difficult to determine a suitable magnitude of the distance tolerance to satisfy the accuracy and stability requirements. In this study, the critical plastic strain criterion is, therefore, used. Based on the stress-

strain relation of the material, if the equivalent plastic strain (ϵ_{cr}) is beyond a certain value (e.g., 0.12 for AISI 1020 steel and 0.32 for 6061-T6 aluminum alloy), the material will be fractured [Boy 87]. This critical plastic strain is fixed throughout the study as the criterion to determine the chip separation condition.

4.3.3 Finite Element Solution Phase

A commercially available finite element program is used to perform the solution part of this study [MARC 91]. The program allows contact between solid bodies such as the tool-work interface in this study. The contact option that governs the contact interface prevents penetration of one body into the other as well as sliding with separation when the tool is in contact with the workpiece. The updated Lagrange formulation, as mentioned in Section 4.3.2, is also integrated as an option of the plasticity algorithms in this finite element program. The solution phase of the finite element program can be briefly divided into two steps; i.e., 1) the integration of the rate equations to the nonlinear incremental equations, and 2) the solution of the nonlinear incremental equations where a maximum number of 15 iterations are allowed to meet a given convergence criterion as described below.

To guarantee the convergence, the *nodal force equilibrium* criterion is used in this analysis. A prescribed nodal force tolerance (F_{tol}) should be a small fraction of the expected force in the solution phase. A value of 10 N is chosen as the tolerance since it is less than 0.5% of the mean values of the force generated in the solution phase. If the convergence (or the stability) of each increment is satisfied, the tool, which is treated as a rigid body in this study, is then *advanced* along the cutting direction by an amount equivalent to a preset increment size

(ΔZ) for the next computation cycle. The optimal increment size is determined by preliminary simulations of choosing different quantities between 0.01 and 0.9 times the size in the cutting direction of an element (0.2 mm in this study). It is found that when ΔZ is below 0.01 times the element size (or 0.002 mm), the stability and accuracy of the solution are well controlled (i.e., no undesirable interrupts) during the calculation. Based on the preliminary simulations, the increment size is fixed at 0.002 mm in this study.

The solution phase is stopped when the number of increments reaches a preset number. The stress/strain fields calculated from each increment can be restored as the initial conditions for further analysis if necessary. This provides the flexibility for debugging the calculation in the middle of the analysis since the result from each increment can be checked for accuracy before the next one is proceeded. It is also convenient to use the restart data file for further calculation if some problems interrupted the previous run in the middle of calculation. The special features and parameters used in this three-dimensional finite element analysis are summarized in Table 4.2.

Table 4.2: Special Features and Parameters Used in the Analysis

Special Features	Updated Lagrange Formulation, *Tying* Conditions, *Contact* Options.
F.E.M. Parameters	F_{tol}=10 N, ΔZ=0.002 mm., ϵ_{cr} = 0.32 for 6061-T6 aluminum alloy, ϵ_{cr} = 0.12 for AISI 1020 steel
Cutting Conditions	Feed Rate = 0.05 through 0.38 mm/rev., Depth of Cut=0.13 through 0.25 mm.
Tool Settings	Tool Nose Radius=0.8 mm, Rake Angle=5°, Lead Angle=−5° (for carbon steel), 45° (for aluminum).

4.4 Description of Results from Analysis

Based on the aforementioned procedure used in the finite element analysis, analysis results under different cutting conditions and workpiece materials are explained in this section. The effects of cutting conditions (feed and depth of cut as listed in Table 4.2) on the elastoplastic deformation of a machined surface are examined. Different cutting conditions for each of carbon steel and aluminum materials are applied. From the analysis, results such as deformed meshes, equivalent plastic strain (ϵ_p^{eq}) and equivalent *von Mises* stress (σ_M^{eq}) are obtained. Then a specific surface quality index, i.e., average slope of surface profile (dq), is evaluated from the deflections of nodal points on the deformed surface, and dq is used as a performance index for comparison.

Figure 4.6 shows the deformed shapes of steel being cut under one cutting condition (as indicated in the figure) at different load steps near the cutting zone. In this figure, as well as in the subsequent figures with deformed shapes, the deflections are not exaggerated. In other words, the actually calculated deflections of the chip and workpiece are represented. It is also noticed that the figure only displays a portion of the original finite element meshes since we are interested in the region near the cutting zone in the material being cut. To have a better view of the cutting zone, five *clip planes* (four sides and the bottom one) are applied to the model to *cut out* a portion of the finite element model from Fig. 4.5. The cutting tool is also excluded from Fig. 4.6 to give a clearer view of the cutting zone.

As can be seen in Figs. 4.6a to 4.6d, the deformed shapes yield a qualitative assessment of the expected physical behavior in metal cutting. For example, it

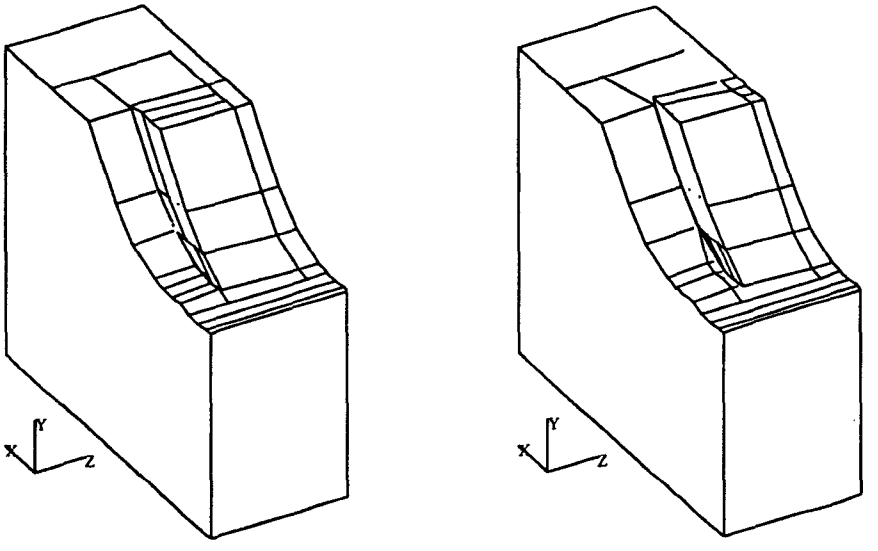

(a) Load Step = 10 (b) Load Step = 30

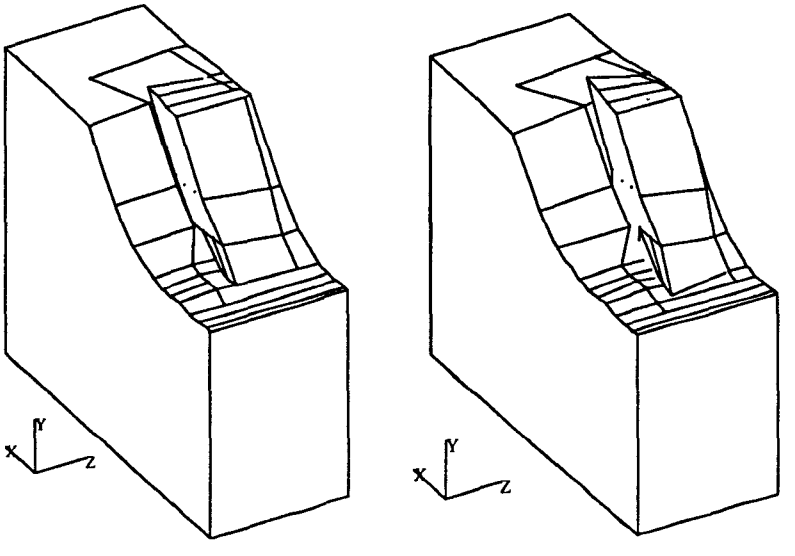

(c) Load Step = 50 (d) Load Step = 80

Figure 4.6: Deformed Shapes of Steel at Different Load Step
(Cutting Condition: feed = 0.10 mm, depth of cut = 0.25 mm)

can be seen from the time history as shown in Figs. 4.6a to 4.6d that the chip is traveling up toward the tool rake face and the shearing process is developing progressively near the tool-work interface region (e.g., the separation of the just-formed chip from the machined surface).

Iso-strain contours of the equivalent plastic strain (ϵ_p^{eq}), corresponding to the deformed shapes under different load steps are displayed in Figs. 4.7a to 4.7 d as well. Figure 4.7a is the total picture of the equivalent strain on the model under load step 30 which gives a picture of the range of plastic strain distributed in the material. This information also gives a quantitative assessment of the development of plastic strain as the tool advancing forward. Similarly, iso-stress contours of the equivalent von Mises stress (σ_M^{eq}) corresponding to the deformed shapes under different load steps are displayed in Figs. 4.8a to 4.8 d.

By finding the resultant reaction forces from the nodal points on the tool-work interface, the steady-state cutting forces in the tangential (z) and feed (x) directions can be estimated from the analysis. Moreover, from the deformed shapes, the deflections of each node on the machined surface can be calculated and compared with those deduced from the turning tests of AISI 1020 carbon steel and 6061-T6 aluminum alloy cut under the same cutting conditions as described in this finite element analysis.

Figure 4.9a displays a close-up view of a plastically deflected cross section from the machined surface of the AISI 1020 steel along the feed direction. Figure 4.9b shows the surface profile taken from the machined surface of the 6061-T6 aluminum alloy. In the same Figure, the surface profiles taken from the results of finite element analysis for both steel and aluminum alloy material under the same cutting conditions are also shown. The thinner lines represent the ideal

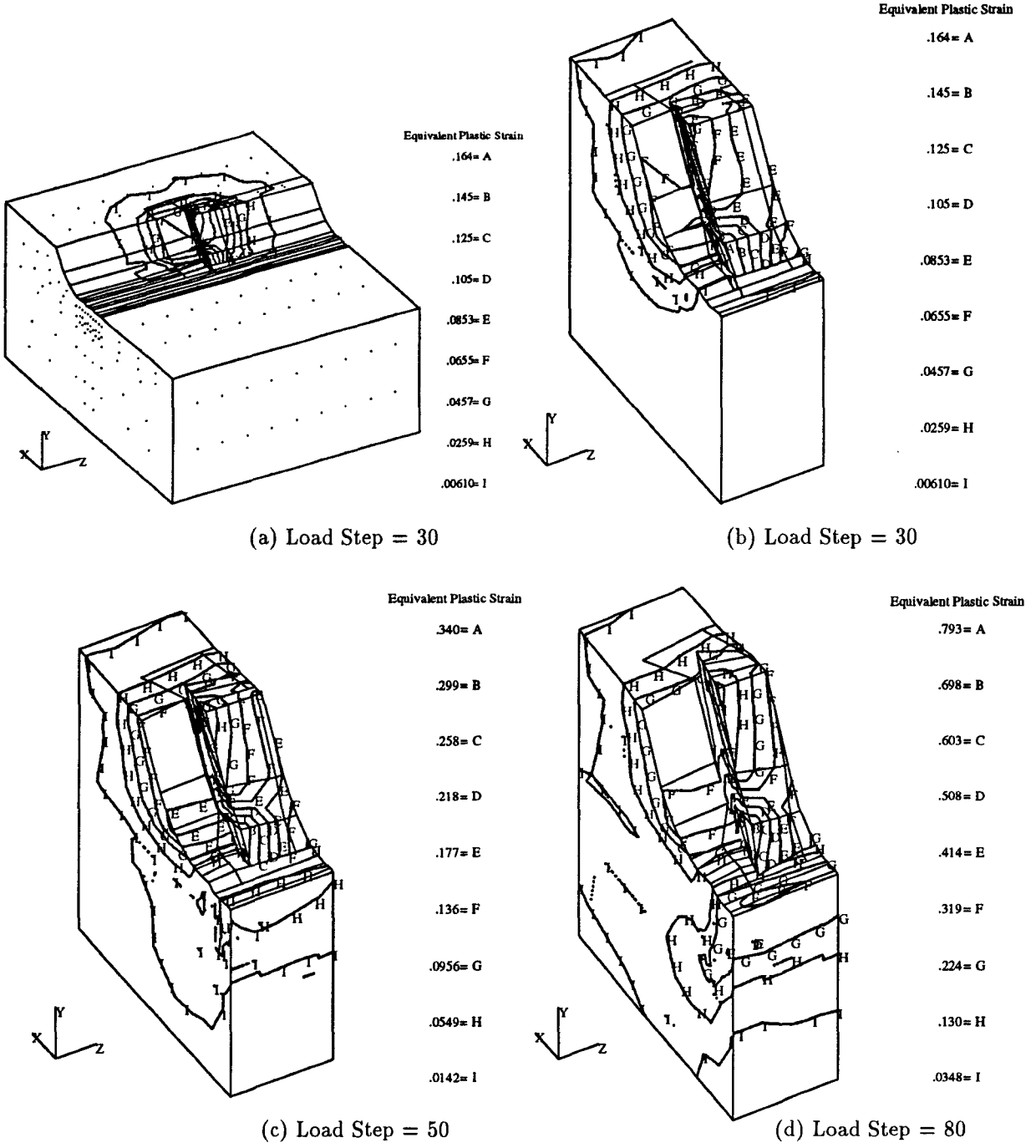

(a) Load Step = 30

(b) Load Step = 30

(c) Load Step = 50

(d) Load Step = 80

Figure 4.7: Iso-Strain Contours with Deformed Shapes of Steel at Different Load Step
(Cutting Condition: feed = 0.10 mm, depth of cut = 0.25 mm)

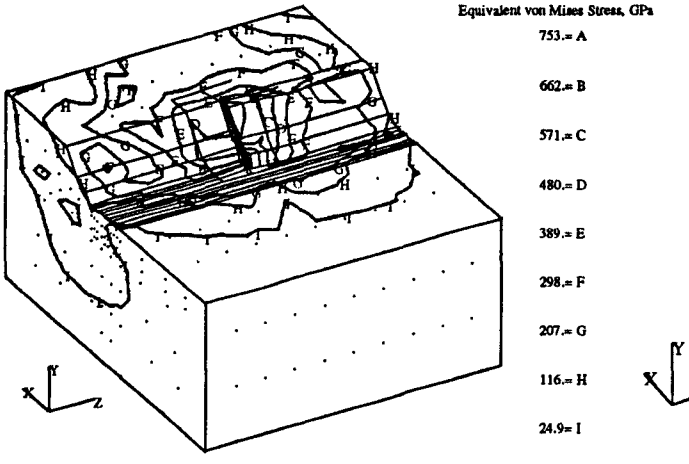

(a) Load Step = 30

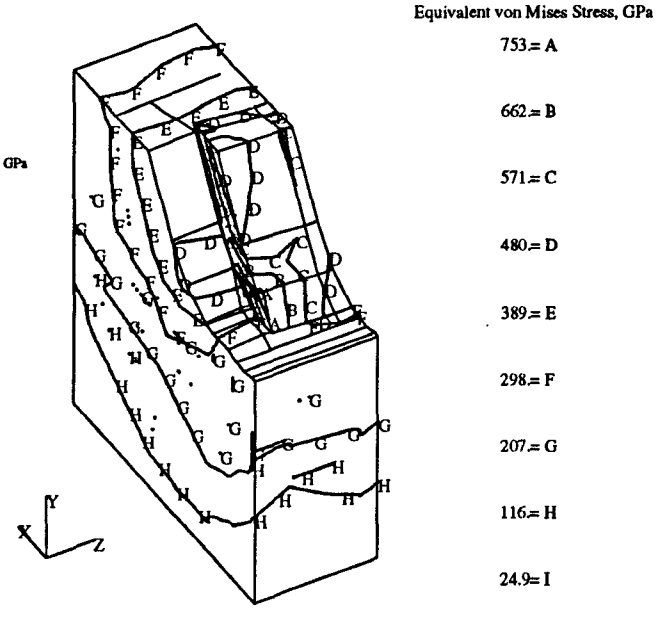

(b) Load Step = 30

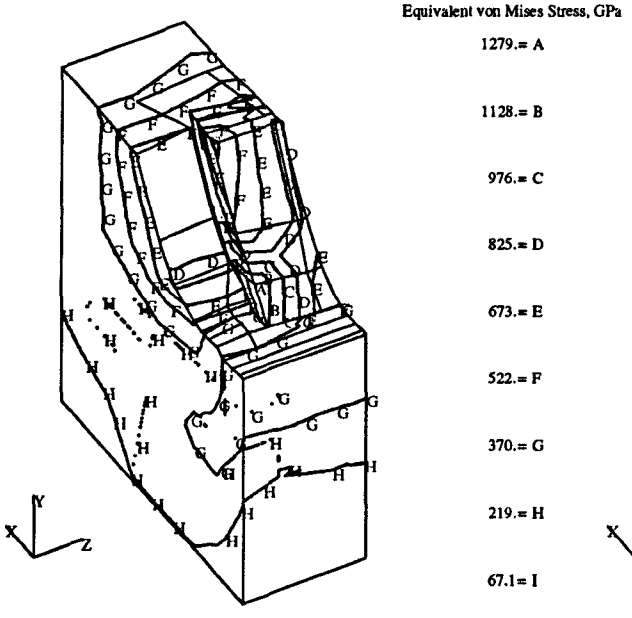

(c) Load Step = 50

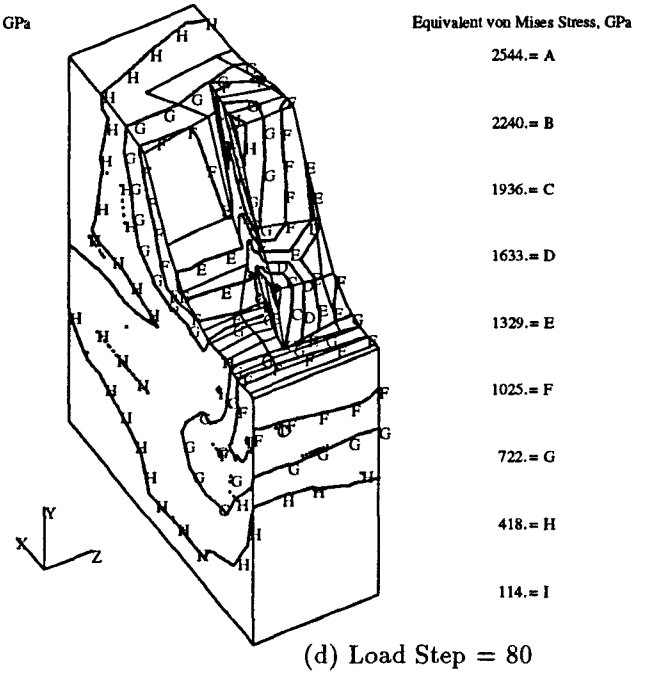

(d) Load Step = 80

Figure 4.8: Iso-Stress Contours with Deformed Shapes of Steel at Different Load Increment
(Cutting Condition: feed = 0.10 mm, depth of cut = 0.25 mm)

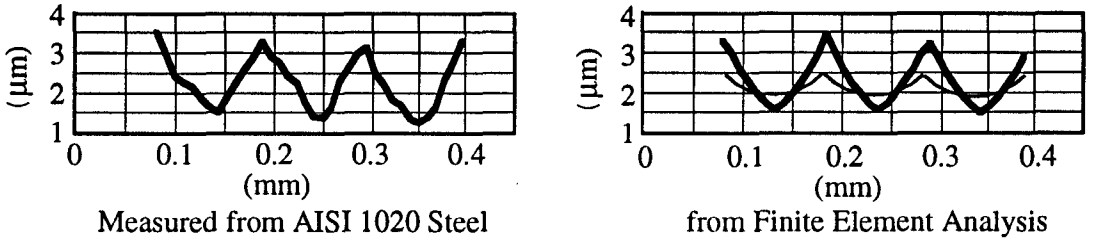

(a) Surface Profiles of AISI 1020 Carbon Steel

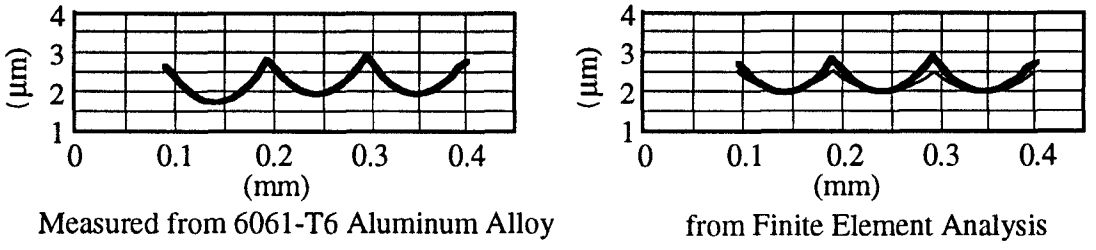

(b) Surface Profiles of 6061-T6 Aluminum Alloy

Figure 4.9: A Close-up View of the Deflections of Machined Surface Profiles (Cutting Condition: feed = 0.10 mm, depth of cut = 0.25 mm)

machined surface profile, which is just a duplicate of the cutting tool geometry, if no elastoplastic deformation and tool vibration is occurred on the machined surface. Comparisons between the deformed surface profiles from experimental results and finite element analysis will be discussed in the next section.

4.5 Experimental Verification and Discussion of Results

4.5.1 Experimental Work

A turning operation of machining an AISI 1020 steel bar and 6061-T6 aluminum alloy bar with diameter of 76 *mm* (3 *in*) and length of 102 *mm* (4 *in*) was performed to verify the developed finite element model for elastoplastic deformation observed on machined surfaces. The experimental procedure is similar to what was discussed in Section 3.5.1. The machine tool used is a CNC lathe, and the tool inserts are tungsten carbide inserts.

It is important, however, that the tool vibration, tool wear and built-up edges, which can alter the machined surface significantly, should be carefully controlled to their minimum levels such that the surface finish due to elastoplastic deformation process during machining tests can be identified and compared with those from the finite element analysis.

As mentioned in Section 2.3.2, the effect due to built-up edges can be reduced by high cutting speed. In this study, we choose the spindle speed in the range between 1500 to 1900 *rpm* (360 - 450 surface meter per minute) which is high enough for preventing the built-up edges from occurring on both the steel and

aluminum alloy [Shaw 84]. On the other hand, the effect on surface finish due to tool wear can be prevented if each test performed lasts for a very limited time duration. In this study, each cutting test only cuts less than ten seconds and new tool insert is used for each material type.

As for the effect due to tool vibration, it is obvious that the length to diameter ratio of the workpiece ($4/3 = 1.33$) in this test can provide a very high stiffness between the workpiece and tool during machining. As a result, the vibration during cutting can be reduced significantly compared with those have higher length to diameter ratios. However, the random tool vibration due to material properties as discussed in Chapter 3 can never be suppressed in the cutting tests.

To solve this problem, we use a specific surface index, called root mean squared slope or average slope (dq defined in Section 2.2), which is least sensitive to the tool vibration and most sensitive to the effect of elastoplastic deformation on machined surfaces, to characterize the average slopes of surface profiles [Sa 63, Wh. 74]. Usually, the surface quality indices such as the surface roughness average, root mean squared value and peak-to-valley value, are used for characterizing an engineering surface. These indices are directly related to the tool vibration. In other words, the stronger the tool vibratory motion during machining, the rougher the surface finish and higher the values of these indices will be. Therefore, dq will be used as the surface quality index for comparing the results from turning tests and finite element analysis in the following sections.

4.5.2 Effects of Feed Rate, Depth of Cut and Workpiece Material

Feed Rate Effect

Four different feed rates (0.05, 0.1, 0.25 and 0.38 mm/rev) are used in the machining tests. Same cutting conditions (depth of cut is fixed at 0.22 mm/rev and spindle speed is 1500 rpm) are then applied to the finite element model and analyzed for each feed rate.

Similar to Figure 4.9, the deformed profiles along the feed direction taken from the cutting zone of the finite element model under different feed rates can be evaluated. Moreover, the deflections in the x and y directions of each node are also available from the results of finite element analysis. Based on these deflections, the new coordinates of the nodes on the deformed surface profile and, thus, the average slope of the deformed surface profile can be calculated.

The average slopes of surface profiles (dq) evaluated from the finite element analyses under four feed rates are then compared with those obtained from machining tests. The dq's of both the ideal and deformed surface profiles are calculated based on Eq. 2.3 and plotted against the dq's measured from the machined surfaces as shown in Fig. 4.10a for AISI 1020 carbon steel and Fig. 4.10b for 6061-T6 aluminum alloy.

The figure shows that the ideal dq linearly increases with the feed rate. It also shows that the dq's measured from machined surfaces possess a similar trend as the feed rate increases. However, there is a big gap in the actual values between the measured and ideal ones. The cause of this gap is mainly from the elastoplastic deformation process occurred on the machined surface during

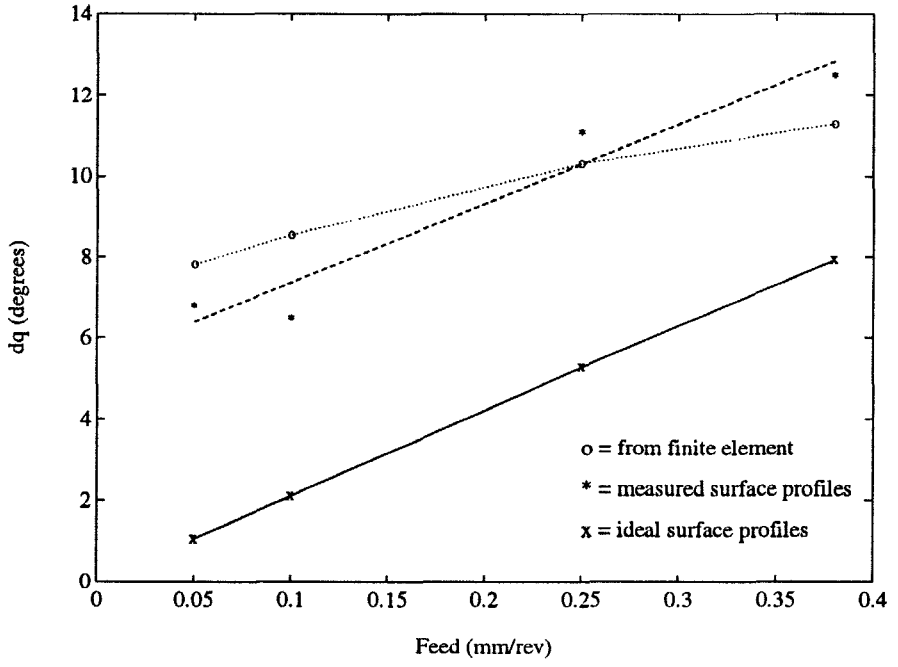

(a) from AISI 1020 Carbon Steel

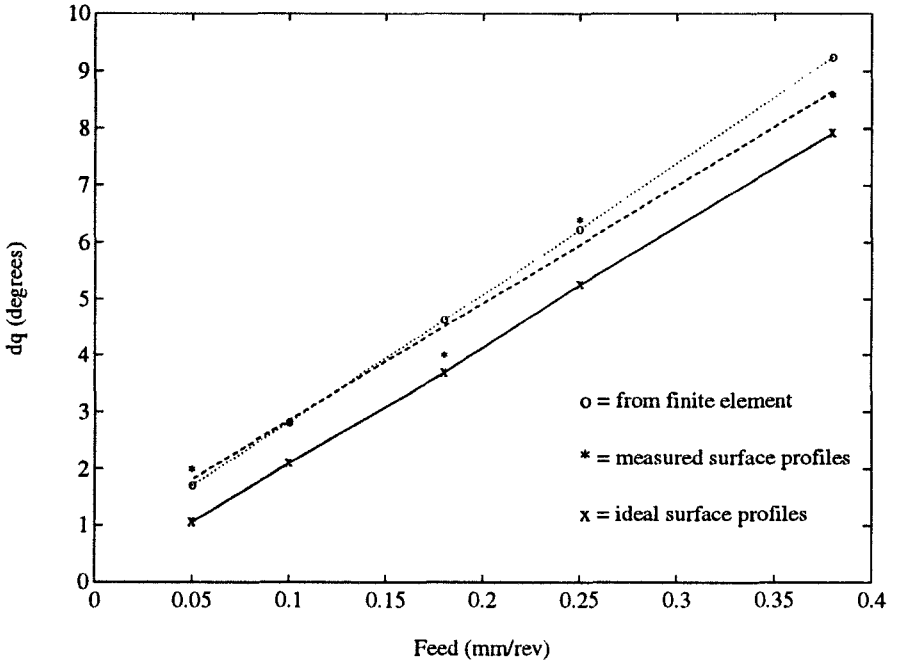

(b) from 6061-T6 Aluminum Alloy

Figure 4.10: Effect of Feed Rate Change on the Average Slopes (dq) of Machined Surfaces

cutting. As shown in the same figure, the estimated dq's from the finite element analyses well match with those measured ones. This indicates that the validity of the finite element analysis applied in this study is very promising.

Depth of Cut Effect

Comparisons are also made for four different depth of cuts (0.13, 0.15, 0.20 and 0.25 mm). Turning tests are carried out under the four depth of cuts. Same cutting conditions (feed rate is fixed at 0.1 mm/rev and spindle speed is 1900 rpm) are applied to the finite element model and analyzed for each depth of cut. Similar to what was discussed for feed rate effect, the average slopes of surface profiles (dq) under four depth of cuts can be evaluated from the results of the finite element analyses. Figure 4.11 shows the ideal average slopes (a constant), the measured average slopes, and the estimated average slopes from the finite element analyses under four depth of cuts for both AISI 1020 carbon steel and 6061-T6 aluminum alloy.

This figure shows that when the depth of cut increases, the average slopes of machined surface profiles reduce, which is opposite to what was observed from the effect of varying the feed rate. This can be explained by the fact that when the depth of cut increases, the cutting force increases more dramatically than that of the increase due to the feed rate change. As a result, the stress and strain distributed on the tool-work interface tend to be so high that most of the material particles under it will sustain the plastical deformation and make the machined surface profile closer to the tool geometrical shape (or the ideal surface profile).

Again, the estimated dq's from the results of finite element analyses match

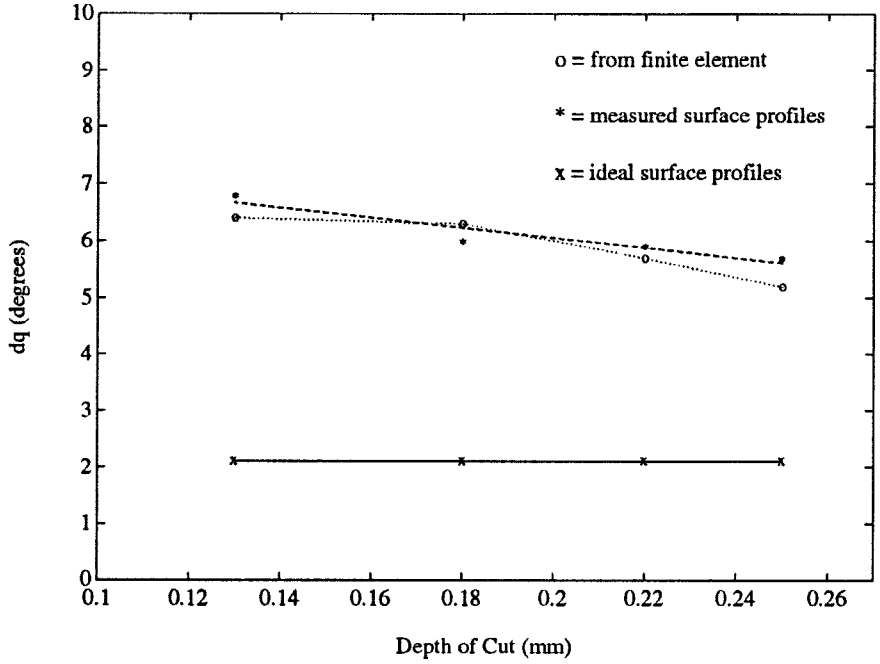

(a) from AISI 1020 Carbon Steel

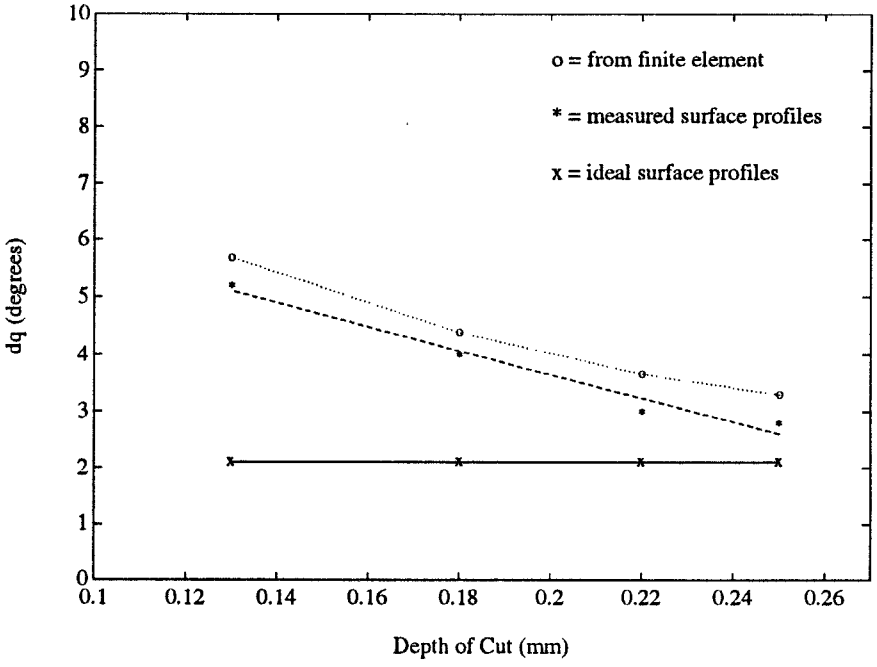

(b) from 6061-T6 Aluminum Alloy

Figure 4.11: Effect of Depth of Cut on the Average Slopes (dq) of Machined Surfaces

well with the measured ones as can be seen in the figure. This suggests that the finite element model as well as the analysis approach in this study is necessary to predict the elastoplastic deformation and recovery processes in metal cutting. The predicted average slopes, dq's, are important for the tribological performance of mating parts with relative motions such as bearings, shafts, cylinder bores, brakes, etc... [StDa 84].

Effect of Workpiece Material

As can be seen from Figs. 4.10 and 4.11, the average slopes of machined surface profiles from both the carbon steel and aluminum alloy are higher than those from the ideal surface profiles. From the same figures, it is also evident that the average slopes of machined surfaces from carbon steel are always higher than those from aluminum alloy. For example, the difference between the measured dq's on steel and those from ideal surface profiles is about five degrees. The difference between those from aluminum alloy and ideal surface profiles is only about one degree.

It can be explained by the properties of different materials. Suppose material A (e.g., carbon steel) possesses higher yield strength and Young's modulus (E) than those of material B (e.g., aluminum alloy) as shown in Fig. 4.12. When the stress exerted by cutting tool in material A reaches the plastic region and is released after the tool moving away, the remaining strain (permanent set) on the machined surface is $d\epsilon_a$. If the material being cut is material B, the remaining strain on the machined surface will become $d\epsilon_b$, which is larger than $d\epsilon_a$. This suggests that the elements in material A *recovers* more from the plastically deformed state than those from material B. As a result, the machined

surface profiles of material A will sustain less geometric shape of the cutting tool. This can also be verified by looking at the profiles in Fig. 4.9a in which the *spring-back* of the profile is more prominent than that in Fig. 4.9b. From the observation, it can be asserted that the elastoplastic deformation process is more prominent on higher strength materials such as carbon steel than that of lower strength materials such as aluminum alloy.

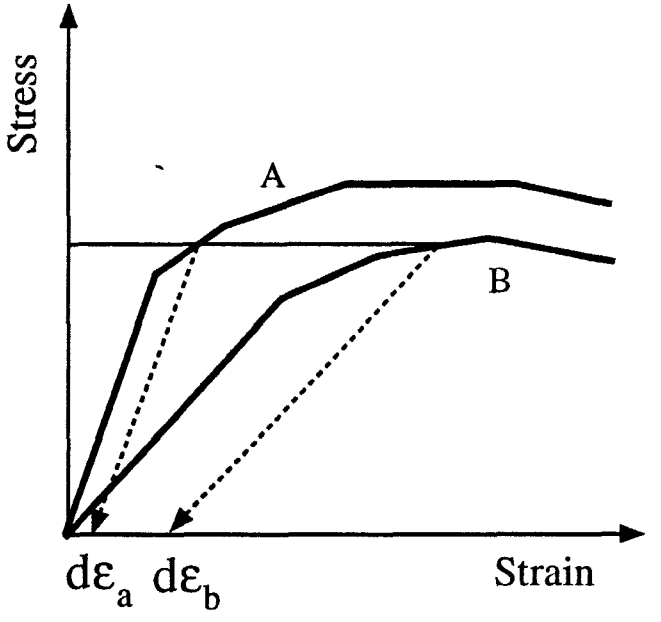

Figure 4.12: Example of Elastoplastic Deformation and Recovery Processes

4.5.3 Development of a Surface Texture Modification Model

As mentioned in the beginning of this Chapter, the results from this finite element analysis can be applied as a surface texture modification model to enhance the accuracy of the prediction on machined surface quality. However, the need for this modification depends on the material being cut as discussed

in the previous section. If the material is low in strength (or soft), such as the aluminum alloy used in this study or brass, the surface texture variation due to the elastoplastic deformation process can be neglected.

To develop such a surface texture modification model, the idea is to use the deflections of surface profiles calculated from the results of the finite element analyses for different cutting conditions. For example, given different cutting parameter settings, but with a same cutting tool with no tool wear and built-up edges (if high cutting speed is used), one can use the finite element models in this study to find the elastically-plastically deformed points along the cutting edge. The estimated deflections on these points can be presented as functions of the cutting parameters (feed rate and depth of cut). As demonstrated in the previous sections, the variation of dq's can be linearly related to the feed rate change or the depth of cut change. Similarly, the functional relations between the deflections on each nodal points along the cutting tool edge and the cutting parameters can be found.

One such example is shown in Fig. 4.13. The measured surface profile is taken from a machined AISI 1020 steel bar under the same cutting condition as those in Fig. 4.9. The simulated profile is from a computer-aided surface texture simulator, which is discussed in the next chapter. The modified profile is based on the results from the finite element analysis discussed in this chapter. By comparing the three dq values, the measured one (6.5°) and the modified one (6.9°) are very close to each other, while the simulated one (2.7°) is far below the measured one. This example shows that the improvement on dq prediction after the surface texture modification is about 65%. Other cutting conditions are also examined after the modification, and the average improvement on the

dq prediction is more than 50%. This gives a strong indication that the finite element analysis is a very promising tool for enhancing the accuracy of the computer simulator which can never predict the effect of elastoplastic deformation observed on the machined surfaces.

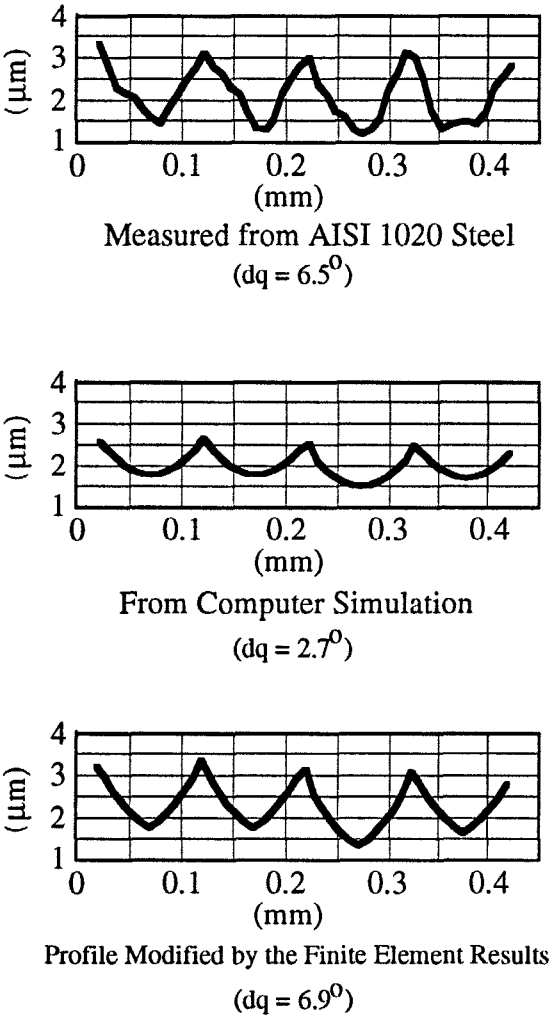

Figure 4.13: dq's from the Measured, Simulated, and Modified Surface Profiles

4.6 Summary

In this study, an updated Lagrange approach based on a three-dimensional finite element model is used for analyzing the elastoplastic deformation processes observed on machined surfaces. The emphasis is on simulating a single-point cutting process, in particular, on the modeling approach and the effects of cutting parameters (feed rate, depth of cut, and material property) on the elastoplastic deformation process associated with machining.

The obtained results are in reasonable quantitative agreement with the experimental results when the average slopes of surface profiles (dq's) are compared. It has been shown that the dq's have linear relations with the feed rate as well as the depth of cut (with opposite trends). On the other hand, soft materials (such as aluminum alloy or brass) tend to have less effect of plastic recovery on machined surfaces; thus, the average slopes are smaller and closer to the ideal ones as opposed to the hard materials (such as carbon steel). This phenomenon is also observed from the results of finite element analysis. This enlightens the necessity of applying the results from the finite element analysis as a surface texture modification model. This modification can enhance the accuracy of a surface texture simulator by 50% on predicting the average slopes of machined steel, an important index for tribological performance of mating parts.

The developed finite element model can be extended to account for more complex metal cutting behavior, such as frictions between tool-work or tool-chip interface under low cutting speed, effect of built-up edges or tool wear phenomenon. It could also be applied to the study of machining of non-metallic materials such as advanced ceramics.

Chapter 5

Development of a Computer-Based Surface Topography Simulator

5.1 Introduction

The surface characteristics of machined parts have been recognized as important factors of the quality control in production. Consistent fine finish surfaces not only provide customer satisfaction but also assure the functionality and reliability of the product.

Traditional manufacturing techniques have often been based on a one-person, one-process, one-machine system. The same operator not only generates a specific part but is also responsible for the control of the process. This includes the required changes to the process as caused by tool wear, machine conditions and material composition. The operator is also required to be responsive to changes in dimension and tolerance dictated by a design engineer.

Problems may arise when a part (or design changes) is designed by a design engineer. For example, what is the tolerance he/she could use such that a) it

is tight enough to guarantee the part is functional, and b) the part is manufacturable? As for a production engineer (or machine tool operator), he/she may ask what machining parameters should be chosen such that a) the dimensional and tolerance requirement can be achieved, and b) the surface quality is optimum. All of these problems become serious as the demand for a shortened product cycle time, reduced waste, and a consistent, high level of quality has increased in recent years to keep pace with the marketplace competition. It also has become more evident when new advances in machining processes, such as untended *cell* type machine centers, are introduced to the manufacturing industry or new advanced materials (such as advanced ceramics) are to be used.

How does one design and make a product in such a complex, automated environment? People from both parties may agree on one thing; i.e., they need a reliable tool that can provide the information for assessing the process capability and finish quality even before the part is designed. Hence, there is a pressing need to develop such a system for both design engineers and production engineers.

The main topic discussed in this chapter is the design of a computer software package which can serve as a tool for assessing the process capability and surface quality of machining processes. By integrating material science, machining science and metrology science, a framework which provides a systematic approach to simulate the surface irregularity formed during machining is proposed. The framework combines a) the analytical work discussed in previous chapters which includes the stochastic modeling of random excitation source (material nonhomogeneity) and the elastoplastic deformation process observed on machined surfaces, and b) the results from machining different materials which provide necessary information of parameters used in the software. The validity

of this computer-aided surface topography simulator is verified by comparing the predicted surface quality indices from the simulator and those from experimental tests.

5.2 Basic Methodology

5.2.1 Framework Structure

The framework structure of the surface topography simulator, as closely related to the analytical work presented in Chapters 3 and 4, is listed below:

1. Study the microstructure of workpiece material to be machined. This will provide a quantitative estimation of the variation levels of the basic material properties relevant to machining (such as microhardness). As presented in Chapter 3, the stochastic model (Markov chain model) can be applied to characterize the microhardness variation pattern along a specific direction in the workpiece material.

2. Find a mapping function between the microhardness variation information and the tool vibratory motion in the machining process. This requires a mathematical model which can link the material variability as a random excitation source to the machine tool structural dynamics [Zh 86]. As a result, the tool tip's dynamic response (both deterministic and stochastic) can be evaluated for the machining of a specific type of workpiece material under different cutting conditions.

3. Generate the surface topography through the dynamic response of the cutting tool. Based on the evaluated tool tip positions, tool geometry,

and cutting parameter settings, the machined surface topography can be formed as a concatenation of each tool profile segment according to the time sequence. This simulated surface topography persists a portion of the irregularities observed on a real machined surface.

4. Analyze the elastoplastic deformation and recovery processes observed on machined surfaces. Through this analysis, a systematic approach to estimate the non-linearly deformed elements on the machined workpiece under different cutting conditions can be made. This information is especially important for higher strength materials as asserted in Chapter 4. The estimated elastoplastic deformation on machined surfaces under different cutting conditions and different materials are then stored as a database. This database provides the information for modifying the predicted surface topography from 3. The simulated surface profiles are then modified based on the said database.

5. Characterize the simulated surface quality. Here we calculate the characteristic indices of the simulated surface; e.g., R_a, R_q, R_t, and dq. Furthermore, the dimensional quality indices such as the roundness, straightness, and cylindricity of the machined part can also be calculated based on the simulated surface topography and statistical methods [ZhHw 90b].

Based on the above framework structure, a block diagram consisting of six modules is shown in Fig. 5.1 to depict the framework structure, and a computer-based surface texture simulator which synthesizes the factors contributing to the generation of surface texture during machining is developed. This simulator, if combined with its generated data base, can serve as a unique resource as a tool

for assessing process capability and assuring surface quality.

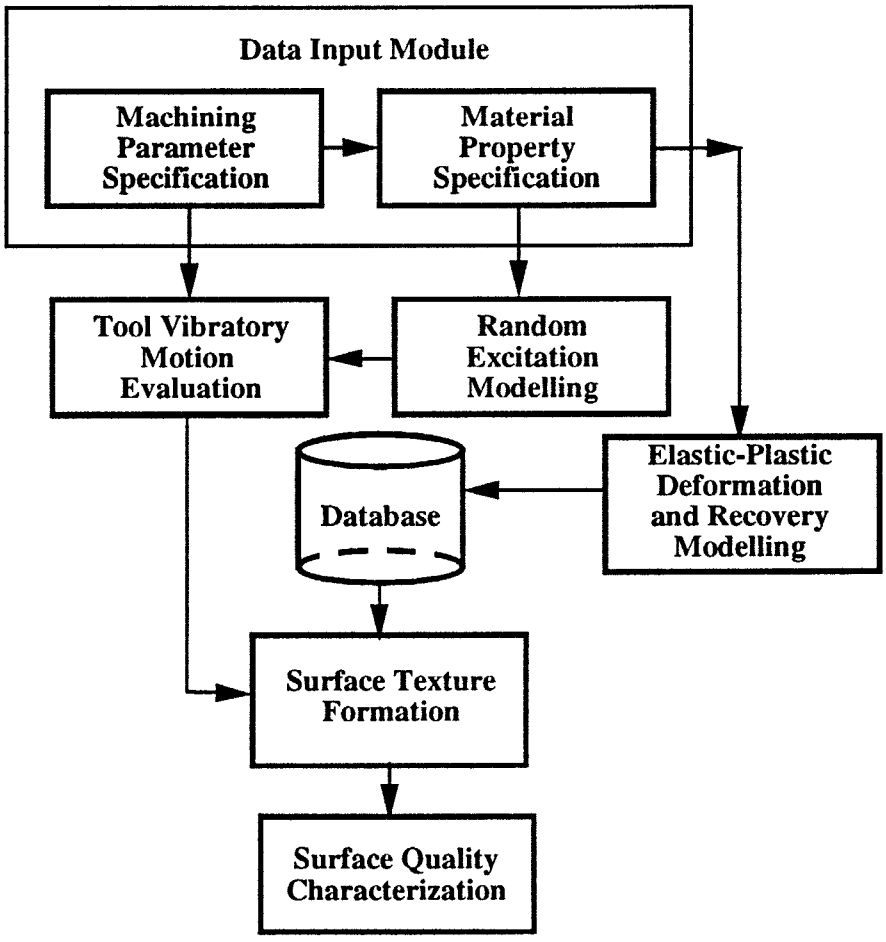

Figure 5.1: Framework Structure of the Simulator

5.2.2 Development of the Simulator

Each module in Fig. 5.1 is explained in this section.

Data Input Module

Based on the framework structure, information, such as the cutting parameters (feed, depth of cut, cutting speed), tool geometry specifications (tool

nose radius, rake angle, lead angle), machine tool dynamic system parameters (equivalent damping, mass, stiffness), workpiece material related parameters (microstructures, unit cutting force), and product dimensional specifications (e.g., initial diameter and cutting length of a bar as in turning), is necessary for the simulator. Table 5.1 lists the parameters required by the simulator.

Table 5.1: List of Required (Major) Inputs for the Computer-Based Simulator

Description	Units	Default Ranges
Machining Parameters:		
Feed (f)	mm/rev	$0 \sim 1.0$
Depth of Cut ($dcut$)	mm	$0 \sim 1.5$
Spindle Speed ($mrpm$)	rpm	$100 \sim 3500$
Tool Geometry:		
Tool Nose Radius (t_r or R)	mm	$0 \sim 10.0$
Rake Angle (α_r)	degrees	$-10.0° \sim 10.0°$
Lead Angle (C_s)	degrees	$-10.0° \sim 75.0°$
Machine Tool Dynamic Model:		
Equivalent Mass (M)	kg	$0.05 \sim 10.0$
Equivalent Damping Coefficient (ξ)	none	$0 \sim 0.1$
Equivalent Primary Stiffness 1 (K_1)	N/m	in the order of 10^7
Equivalent Primary Stiffness 2 (K_2)	N/m	in the order of 10^7
Workpiece Material Related Parameters:		
Unit Cutting Force (K_s)	N/m^2	from [Kr 66]
Hardness Index ($hindex$)	none	from [Kr 66]
Diameter of a Feature ($diam$)	mm	$100.0 \sim 400.0$

Some of the parameters needed for the simulator which are not listed in the table are derived from the input data. For example, the calculation of *overlapping factors* (μ, for regenerative feedback loop [Zh 86]) is based on the cutting tool geometry and cutting parameter settings (feed, depth of cut). Computer subroutines are developed for such special calculations.

Random Excitation Modeling Module

This module applies the stochastic approach mentioned in Chapter 3 to quantitatively characterize the microhardness variation through a Markov chain model if a specific trend of microstructural distribution exists. If such a trend does not exist, a *sample variance model* [ZhKa 90] is applied instead of the Markov chain model.

Based on the idea discussed in Chapter 3, steps for the Markov chain modeling of the microhardness distribution can be outlined as follows:

1. Input the cutting parameters (feed, depth of cut, and speed) and binary image file(s) (a matrix of 0's and 1's) of the workpiece material taken from its samples (see Appendix B). Set the number of states, N.

2. Divide the image data (a matrix of 0's and 1's) into subdivisions based on the cutting parameter settings. Calculate the following parameters:

   (a) *state ratio*, r_{kl}, of each subdivision based on Eq. 3.8,

   (b) statistics of possible *group distributions* (μ_{g_j}, σ_{g_j}, and p_{g_j}) if they appeared to be statistically different from each other, and

   (c) state boundaries of each *group distribution.*

3. Estimate the probability transition matrix, $[p]$, based on the *state ratio* (r_{kl}) of each subdivision and those equations discussed in Chapter 3.

4. Assign the group distributions to each cutting cycle based on the probability of each group distribution (p_{g_j}).

5. Assign random hardness values for each of the *sample blocks* in the *first* cutting cycle according to the mean and standard deviation of the associated group distribution.

6. Determine the corresponding *state* of each sample block in the first cycle by checking its assigned microhardness value against the state boundaries in this cutting cycle.

7. Assign the *state* of each sample block in the next cutting cycle along the direction of microstructural distribution (it's in the feed direction under turning process) by applying the transition probabilities ($[p]$ matrix).

8. Determine the microhardness value of each sample block in this cutting cycle based on its assigned *state* which is governed by the group distribution in this cycle. Care should be taken such that the microhardness values determined in this cutting cycle should have the same (or close to the) mean value and standard deviation as those of the group distribution in this cycle.

9. Repeat steps 7 and 8 until the required cutting cycles are reached.

10. Store the microhardness values in all the sample blocks of the workpiece material to be machined as a matrix data file. This file will be used as the random excitation source to evaluate the dynamic response of the cutting tool which is discussed next.

Tool Vibration Evaluation Module

In this module, the tool deterministic motion as well as the random motion will be evaluated. The random excitation source stored as a matrix of microhardness values are read as the input to the tool structural dynamic system. The interaction between the cutting dynamics (or the cutting force generated during machining) and microhardness variation can be linked by a nonlinear relation

$$F = K_s A_c \left[\frac{\mu_i}{\overline{\mu}}\right]^{hindex} \tag{5.1}$$

where K_s is the unit cutting force, A_c is the cutting area (a product of feed and depth of cut), μ_i is the averaged microhardness value of a sample block under cutting, $\overline{\mu}$ is the mean hardness value of the workpiece material, and the exponent *hindex* presents the nonlinear relation between the instantaneous cutting force (F) and the ratio $\mu_i/\overline{\mu}$. The details about cutting dynamics in machining can be found in Appendix C [ZhKa 90, ZhHw 90a]).

On the other hand, a two-degree of freedom, lumped mass-spring-damper mechanistic model as depicted in Fig. 5.2a is used to simulate the machine tool structure [El. 83, Ni 85, Zh 86]. The well known *Merritt* block diagram as shown in Fig. 5.2b explicitly illustrates the interaction between the cutting mechanism and the structural dynamics of the machine tool. The input to the cutting mechanism consists of the chip load and the output is the cutting force. In the mean time, the cutting force serves as the input to the structural dynamics of the machine tool for which the tool vibratory motion is the output. This vibratory motion in turn changes the chip load through the primary and regenerative feedback paths. A symbol of three group distributions in Fig. 5.2b represents

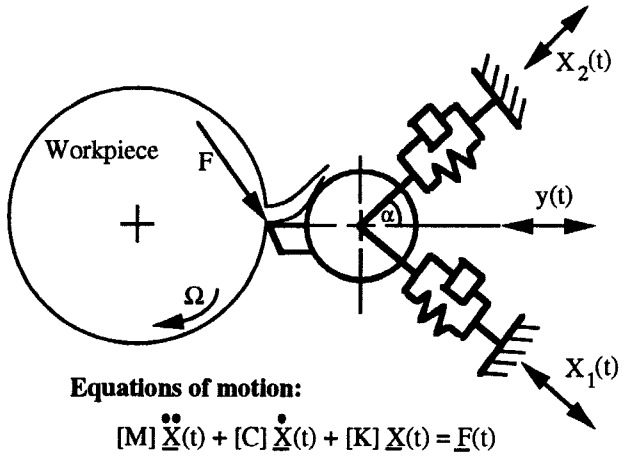

(a) Dynamic Model of Machining Process

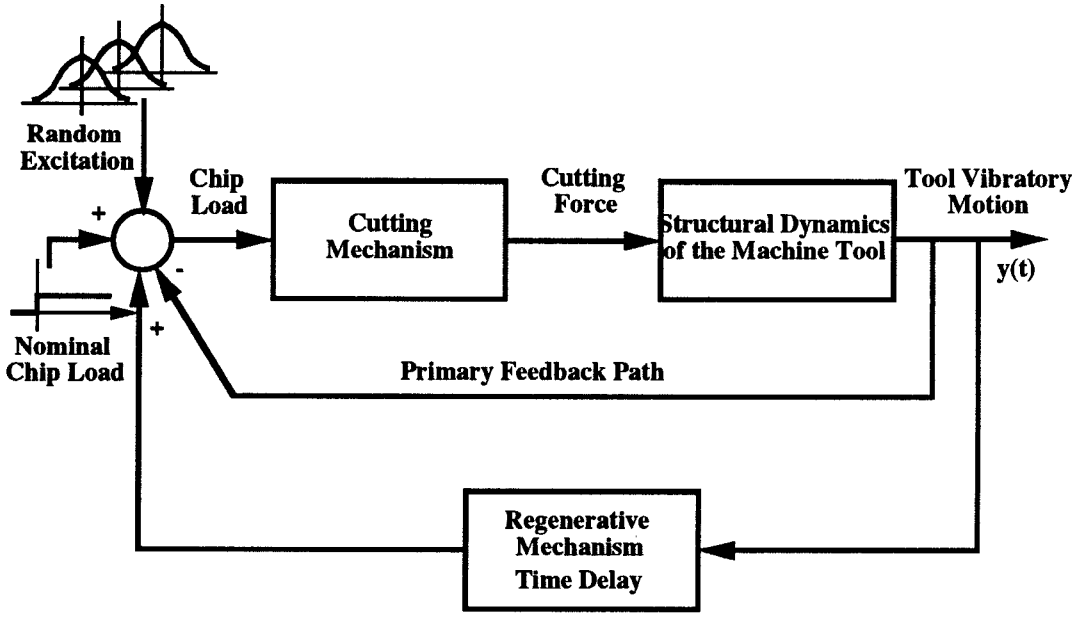

(b) Merritt Block Diagram Representing the Machining System

Figure 5.2: Dynamic Model and Merritt Block Diagram for Machining Process

the random excitation source to the cutting force evaluation through the cutting dynamics in microscale.

Surface Topography Formation Module

The mechanism to form the surface texture during machining is to trace how the tool removes the material from the workpiece instantaneously. The evaluation of the tool vibratory motion provides an instant deviation of the tool motion away from its ideal, or undisturbed, tool path determined by the tool kinematic motion during machining. This makes it possible to identify the relative position between the workpiece and the tool at a given location on the machined surface. Regarding the turning operation, the surface texture formed during machining should be examined along both the circumferential and the axial directions of the workpiece.

Figure 5.3 presents an intuitive view to explain how the surface texture is formed on the workpiece circumference. The three points marked as A, B, and C represent the three cutting locations on the cutting edge of the tool. From the viewpoint of kinematics, points A, B, and C have an identical path trajectory, which is the tool vibratory motion about the ideal tool path indicated by the dashed straight line shown in Fig. 5.3.

Consequently, the geometry of the surface texture formed on the circumference at a given instant should be a copy of the outline of the tool at a specific location. The surface texture along the axial direction of the workpiece, or the surface profile, is formed by a series of adjacent outlines of the cutting tool, as shown in Fig. 5.4. A pair of two neighboring tool outlines represents two specific tool positions during machining, which are separated by a time interval equal

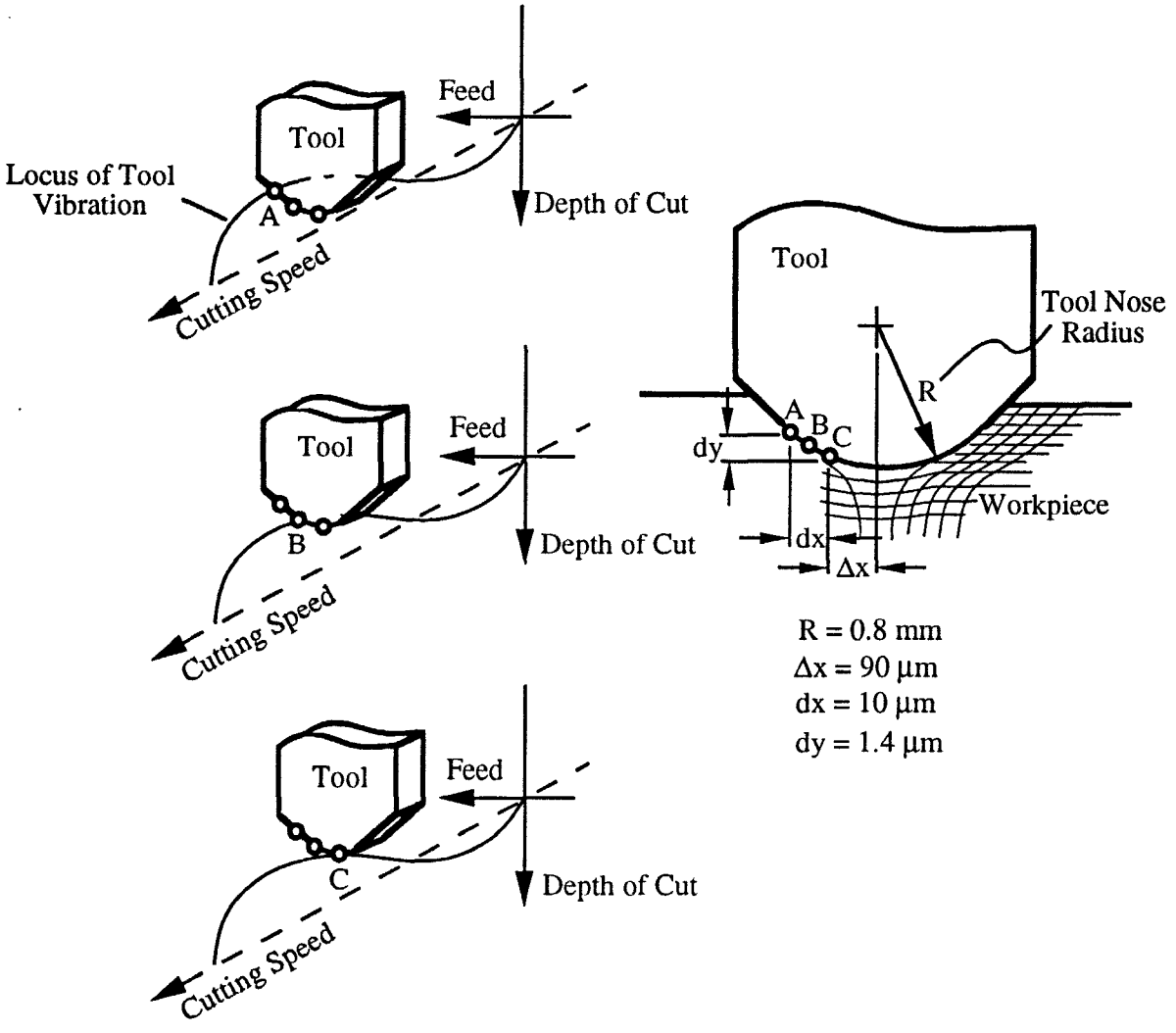

Figure 5.3: Intuitive View of Surface Texture Formed during Machining

to the time needed for one revolution of the workpiece during machining. As a result, the surface texture formed during machining can be visualized as a dynamic process, in which the outlines of the cutting tool are concatenated on the workpiece circumference, and at the same time, each outline of the cutting tool links to that of the previous revolution, so as to form a surface profile in the axial direction. The deviation of the tool position from the ideal tool path results in the variation of the heights of the tool outline both on the circumference and along the axial direction of the workpiece.

To uniquely determine the surface texture formed during machining, it is necessary to know the coordinates of each of the individual points for a given surface profile, such as the one shown in Fig. 5.4. By examining the geometrical constraints indicated in Fig. 5.4, the coordinates of the intersection point between a pair of the two neighboring outlines can be calculated based on the following two equations.

$$\left.\begin{aligned} (x_k - C_{x_k})^2 &+ (y_k - C_{y_k})^2 = R^2 \\ (x_k - C_{x_{k+1}})^2 &+ (y_k - C_{y_{k+1}})^2 = R^2 \end{aligned}\right\}, \text{ for } k = 1, 2, ..., (n_f - 1) \qquad (5.2)$$

where

x_k, y_k = coordinates of the k^{th} intersection point,

C_{x_k}, C_{y_k} = coordinates of the k^{th} tool center position,

R = tool nose radius, and

n_f = number of feeds (or revolutions) under consideration.

The coordinates of the other points on the surface profile can be determined

by referring to the coordinates of the relevant intersection points. For example, the coordinates of point D in Fig. 5.4, which is next to the intersection point C, can be written in $x_k + \Delta x$ and $y_k + \Delta y$ where Δx and Δy are constrained by Eq. 5.2 because point D is located on the circle. A surface profile can be uniquely visualized in a two dimensional space when the coordinates of all the points are known. Note that the two dimensions are related to the directions of feed and depth of cut.

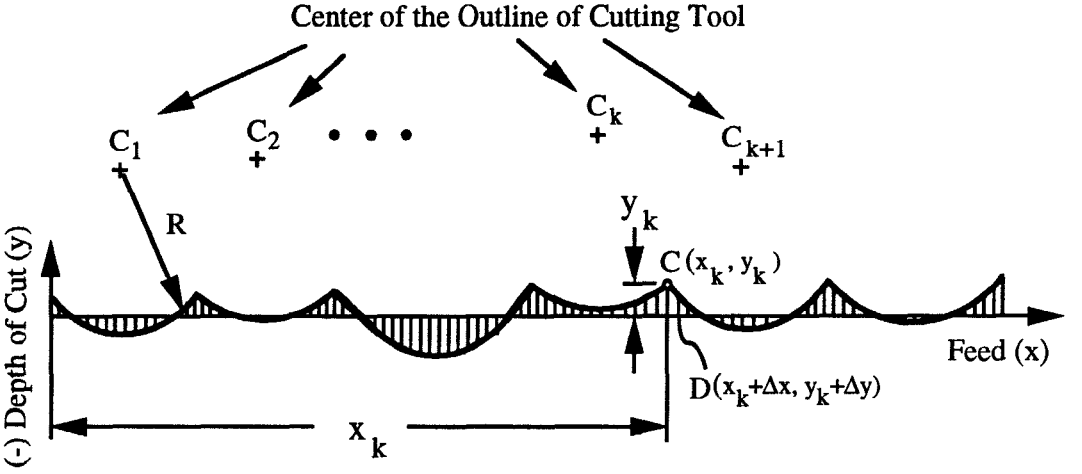

Figure 5.4: Formation of Surface Profile along Feed Direction

The above method to identify the surface profile in a two-dimensional space forms the basis for the three-dimensional surface topography generation. By constructing the two dimensional surface profiles formed at different time instants during machining and by linking and ordering them in time, the framework is capable of displaying the dynamic formation of the surface texture by the machining process.

Elastoplastic Deformation and Recovery Modeling Module

As mentioned in Chapter 4, a series of analyses are needed to take different cutting conditions and materials into consideration. The results of these analyses are able to provide the information for modeling the surface texture deformation and recovery process during machining.

To develop such a model, following steps are required after the finite element analyses:

1. Extract the deformations of the nodal points on the finite element model which forms the machined surface.

2. Apply the least square curve fitting, the relation between the deformations of each node and different cutting conditions can be obtained as a quadratic function. For example, Fig. 5.5 shows the deformation in the y direction as a function of the feed rate change. A bunch of such curves can be found under different cutting conditions for deformations of each node in both the x and y directions.

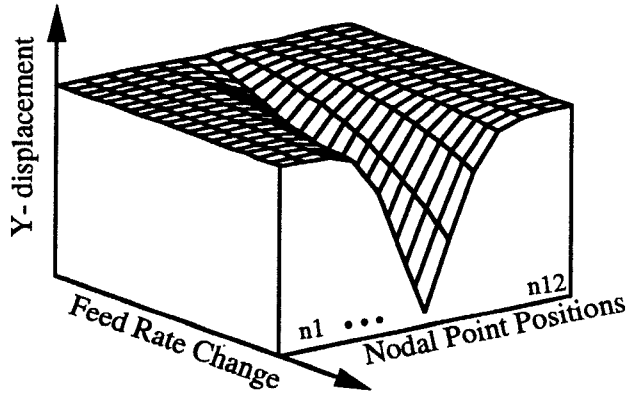

Figure 5.5: Deformation of Nodes as a Function of Feed Rate Change

3. Store the coefficients of each quadratic function as a database. This database can be used as the required elastoplastic deformation and recovery model.

4. Apply this model to modify the simulated surface from the surface texture formation module based on the cutting conditions.

Surface Quality Characterization Module

This module calculates the quality indices of a simulated surface, such as the R_a, R_q, R_t, and dq as defined in Chapter 2. Furthermore, this module applies the statistical metrological method to assess the dimensional quality indices such as the roundness, straightness, and cylindricity from the simulated surface topographies. Reference [ZhHw 90b] explains the methodology used for the calculation of the geometric dimensions and tolerances.

The uniqueness of this simulator in quantifying the natural variations associated with dimensions and geometric tolerances can help the design engineer to properly select tolerances, effectively pushing the quality control upstream into the design stage. This capability can further support the decision-making process of selecting cutting parameters, such as feed, depth of cut, and cutting speed. Such a capability meets the increasing demand in machining operation planning, especially in NC machining, where the selection of the cutting parameters has to be made during the programming stage.

5.3 Computer Simulations and Experimental Work

5.3.1 Computer Simulations

A two-level full factorial design is applied to compare the results under different cutting conditions. Table 5.2 lists the cutting conditions used in the computer simulations and experimental work. Other parameters used are listed under the table.

Table 5.2: A Two-Level Full Factorial Design of Experiment

Test Condition Number	Depth of Cut (mm)	Feed Rate (mm/rev)	Spindle Speed (rpm)	Surface Quality Indices (R_a,R_q,R_t,dq)
1	0.13	0.05	1000	
2	0.25	0.05	1000	
3	0.13	0.2	1000	
4	0.25	0.2	1000	
5	0.13	0.05	1500	
6	0.25	0.05	1500	
7	0.13	0.2	1500	
8	0.25	0.2	1500	

Workpiece Material:	AISI 1020 Rolled Carbon Steel Bars
Microhardness Distribution:	Longitudinal Trend
Workpiece Geometry:	Length $\times$ Diameter = 100 $\times$ 70 mm
Tool Geometry:	Nose Radius = 0.8 mm, Rake Angle= $+5°$, Lead Angle = $45°$
Unit Cutting Force:	2.0 GPa
Equivalent Mass:	2.0 kg
Damping Coefficient:	0.05
Natural Frequency 1:	1260 Hz
Natural Frequency 2:	1870 Hz

The simulation programs are written in FORTRAN 77 language and compiled

under the Unix operating system. When the program is running, the user will be prompted by a simple menu system with options similar to the following:

```
======== Computer-Aided Surface Topography Simulator ========

    1. Microstructural Analysis (Random Excitation Modeling)
    2. Tool Vibration Motion Evaluation
    3. Surface Texture Formation and Quality Analysis
    4. Help
    5. Quit

Please choose a number (default = Quit):
```

Each option in the menu stands for the modules discussed in the previous sections. The surface texture formation and quality analysis option will load the output from the tool vibration motion evaluation module, visually display the simulated surface topography on the computer screen (it is device dependent), and calculate the simulated surface quality indices values. Figure 5.6a shows a screen of simulated surface topography under test number 1. Surface quality indices calculated by the simulator under the 8 cutting conditions in Table 5.2 are listed in the left half of Table 5.3. It is noted that these numbers are after the modifications from the elastoplastic deformation model as described earlier.

Beside the surface texture and quality indices, cutting force signals can also be simulated. Figure 5.6b shows the cutting force signals evaluated from the simulator under test number 1. By checking the frequency spectrum of this signal, one can verify the system parameters (natural frequencies) of the machine

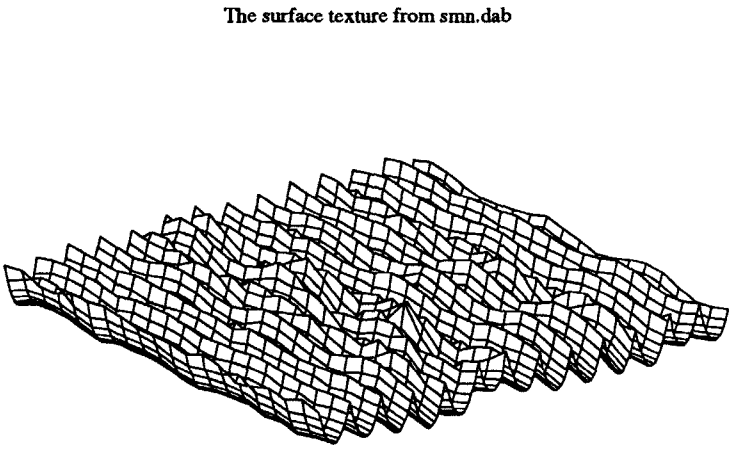

(a) Simulated Surface Topography Shown on the Screen

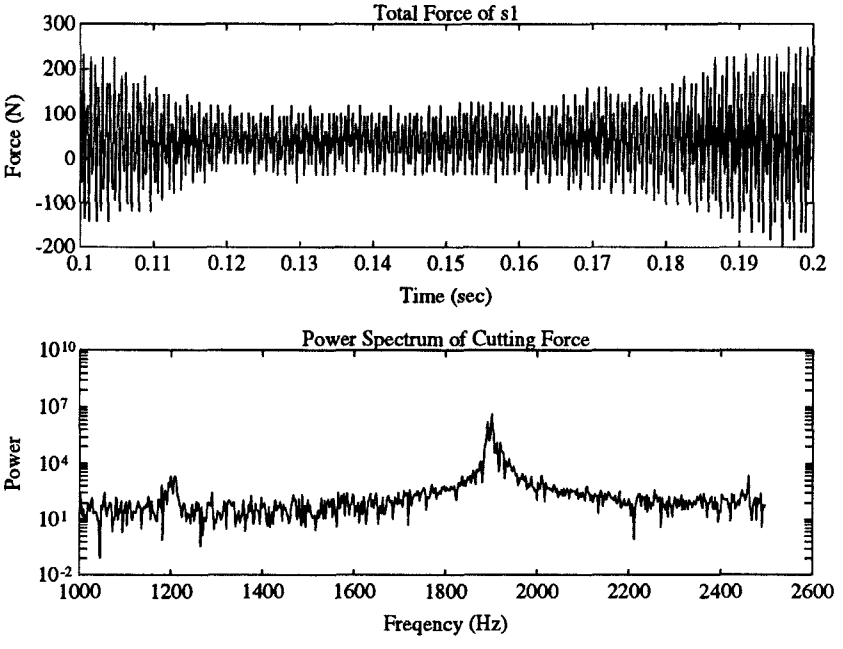

(b) Simulated Cutting Force and Power Spectrum

Figure 5.6: Simulated Surface Texture and Cutting Force Signals

tool used in the simulation. For example, the peaks shown in the frequency spectrum are around 1260 Hz and 1870 Hz, which are close to what we measured in the cutting tests (see the next section).

Table 5.3: Surface Quality Indices under 8 Cutting Conditions

Test Condition Number	Computer Simulation Results				Measured from Machined Surfaces			
	R_a (μm)	R_q (μm)	R_t (μm)	dq (degrees)	R_a (μm)	R_q (μm)	R_t (μm)	dq (degrees)
1	1.09	1.37	5.52	7.32	1.16	1.40	5.70	7.90
2	1.80	2.05	6.74	6.63	1.88	2.10	7.00	6.50
3	0.99	1.14	4.67	5.55	1.02	1.20	4.80	5.70
4	1.86	2.08	7.11	5.94	1.90	2.13	7.20	6.00
5	1.07	1.22	5.34	6.24	1.09	1.30	5.40	6.20
6	1.87	2.10	7.32	6.99	1.91	2.15	7.40	6.90
7	0.90	1.19	5.04	6.71	0.98	1.21	5.10	6.80
8	1.77	1.97	7.05	6.21	1.82	2.04	7.10	6.10

5.3.2 Experimental Work

To validate the methodology used in developing the simulator for the visualization of surface texture formed during machining, experiments were carried out and the experimental results were compared with the results derived from the developed framework. A series of turning tests using AISI 1020 steel and 6061-T6 aluminum alloy bars are performed on a CNC lathe. The cutting parameters are kept the same as those used in the computer simulations to compare the results.

Microstructures of different materials are characterized as discussed in Chapter 3 and Appendix B. Cutting force signals are acquired during machining tests to provide the average cutting forces in the feed and tangential directions, which in turn provide the information for estimating the cutting force angle (θ) in the

simulation. Figure 5.7 (from [Shaw 84]) shows the relation between the force angle, rake angle, and the cutting forces (tangential and feed directions) and can be expressed as follows:

$$\theta = \frac{\pi}{2} - \alpha_r - tan^{-1}\left(\frac{F_f}{F_t}\right) \tag{5.3}$$

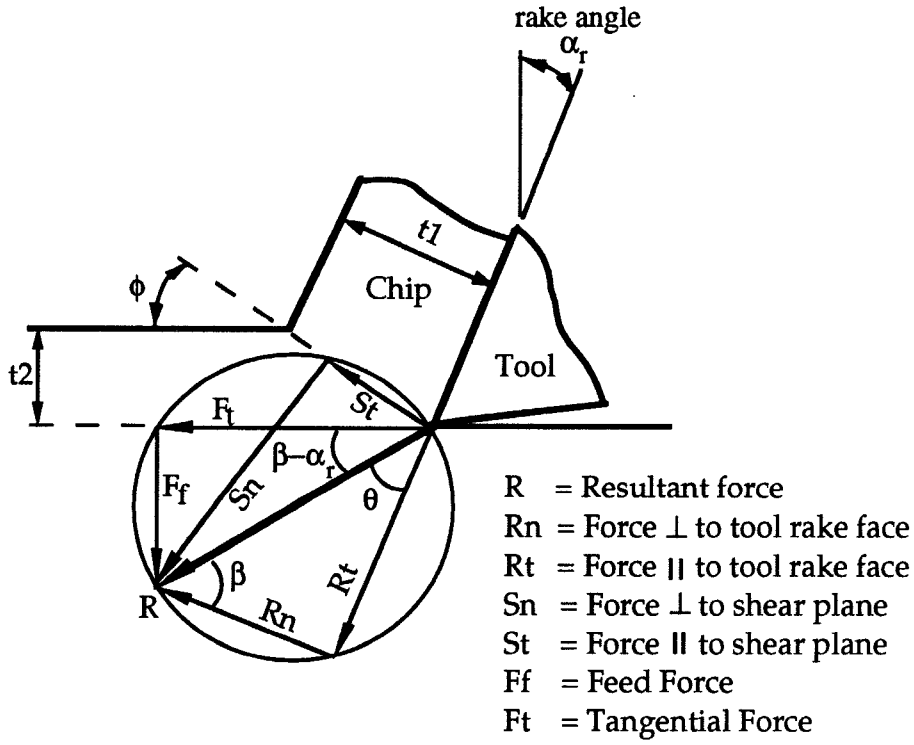

Figure 5.7: Composite Cutting Force Circle

Natural frequencies can also be estimated from the acquired signals through the spectral analysis. These information can be used to fine tune the parameters used in the simulator. After machining tests, surface profiles on the machined surfaces are also measured by the surface profilometer to get the quality indices for comparison.

Cutting Force Measurement

Cutting force signals are required to find the average ratio of the feed to tangential forces. Therefore, a transducer which can measure the two cutting forces is needed as shown in Fig. 5.8a. The force transducer basically consists of three parts: strain gages, a bridge conditioning system, and a data acquisition system. A brief description of the development of the force transducer is given below.

1. *Layout Design of Strain Gages:* A Wheatstone bridge is usually applied to measure the change in resistance when active gages are subjected to strains. In Fig. 5.8b, one gage on the top face and another one on the bottom face of the tool holder are mounted along the central axis of the tool holder to measure the tangential cutting force [Da. 84]. Similarly, two other gages are mounted on the left and right faces of the tool holder along the central axis to measure the feed cutting force. As a result, two half-bridge configurations are used in this force transducer to measure the two forces. The gages used are thin-foil type strain gages with the same gage factor, 2.115.

2. *Signal Conditioning and Data Acquisition Systems:* The two Wheatstone bridges need to be first balanced before they can be used. Two strain indicators are, therefore, connected to each of the bridges for this purpose. The signals (or voltages) from the strain indicators are still too weak to be picked up by data acquisition system. Therefore, a signal amplification circuit which consists of operational amplifiers and resistors (100 $K\Omega$ and 1 $K\Omega$) is built to amplify the signals with a gain of 100. A microcomputer-

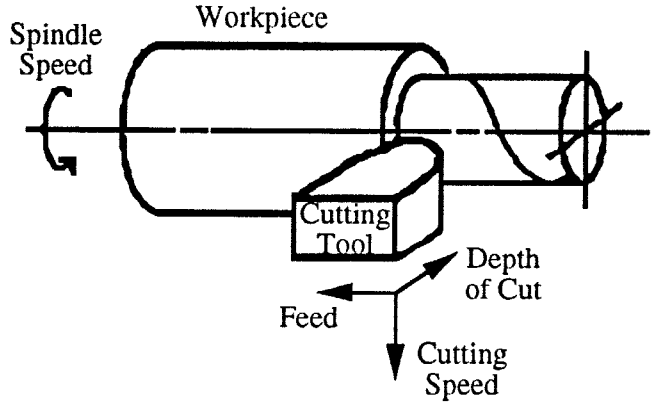

(a) A single-point cutting process

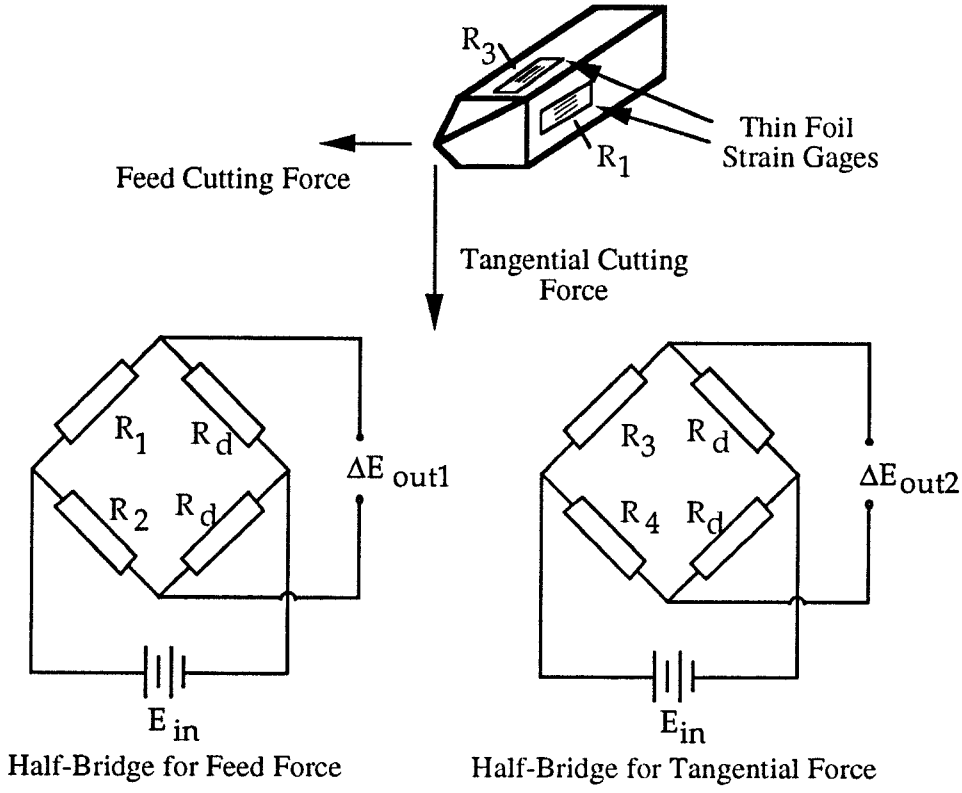

(b) Layout design of strain gages

Figure 5.8: Design of a Force Transducer

based data acquisition system is used to a) convert analog signals to digital signals, and b) store the signals for further analysis. Figure 5.9 shows the connections of the whole signal conditioning and data acquisition systems.

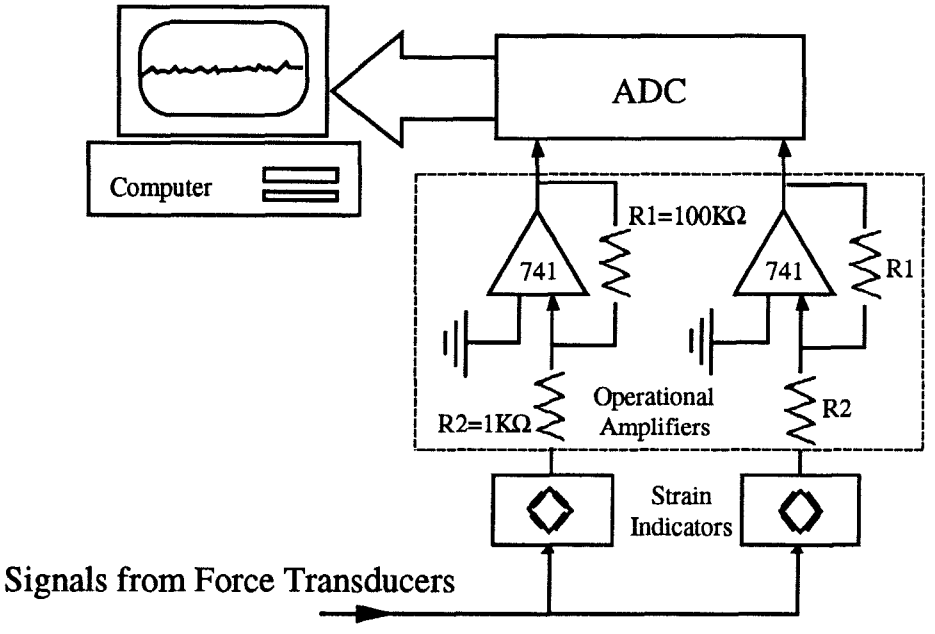

Figure 5.9: Signal Conditioning and Data Acquisition System

3. *Calibration:* Before the force transducer can be used to measure the cutting forces, a relation between the voltage readings from the data acquisition system and the acting forces must be found. Calibration of the system is, therefore, performed for this purpose.

   As shown in Fig. 5.10a, static loads are applied (first increasing the load then decreasing it) along the feed (X) direction first. Readings from each bridge are recorded. Similarly, static loads are applied along the tangential (Y) directions and readings from each bridge are also recorded. Figure 5.10b shows the recorded data plotted against the loads in both

X and Y directions. From the recorded data, the relation between the voltage readings and the load is formed as follows.

$$\begin{bmatrix} V_x \\ V_y \end{bmatrix} = \begin{bmatrix} \frac{\Delta V_x}{\Delta F_x} & \frac{\Delta V_x}{\Delta F_y} \\ \frac{\Delta V_y}{\Delta F_x} & \frac{\Delta V_y}{\Delta F_y} \end{bmatrix} \begin{bmatrix} F_x \\ F_y \end{bmatrix} \tag{5.4}$$

or

$$[V] = [T][F] \tag{5.5}$$

where the matrix $[T]$ is a transformation matrix which consists of the slopes of the four "curves" shown in Fig. 5.10b. Based on this matrix, when the force transducer is used during machining, the readings from the computer can be transformed into the cutting forces along feed and tangential directions, or $[F] = [T]^{-1}[V]$.

The actual values in the transformation matrix evaluated from Fig. 5.10b are

$$[T] = \begin{bmatrix} 0.0153 & 0.0001 \\ 0.0006 & 0.0312 \end{bmatrix}. \tag{5.6}$$

4. *On-Line Testing and Spectrum Analysis:* By using the force transducer and data acquisition system mentioned above, cutting force signals are measured on-line during machining. Figure 5.11 shows the measured feed and tangential forces under test condition 1. Frequency spectra of both force signals are also calculated through the *FFT* algorithm [Bri 88]. The most significant two peaks in both frequency spectra are at frequencies around 1260 Hz and 1870 Hz, respectively. By observing spectra of other cutting conditions, these two peaks are always there. It is, therefore,

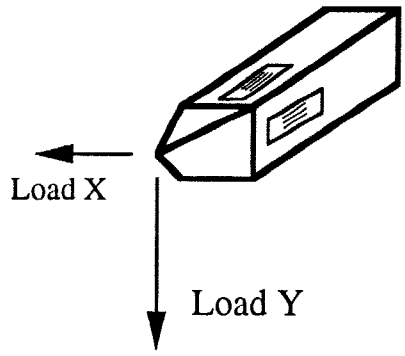

(a) Loading Directions

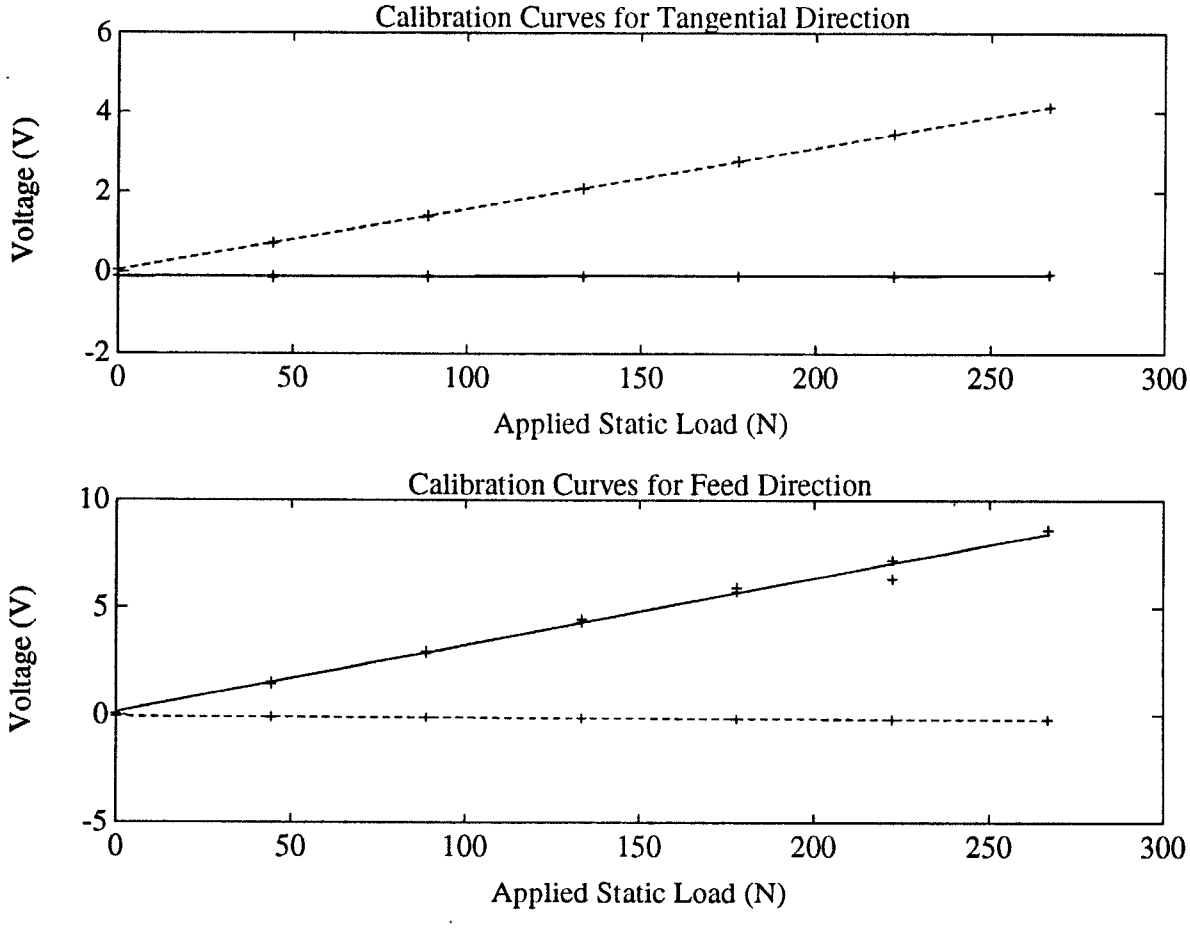

(b) Calibration Curves

Figure 5.10: Calibration of the Force Transducer

reasonable to assume that the natural frequencies of the machine tool structure are pretty close to the above two values.

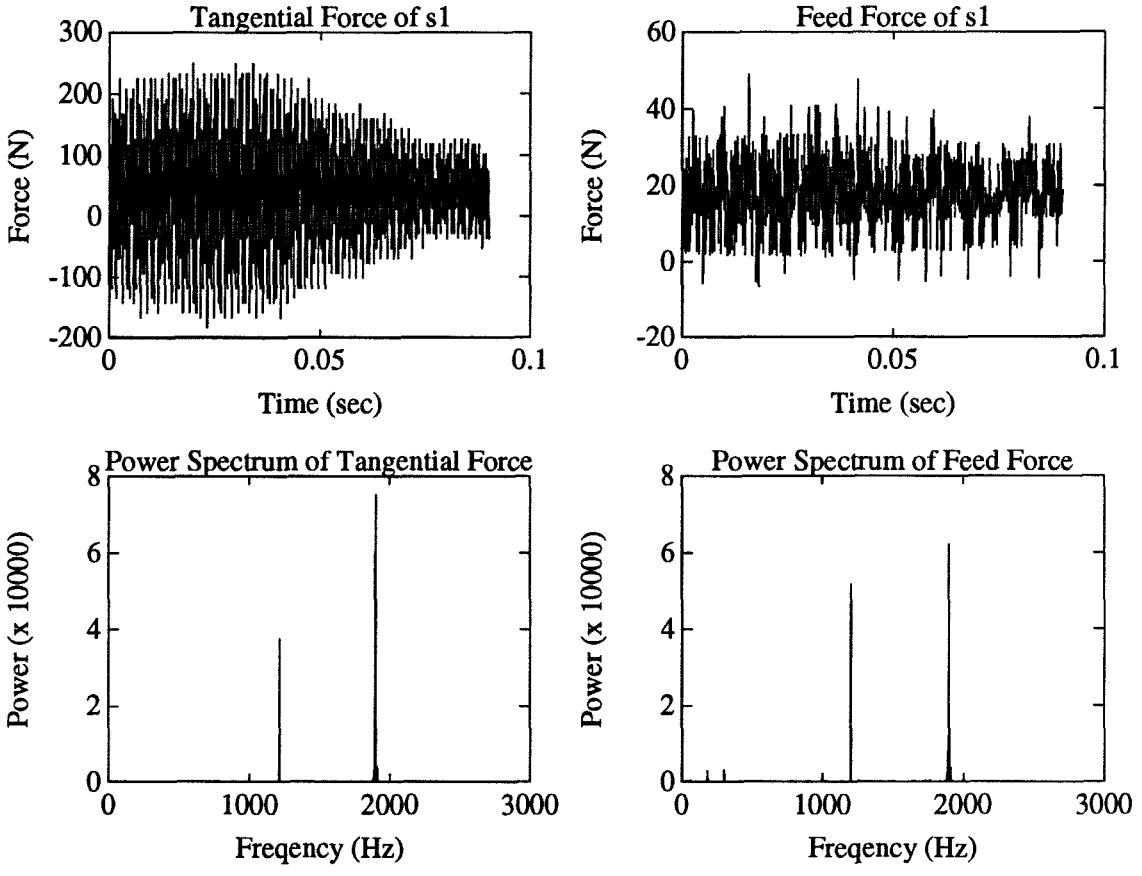

Figure 5.11: Cutting Force Signals Acquired during Machining

Surface Profiles Measurement

A Talysurf 6 surface profilometer was used to measure the machined surface profiles along the feed direction. Figure 5.12 displays the equipment setup of the profilometer at the National Institute of Standards and Technology. Surface quality indices of each machined surface are also calculated and averaged after

three profile measurements. The results of each machined surface are listed in the right half of Table 5.3.

Figure 5.12: Setup of the Surface Profilometer

5.4 Discussion of Results

By comparing the results of the 8 cutting tests with the simulation results listed in Table 5.3, it is evident that the simulator can predict the surface quality relatively close to the measured indices of machined surfaces. By changing the cutting conditions, both the surface quality predicted from the simulator and those measured from machined surfaces change with similar trends. The system parameters such as the natural frequencies of the tool structure used in this study are estimated by on-line sensed cutting force signals if frequency spectra of the

signals are analyzed. It indicates that a careful calibration to set the system parameters of the developed simulator is necessary to ensure the accuracy of the surface quality prediction.

At the present stage, the developed simulator serves as a prototype model of the computer-based metrological system for industrial control and diagnostics of the quality of machined surfaces formed during machining. It can clearly depict how the parameters of a machining operation system affect the surface texture formation during machining, thus resolving the problem of relating the surface functional requirements and pertinent manufacturing parameters. For example, through evaluating the effect of microstructures in the material to be machined, the simulator is capable of advising the improvement of surface texture by controlling the size, shape, and segregation of the microstructures in the material. Therefore, the visualization of surface texture formed during machining has linked the design of surface texture to meet the functionality in a tribological environment to the control of the surface texture actually formed during manufacturing.

The development of this computer-based surface topography simulator has made a significant contribution to the quality control of machined surfaces, especially in an environment of automated production. For NC machining, the simulator can be used as a simulation tool to perform an off-line optimization in setting machining parameters during the programming stage. The availability of the database generated through simulation makes it possible to construct a surface profile either on the circumferential, or on the axial, direction of the workpiece, thus characterizing the spatial relationships between profile heights which, basically, differ with direction. As a result, the simulator could be used

to predict the finish quality of a machined surface, instead of taking actual measurements from the machined surface. This capability would facilitate assessing the finish quality of holes with a small diameter and a large ratio of length to diameter. Such assessments usually pose a serious technical problem on the shop floor.

By providing information on the variation of surface profiles taken at different locations on a machined surface, it fits the need to guide the quality inspection by suggesting the number of traces to be taken on the machined surface being inspected. By combining this simulator with sensor technology to detect the tool vibration on-line during machining, it may become an essential tool for performing in-process inspection.

5.5 Summary

1. The work presented in this chapter successfully demonstrates a conceptual framework and the development of a prototype computer-based system for the visualization of surface texture formed during machining. The topography of a machined surface through computer visualization, confirmed by experimental verification, vividly depicts the dynamic process of surface texture formation during machining. The framework offers great potential for industrial applications in controlling the finish quality.

2. The basic methodology is built through the integration of three scientific branches, i.e., material science, machining science, and metrology science. Considering the variability of basic material properties as a major source of random tool motion, the tool vibratory motion is quantitatively evaluated

in microscale. Such an evaluation bridges the gap between the control of surface functional requirement and the control of pertinent manufacturing parameters. The study of the microstructure of machined surfaces through the analysis of cutting dynamics in micro-scale represents an innovative approach to establishing hardness variability as one of the standard material properties for machining. On the other hand, the elastoplastic deformation and recovery processes observed during machining have also been considered in this simulator which has greatly improved the accuracy of predicting machined surface quality (especially, the dq index).

3. The computer-based prototype system for the visualization of surface texture is capable of generating the data representing a machined surface in a three-dimensional space characterized by the three machining parameters; i.e., depth of cut, feed, and cutting speed. The uniqueness of this data base is that it clearly defines the spatial relationships as a whole, rather than as a set of parallel profiles. As demonstrated in this chapter, this information is very useful for guiding the control of finish quality on the shop floor. If an accurate calibration of the system parameters is made, the developed prototype system can be used as a comprehensive metrological system for industrial control and diagnostics of surface quality. This prototype system may also become an important component of a quality assurance system to perform in-process inspection for the certification of the machining process.

Chapter 6

Study of the Material Removal Mechanisms in Machining of Advanced Ceramics

This chapter presents a preliminary investigation of fundamentals behind the machining of advanced engineering ceramic materials. The investigation consists of analytical and experimental aspects. In the experimental study, turning and milling operations were used to machine aluminum oxide (Al_2O_3) and Dicor/MGC. Basic principles of preparing machining operations to achieve a meaningful and practical machining process are suggested. A fracture-dominant mechanism to describe the material removal process is proposed. Method to evaluate the unit cutting force or the minimum threshold load based on the measured cutting force is developed. The design of experimentation approach is used to study the effects of cutting parameters and cutting fluids on machining efficiency. Special attention has been paid to chemical-assisted machining to control the impairment on the machined surface introduced during machining.

Results from this research provide rich information on the cutting mechanisms during the machining of ceramics.

6.1 Introduction

The need for high strength materials has led to the development of advanced ceramics used in engineering. Advantages that ceramics have over other materials include superior heat resistance, wear and abrasion resistance, hardness, corrosion resistance, lightness and aesthetics. As a result, strategic material considerations and economic factors are forcing modern industries towards the use of ceramic components. New interests, especially for structural applications, are markedly increasing.

Although most ceramic parts are manufactured to near net shape by pressing and sintering processes, machining processes are desperately needed to ensure dimensional and geometrical accuracy. However, ceramic materials are very hard to machine. The traditional technology to machine ceramics is grinding. As an abrasive machining operation, very small chips are produced by the cutting edges of abrasive particles. Consequently, the grinding process removes ceramic material with a low productivity. On the other hand, due to natural brittleness, micro-cracking of the machined surface often leads to premature failure of ceramic components during service. With the ever increasing number of ceramic materials in the marketplace, there is a pressing need to improve the traditional methods and search for new, innovative processing methods to achieve cost reduction and quality assurance. As reported in [Ch. 86], a "laser lathe" was developed where the dual beam principle was applied to remove ceramic

materials in a molten form. However, the surface and sub-surface damage induced during laser machining are the drawbacks of the technique. In abrasive jet machining, the high pressure abrasives wash and pierce ceramic materials away [Maz 91]. But, the availability of new equipment and economic factors have limited its wide use on the shop floor. With the availability of making abrasive grains consistently to high levels of performance and dimensional accuracy, the grinding process has maintained its popularity in machining ceramics. Grinding wheels made of hard structural ceramic materials such as Si_3N_4, SiC and alumina (hot pressed silicon nitride ceramics) are capable of achieving high quality of microfinishing. It was reported that the average roughness value (R_a) of the surface ground by 140 $\sim$ 200 mesh diamond wheels was about 0.1 to 2.0 μm [Nak. 85]. However, little work has been conducted in the study for gaining a comprehensive understanding of the mechanisms that remove the ceramic material during machining. Especially, few technical documents report the mechanism in turning and milling ceramic materials. Lack of such knowledge has slowed down the development of new and innovative machining processes that may revolutionize the machining technology of advanced ceramic materials.

This paper presents a preliminary investigation of fundamentals behind the machining of advanced engineering ceramic materials. The experimental work is based on a single-point turning process and a multi-edge milling process. The workpiece materials used in this study were aluminum oxide and Dicor/MGC, a glass-ceramic material designed for use in dental restorations [Gr 91]. The cutting tools used were polycrystalline diamond compact tools for turning aluminum oxide, and cemented tungsten carbide tools and high speed steel end mills for milling Dicor/MGC. Cutting force measurements were taken during machining

tests. After machining, quality of machined surfaces were assessed with respect to surface finish and possible impairments induced during machining. A fracture-dominant mechanism to describe the material removal process is suggested. Method to evaluate the unit cutting force or the minimum threshold load based on the measured cutting force is developed. A two-level experimental design approach was employed to systematically investigate the effects of machining parameters such as feed, depth of cut, and cutting speed on the machining performance. Special attention was paid to the collection of evidence which can support the suggested fracture-dominant machining mechanism. To apply these findings, or more importantly, to develop new and innovative machining methods based on these findings, chemical-assisted machining processes were explored to achieve better machining performance.

6.2 Basic Methodology of Investigation

As a preliminary investigation, our objective was to gain a comprehensive understanding of the fundamental principles in machining ceramics. Starting from the selection of specific ceramic materials as testing materials, our research went on to search proper tool insert materials, establish the machining setup, and determine machining conditions for the investigation.

6.2.1 Selection of Ceramic Materials

In traditional approaches developed in machining science, representative brittle and ductile metals are selected for the study of material removal mechanisms during machining. Following these traditional approaches, aluminum oxide was

selected to represent brittle ceramic materials being machined and Dicor/MGC, a glass-ceramic material designed for use in dental restorations, was selected to represent "ductile" ceramic materials being machined. The selected 99.8% Al_2O_3 is a cylindrical bar with a diameter of 19.0 mm and length of 76.2 mm. It contains 99.8% pure α - alumina with impurities that primarily consist of magnesium oxide which is used as a sintering aid. The material is commercially used in applications of extreme temperature and corrosive environments. The selected Dicor/MGC material is tetrasilicic mica glass-ceramics. The material is produced from glasses based on the quaternary system $K_2O - MgF_2 - MgO - SiO_2$ with additions of Al_2O_3 and ZrO_2 [Gr 91]. This material has a unique microstructure consisting of mica flakes of approximately 70 volume percent dispersed in a non-porous glass matrix. It has been used for dental restorations for its physical properties closely matching human enamel such as hardness, density, thermal conductivity, and translucency. The cleavage, or splitting along the literal planes of mica flakes, functions as stress concentration, a situation similar to the stress concentration around the inclusions presented in free-machining steels, providing a mechanism for its machinability.

6.2.2 Selection of Tool Materials

It has been well known that the material properties of the cutting tool dictate the qualification of tools which can be used in a given machining process. Of these material properties, the hardness stands out, especially the hardness under high temperature conditions. In our study of turning aluminum oxide, two types of tool inserts were used. They are polycrystalline diamond compact and cubic boron nitride (CBN) inserts. In the machining tests, the synthetic diamond

tool inserts sustained the machining action, but the CBN tool inserts did not. Table 6.1 provides a comparison of hardness, modulus of elasticity, flexural strength, and fracture toughness between the two tool materials. A major difference is the hardness. The hardness of the synthetic diamond tool inserts is much higher than the hardness of the CBN tool inserts although the CBN inserts possess a higher value of flexural strength than the synthetic diamond inserts. By comparing the hardness of the synthetic diamond tool material with the hardness of the selected aluminum oxide, a conclusion can be drawn that a minimum ratio of the tool hardness to the hardness of the ceramic material being machined should be, at least, kept at 5:1 or 6:1. Therefore, diamond is most recommended because it is the hardest material known. In addition, it possesses the largest thermal conductivity and chemical inertness which are two important properties for being machining tool materials.

Table 6.1: Tool Insert Materials and Aluminum Oxide Comparison

Mechanical Properties	Unit	Aluminum Oxide	Polycrystalline Diamond Compact	Cubic Boron Nitride
Hardness	GPa	$11 \sim 12$	$60 \sim 90$	29
Modulus of Elasticity	GPa	345	$725 \sim 1049$	680
Flexural Strength	MPa	359	500	750
Fracture Toughness	$MPa\sqrt{m}$	4.0	3.4	-
Grain Size	μm	$10 \sim 12$	-	-

The hardness of the Dicor/MGC is about 3.4 GPa, a value that is relatively low if compared with the selected aluminum oxide. Consequently, the tool materials used for machining the Dicor/MGC material were cemented tungsten carbide and high speed steel tools because their hardness values are about 22 GPa and 18 GPa, respectively.

6.2.3 Description of Experimental Setup

In this study, the aluminum oxide (Al_2O_3) bars were machined on a CNC lathe. An instrumented tool post with attached strain gage sensors was used to perform in-process cutting force measurements. A special cutting fluid system was used for feeding cutting fluid into the cutting area and collecting chips through a filtering device. Figures 6.1a and 6.1b show the experimental setup. As illustrated in Fig. 6.1b, a PC-based computer data acquisition system was used for recording the cutting force signal.

The Dicor/MGC specimens were cylinders with a diameter of 16.0 mm and the length of 12 mm. These specimens were mounted on a metal base plate in epoxy resin to form a block of material to be machined. A Matsuura MC-510 machining center was used to perform a milling operation, which is the major fabrication technique used in dental restorations. Figures 6.2a and 6.2b show the experimental setup.

6.3 Experimental Work

Our investigation focused on the following issues:

1. Investigate the cutting mechanisms through the evaluation of unit cutting force and the effects of machining parameters on the evaluated unit cutting force;

2. Determine the surface finish and its relation to machining conditions; and

3. Explore a new technology that ensures quality and provides adequate machining efficiency.

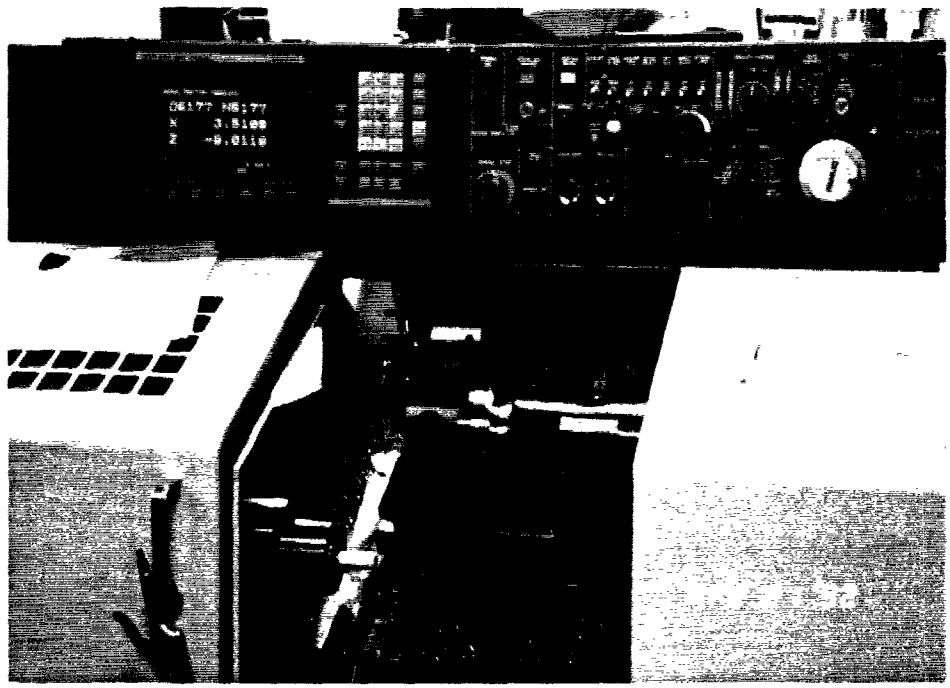

a. Picture of the experimental setup for machining Aluminun oxide.

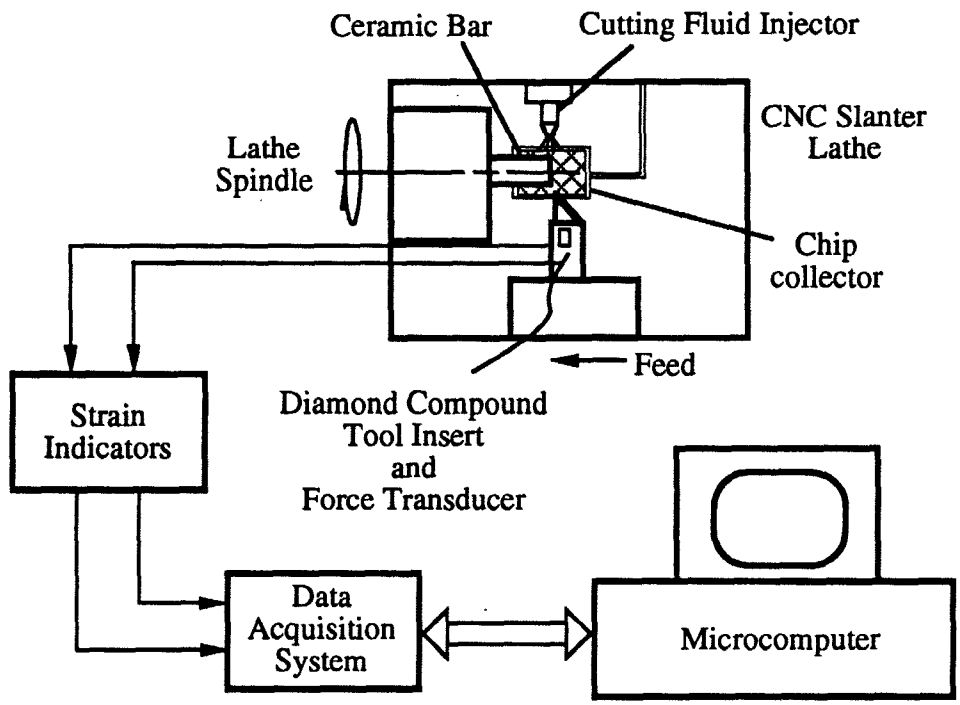

b. Schematic of the experimental setup

Figure 6.1: Experimental Setup for Turning Aluminum Oxide

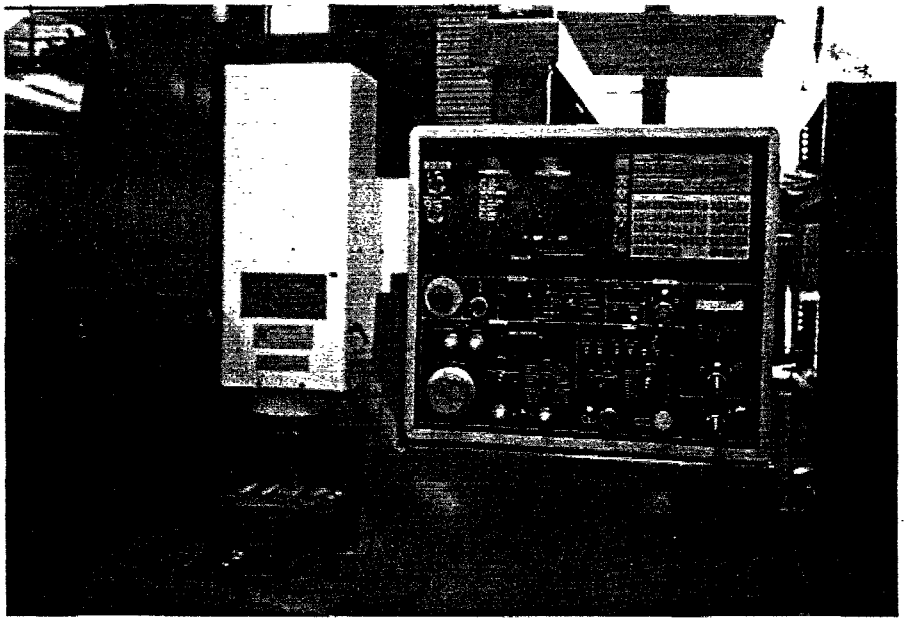

a. Picture of the experimental Setup for Milling DICOR

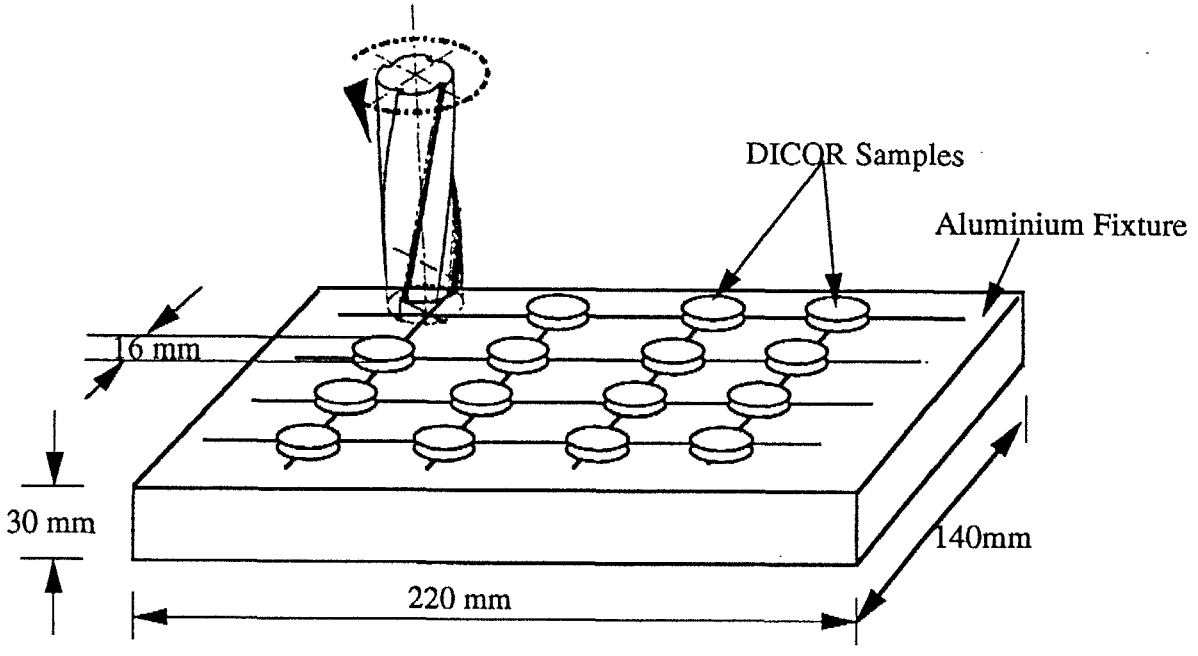

b. Schematic of the Milling operation of DICOR

Figure 6.2: Experimental Setup for Milling DICOR/MGC

6.3.1 Cutting Force Evaluation

A factorial design approach was used for turning the aluminum oxide bars. The approach is based on the principle of orthogonal arrays which provides an insight into the relation between the cutting force and machining parameters. The three parameters under investigation were feed, depth of cut, and cutting speed. Table 6.2 is the design matrix used for turning the aluminum oxide bars.

Table 6.2: Machining Conditions Used in Turning Aluminum Oxide Bars

Test Condition Number	Depth of Cut (mm)	Feed Rate (mm/min)	Spindle Speed (rpm)	Performance Measures of Interest (Cutting Force or Surface Finish)
1	0.1	5	400	
2	0.2	5	400	
3	0.1	10	400	
4	0.2	10	400	
5	0.1	5	600	
6	0.2	5	600	
7	0.1	10	600	
8	0.2	10	600	

In order to block the experimental errors due to the variation in the tool insert quality, a single tool insert was used to cut 16 tests, 8 tests for the distilled water and 8 tests for water plus chemical additives. To get fair estimates, three tool inserts were used to duplicate the 16 tests when turning the aluminum oxide bars. Whenever a new tool insert was used, a coin was tossed to determine which of the two sets of 8 tests should be performed first. Such a randomization unbiasedly distributed the effect of tool wear on the machining performance among the 8 machining tests. Figure 6.3 presents the tangential and feed cutting force signals measured during machining. It also indicates that the average value and standard deviation are calculated from the recorded data. The resultant cutting

force is calculated as a vectorial sum. Table 6.3 lists the data of cutting force measurements.

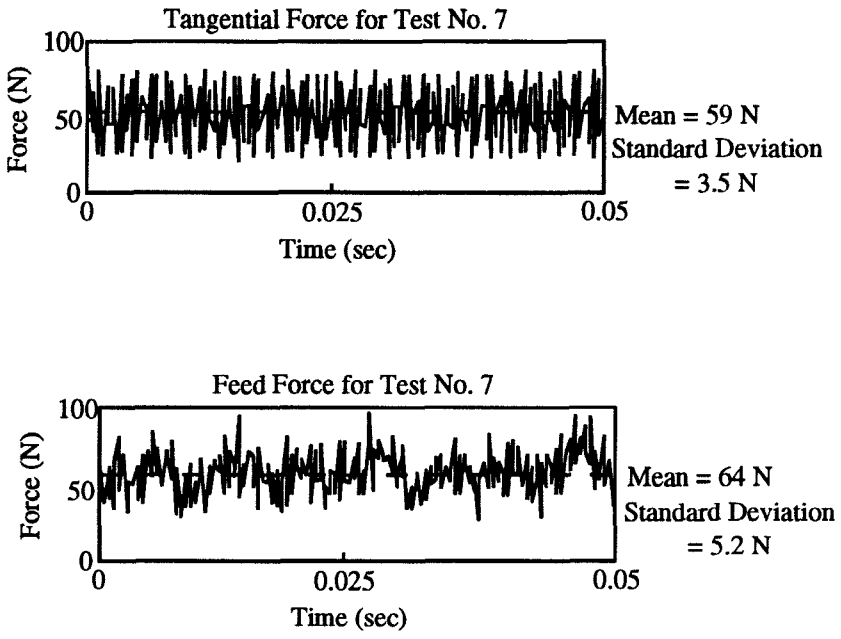

Figure 6.3: Tangential and Feed Cutting Force Signals Acquired from the Cutting of Al_2O_3 with Chemical additives

In order to explore the possibility of using cutting fluids as an efficient means to achieve satisfactory machining performance, four types of cutting fluids were used during the study. They are a type of traditional mineral oil, an oil-based water soluble coolant, pure distilled water, and a mixture of distilled water and a selected chemical additive. In this preliminary study, our finding was that the cutting fluid with the selected chemical additive performed surprisingly well with regard to the machining performance. The data listed in Tables 6.3a and 6.3b are the cutting force measurements from two types of cutting fluids for the purpose of comparison. These two types are the cutting fluid of pure distilled water and the cutting fluid with the selected chemical additive.

Table 6.3: Data of Cutting Force Measurements

a. Cutting Fluid Type: Distilled Water

Test Number	Tangential Force (F_t) (N)	Feed Force (F_f) (N)	Total Force (N)	Unit Cutting Force (GPa)	Surface Roughness (μm)	Ratio of F_t/F_f
1	61	69	92.1	73.7	0.90	0.88
2	71	122	141.2	56.5	0.84	0.58
3	76	73	105.4	42.2	1.00	1.04
4	79	123	146.2	29.2	1.25	0.64
5	53	72	89.4	107.7	0.89	0.74
6	80	116	140.9	82.9	0.65	0.69
7	65	70	95.5	56.2	1.04	0.93
8	102	114	153.0	46.4	1.16	0.89

b. Cutting Fluid Type: Distilled Water Plus a Chemical Additive

Test Number	Tangential Force (F_t) (N)	Feed Force (F_f) (N)	Total Force (N)	Unit Cutting Force (GPa)	Surface Roughness (μm)	Ratio of F_t/F_f
1	56	73	92.0	73.6	0.83	0.77
2	60	144	156.0	62.4	0.75	0.42
3	63	60	87.0	34.8	1.04	1.05
4	75	136	155.3	31.1	0.81	0.55
5	51	68	85.0	102.4	0.55	0.75
6	49	140	148.3	87.3	0.69	0.35
7	59	64	87.0	51.2	0.85	0.92
8	88	116	145.6	44.1	1.23	0.76

6.3.2 Surface Finish Evaluation

After machining, surface profiles were taken from the machined surfaces. The Surface roughness average, R_a, was used as the performance index for the finish quality evaluation. To visualize the surface topography formed during machining, three-dimensional topographies were also constructed. Figure 6.4 depicts two surface topographies. The two surfaces were machined under identical parameter settings but with different cutting fluid conditions. As indicated, one is with pure distilled water and the other is with distilled water and a chemical additive. For the purpose of quantifying the finish quality, three traces were taken from each of the two chosen areas, representing the best, median, and worst traces regarding the roughness characteristics, that are possibly taken from the selected area. In addition, the machined surfaces were examined using a scanning electron microscope. Photographs were taken to gain a qualitative information on topography of the machined surfaces in micro-scale. Figure 6.5 displays the appearances of the two machined surfaces. The geometrical shape and size of the visible marks and the contrasts between the lightest and darkest parts of these two pictures signify a fact that the surface conditions shown in Fig. 6.5b are better than those in Fig. 6.5a, indicating the effectiveness of using the selected chemical additive for improving quality of the machined surface.

Similar procedures and the factorial design approach were used in the investigation of milling Dicor/MGC materials. Table 6.4 is the design matrix and the measured surface finish R_a values.

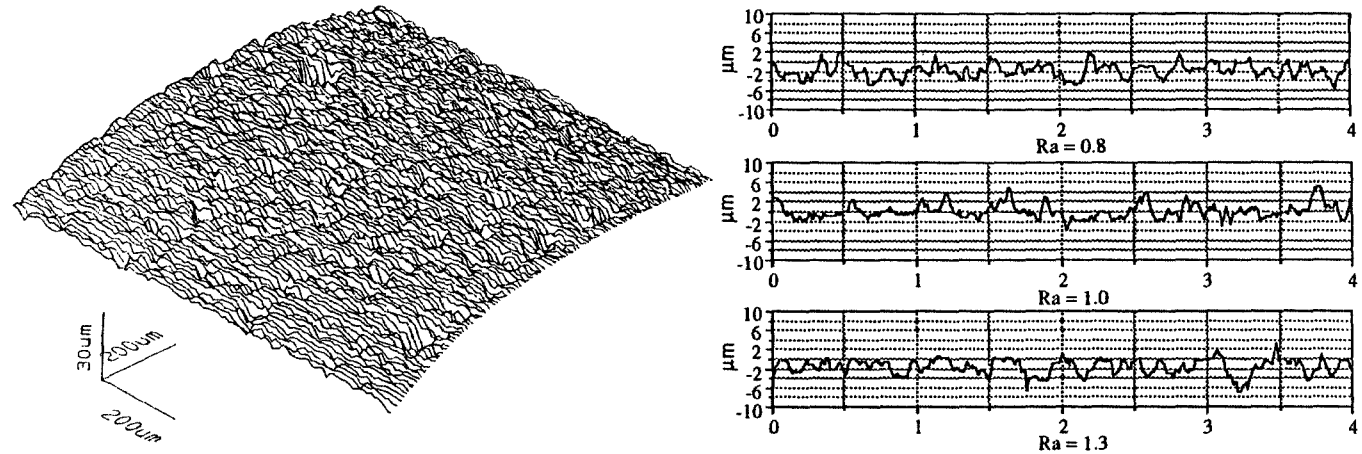

a. Three-Dimensional Surface Topography with Distilled Water and Three Profiles Taken from It

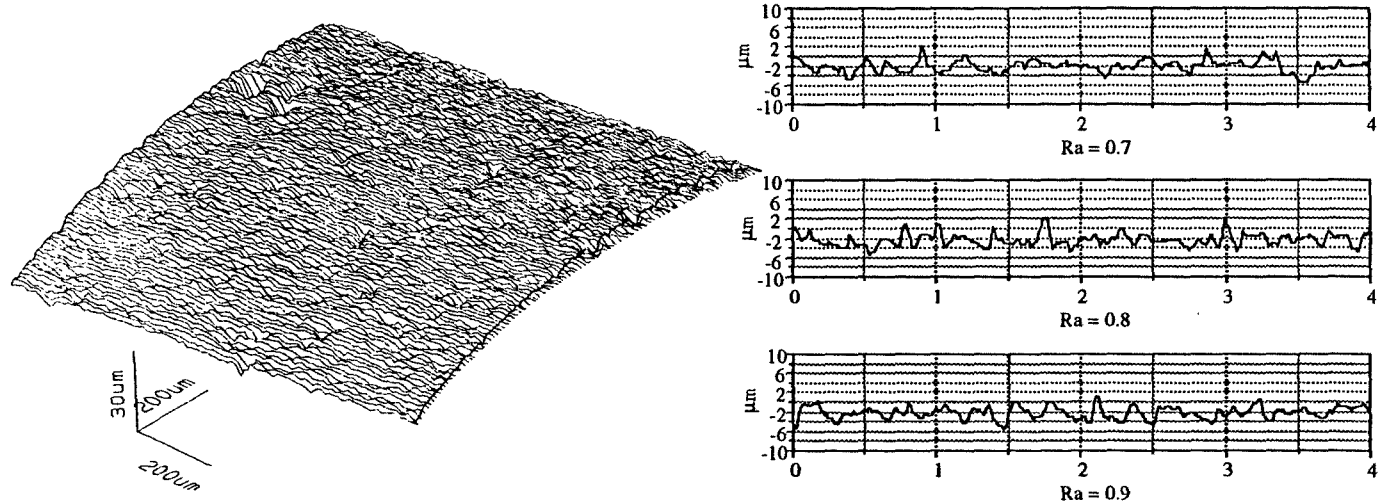

b. Three-Dimensional Surface Topography with Chemical Additives and Three Profiles Taken from It

Figure 6.4: Comparison of Two Machined Surfaces
(Cutting Condition: Feed = 10 mm/min, Depth of Cut = 0.1 mm, Spindle Speed = 600 rpm)

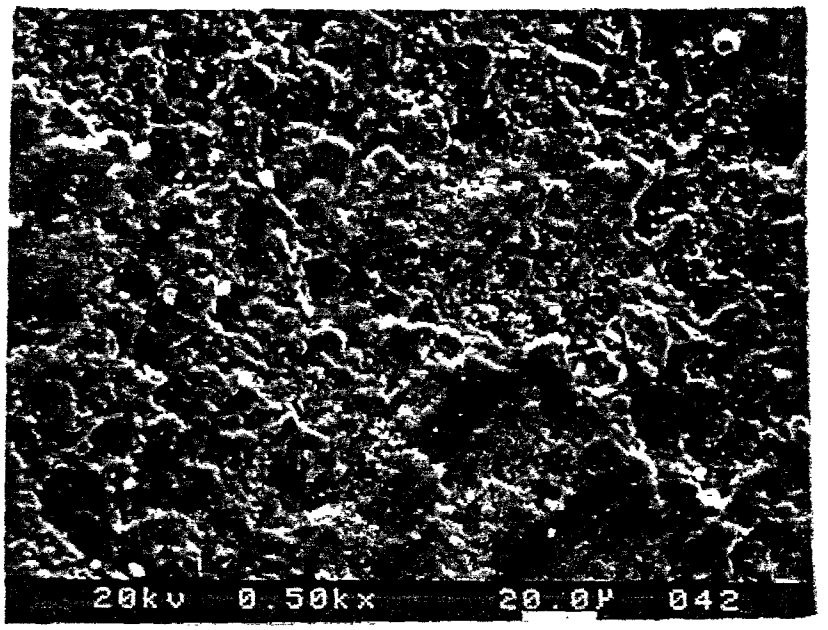

a. Machined Surface Using Distilled Water

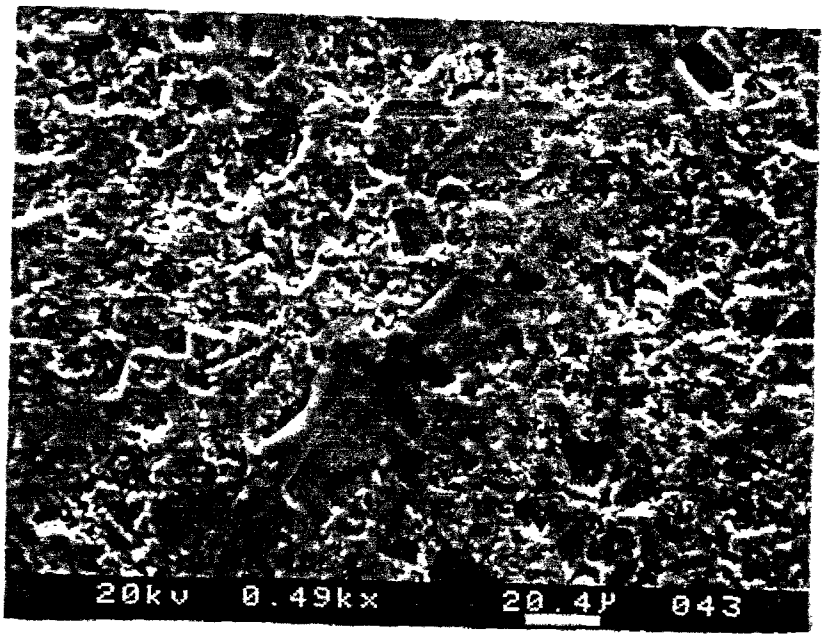

b. Machined Surface Using Chemical Additive

Figure 6.5: Appearances of Two Machined Aluminum Oxide Surfaces

Table 6.4: Machining Conditions Used in Milling DICOR/MGC

a. Cutting Fluid Type: Distilled Water

Test Condition Number	Depth of Cut (mm)	Feed Rate (mm/min)	Spindle Speed (rpm)	Surface Roughness Average (μm)
1	0.05	10	200	2.7
2	0.1	10	200	8.1
3	0.05	20	200	5.6
4	0.1	20	200	4.4
5	0.05	10	400	3.8
6	0.1	10	400	1.8
7	0.05	20	400	6.1
8	0.1	20	400	7.6

b. Cutting Fluid Type: Distilled Water Plus a Chemical Additive

Test Condition Number	Depth of Cut (mm)	Feed Rate (mm/min)	Spindle Speed (rpm)	Surface Roughness Average (μm)
1	0.05	10	200	1.0
2	0.1	10	200	3.0
3	0.05	20	200	4.2
4	0.1	20	200	2.8
5	0.05	10	400	0.8
6	0.1	10	400	3.9
7	0.05	20	400	4.2
8	0.1	20	400	5.6

6.4 Analysis and Discussion of Experimental Results

In this section, results obtained from the experimental study are analyzed. Emphasis will be given to the discussion of *What is the most important mechanism that best describes the material removal process?* Other topics include the control of surface finish quality, tool wear and tribological interaction(s) when chemicals are used as additives to the applied cutting fluid.

6.4.1 Interpretation of Cutting Mechanisms

The cutting mechanism observed during the machining of metals indicates that whenever a cutting tool cuts into a material, elastic deformation starts and three deformation zones are formed as stresses build. In the first, or primary, deformation zone, shear stress develops and elastic and plastic deformations occur to form chips. In the second zone, or the interface between the tool rake face and chip, normal pressure and friction action develop. In the third zone, the tool flank face slides over the machined surface at the cutting speed rate. The unit cutting force that is needed to carry out the material removal process can be estimated from the ultimate tensile strength of the material being machined. In most cases, the ratio of the unit cutting force to the ultimate tensile strength ranges from 1.5 to 4 when the chip compression factor is kept below 2 [Kr 66].

In the machining of aluminum oxide, these three zones are also present. However, the cutting mechanism is mostly characterized by brittle fracture, not by plastic flow although plastic flow and elastic deformation can be observed. It

can be assumed that the tool, traveling across the workpiece surface, acts like an indenter to compress the material, thus inducing the compressive stress to form the three deformation zones [EvMa 80]. As the compressive stress builds up in the cutting zone, crushing and chipping are produced by brittle fracturing through stress wave propagation. Consequently, the indentation fracture chip formation process will result in severe surface damage and sub-surface damage. Therefore, controlling the fracture chip formation process and limiting it within a certain range is a key issue during the machining of ceramic materials.

The results from our experimental investigation strongly support this assertion. The first evidence is that the unit cutting force calculated from the measured cutting force data is far above the ultimate tensile strength of the aluminum oxide material being machined. As indicated in Table 6.2, the average of the calculated unit cutting forces at the 8 testing conditions is about 61 GPa, which is 6 times as high as 359 MPa of the flexural strength of aluminum oxide listed in Table 6.1. Therefore, the chip formation, or the material removal process can not be simply explained based on the metal cutting principles. In machining ceramic materials, there must be something significantly different from machining metals. Since the material removal process is dominated by the fracture mechanism, we apply theory of fracture mechanics to study the machining process. The unit cutting force should be interpreted as the minimum threshold load to the occurrence of cracking and fracturing. As a parallel approach to Evans and Marshall's work [EvMa 80], the unit cutting force and the cutting force produced during machining, as we suggest, can be predicted

by the following two formulas:

$$\text{Unit Cutting Force} = C\left[\frac{H^2}{K_c}\right]\sqrt{r} \tag{6.1}$$

and

$$\text{Cutting Force} = C\left[\frac{H^2}{K_c}\right]\sqrt{r}A \tag{6.2}$$

where H and K_c represent the hardness and fracture toughness of ceramic material to be machined, and their units are in N/m^2 and $N/m^{3/2}$, respectively. The parameter r in these equations represents the average grain size of the ceramic materials to be machined and parameter A represents the cutting area. The proportionality coefficient, C, in Eqs. 6.1 and 6.2 characterizes the effect of machining parameters on the minimum threshold load. Its numerical values can be estimated from experiment. For example, using the data provided in Tables 6.1 and 6.3, $C = 0.65$ for test 1 and $C = 0.50$ for test 2. The difference $(0.50 - 0.65 = -0.15)$ between these two values of the proportionality coefficient indicates the effect of depth of cut on the unit cutting force with negative sign indicating a decrease of the unit cutting force as depth of cut increases. Using the design of experimentation technique, an empirical model to estimate the proportionality coefficient in our investigation can be obtained [Box. 78] and is given by

$$\begin{aligned} C \;=\; & 0.55 - 0.07(\text{Depth of Cut}) - 0.16(\text{Feed}) + 0.10(\text{Spindle Speed}) \\ & +0.02(\text{Depth of Cut} \times \text{Feed}) - 0.03(\text{Feed} \times \text{Spindle Speed}) \end{aligned} \tag{6.3}$$

where the values for Depth of Cut, Feed, and Spindle Speed are in the *design*

unit, i.e., -1 or +1 for low or high levels as listed in Table 6.2. From this empirical model, the negative values of main effects associated with depth of cut and feed indicate that increase of depth of cut or feed will reduce the unit cutting force, and the machining parameter feed seems more effective in the reduction. On the other hand, increase of cutting speed seems to increase the unit cutting force. The numerical values associated with two-factor interactions elucidate the interplay of the three machining parameters on the unit cutting force. Therefore, such an empirical model provides a useful method to set the machining parameters in order to achieve a desired unit cutting force, or a desired minimum threshold load for the purpose of quality and productivity assurance.

6.4.2 Evidence of Plastic Flow during Machining

When the stress developed in the machining region, such as in the second zone on the tool rake face, is below the loading threshold, plastic flow of chip occurs. When the temperature is high, plowing on the back of ceramic chips can be observed. Figure 6.6 is the picture taken from the back of an aluminum oxide chip using SEM. The chip was collected under a machining condition where the temperature measured in the cutting zone was about $750°C$. The smoothness of the chip back surface and plowing tracks on the back surface indicate that the ceramic chip material once was softened under high cutting temperature when it passed through the tool cutting point. Unlike the machining of metals, at high temperature, especially temperature higher than half of the melting point, atomic mobility starts to become significant and behaviors, such as diffusional creep and dislocation climb, start to become possible, even leading to occurrence of severe inter-granular fracture [Do. 91]. Under such circumstances, plastic

flow and inter-granular fracture could increase their contribution to the chip formation process. This contribution could explain the observation that increase of cutting speed leads to a high value of unit cutting force. On the other hand, the increased plastic flow and inter-granular fracture should reduce the cutting force variation, and therefore, attenuate tool vibration. As a result, a better surface finish quality should be anticipated when using a high cutting speed to machine ceramic materials.

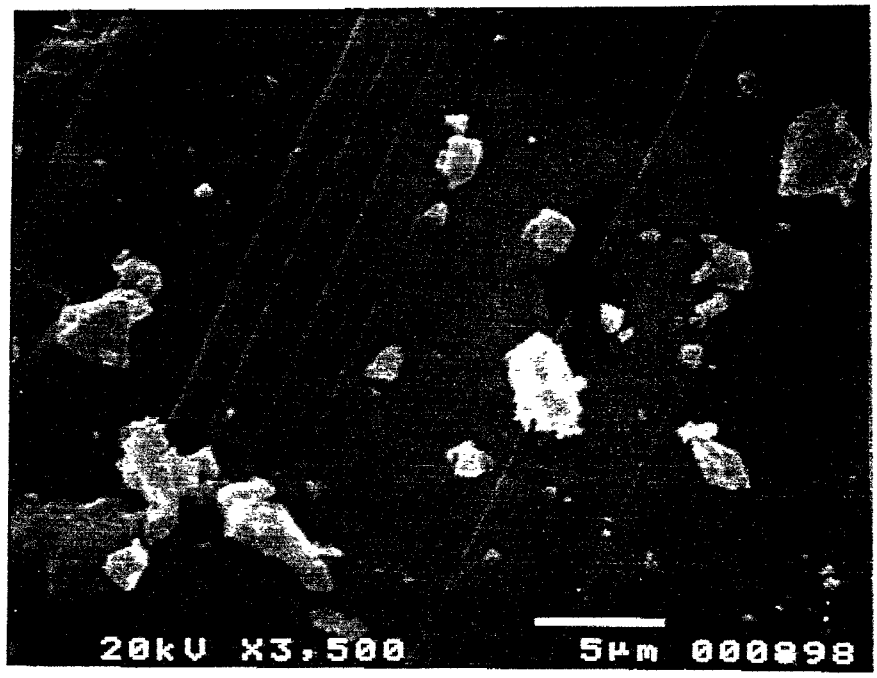

Figure 6.6: Back of a Collected Alumina Chip Showing Signs of Plastic Flow

6.4.3 Relations between Finish Quality and Machining Parameters

By examining the profiles shown in Fig 6.4, the patterns of height variations never constitute the outline of the cutting edge geometry such as the nose radius of the cutting tool. In addition, they never show any tendency of the side and/or end cutting edge angles. The random nature of the height variation patterns suggests that brittle fracture is an essential mechanism to remove the ceramic material when it is being machined.

To gain a deep understanding of the surface generation during machining, chips were collected during machining. Figure 6.7 displays the two types of chips collected during two machining tests with different feed settings. It is evident that the larger the feed setting, the larger the average size of chips which corresponds to a rougher surface after machining.

The effectiveness of using chemical additives to improve surface finish quality can also be evidenced by comparing the six profile traces taken from two machined surfaces. With the presence of chemical additives, both the roughness average values ($0.7\mu m$, $0.8\mu m$, and $0.9\mu m$) and their variation are reduced from the roughness average values ($0.8\mu m$, $1.0\mu m$, and $1.3\mu m$) when the distilled water based cutting fluid was used during machining.

6.4.4 Tribological Interactions

In our preliminary study, distilled water was used as a cutting fluid for the purpose of improving the machining performance. First, water takes away a huge amount of heat generated during machining, leading to a longer tool life.

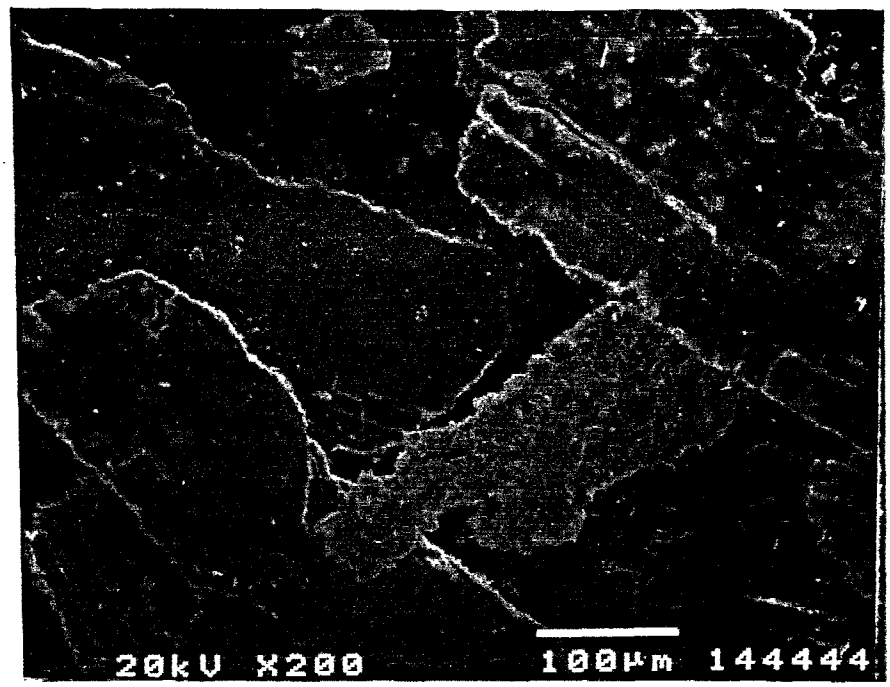

a. Alumina Chips Collected under Cutting Test No. 5 with Distilled Water

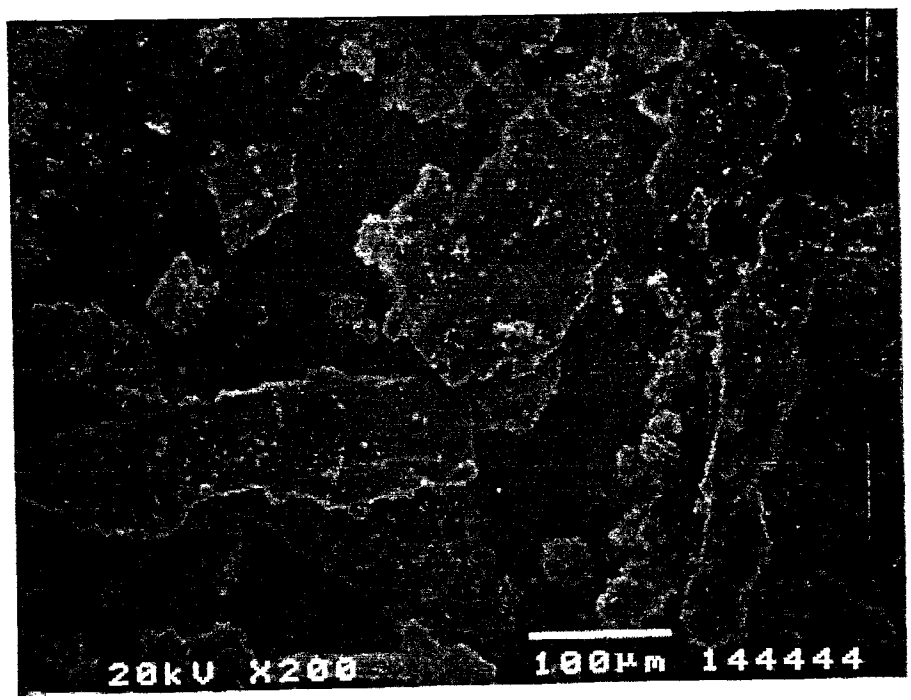

b. Alumina Chips Collected under Cutting Test No. 7 with Distilled Water

Figure 6.7: Comparison of Chips Collected under Different Cutting Conditions

Second, the tribochemical interactions between water and alumina could provide other favorable effects with respect to improving machining performance. In fact, water has been found to exhibit significant effects on the tribological behavior of alumina in the previous study [Ga. 89]. For example, a film-like substance has been found on the wear surfaces of water lubricated alumina , suggesting the possibility of tribochemical reaction between water and alumina in the contact junction. It has been found that at a temperature about $200°C$, aluminum oxide hydroxide (boehmite, $AlO(OH)$) is formed, while at a temperature about $100°C$, the formation of aluminum trihydroxide (bayerite, $Al(OH)_3$) is favored.

To explore the benefits from possible tribological interactions, four types of cutting fluids were tested during machining in this research. As mentioned earlier, the cutting fluid demonstrating the most effectiveness in improving surface finish quality was the water-based cutting fluids with selected chemical additives. It is interesting to report in this paper that the most prominent characteristic when the chemical additives were present is that the ratio of the tangential cutting force component to the feed force component changes significantly while the resultant cutting force, before and after addition of chemical additives, remains unchanged. Such a ratio has been termed as coefficient of friction in engineering. By examining the data of the cutting force measurements listed in Table 6.3, it is evident that the tangential cutting force, or the friction force, is reduced and the feed cutting force, or the normal force, is increased, thus reducing the value of the coefficient of friction. In machining science, the value reduction of coefficient of friction means a change of the action direction of the resultant cutting force with respect to the machined surface. A small ratio, or a small coefficient of friction, indicates that the resultant cutting force action

will produce higher compressive stress in the machining region. Not only does it increase the machining efficiency, but also it keeps the cutting tool within the cutting zone in a more stabile fashion. Such an action attenuates tool vibration effectively and ensures a better finish quality of the machined surface. Figure 6.8 illustrates the effect of the triboligical Interactions on improving the machining performance [Zh. 92]. Figure 6.9 displays the measured roughness average R_a values from milling Dicro/MGC materials under the 16 tests when the two cutting fluids were used. The results of getting a better surface finish when chemical additives were used further confirms the effectiveness of using the chemical-assisted machining technique.

6.4.5 Tool Wear

When machining engineering materials, tool wear is one of the key concerns. When machining ceramic materials with low hardness like Dicor/MGC, adequate tool life can be maintained. However, when machining such ceramic materials as silicon carbide, silicon nitride, and aluminum oxide, tool life will be the top concern. In fact, the high cost of machining has been the major barrier to widespread introduction of advanced structural ceramics.

In machining science, wear mechanisms have been known for long. In this study, emphasis is given to the cutting tools coated with synthetic diamond films, which provide superior hardness, wear-resistance, and thermal conductivity. The observation from our research dictates that the first important issue is surface roughness of the synthesized diamond coating. Figure 6.10 provides pictures taken during the initial and final stages of tool wear during the machining of the aluminum oxide bars. By examining the progress of tool wear on the rake face,

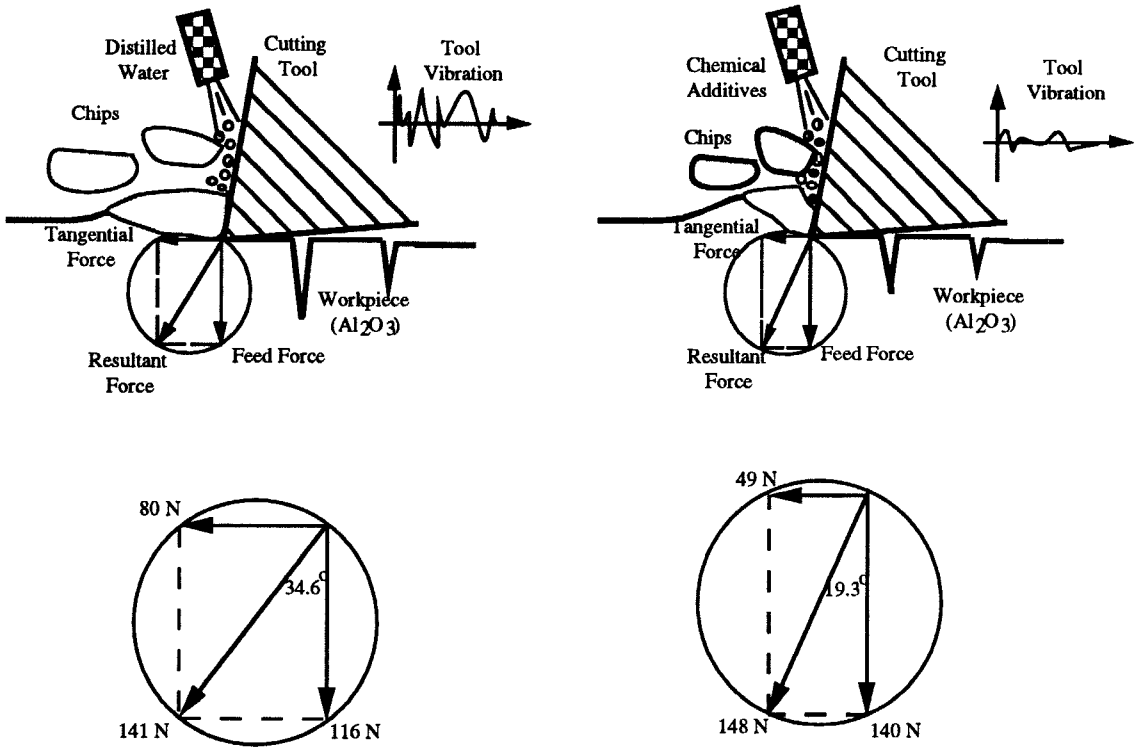

a. A Large Ratio of the Tangential Cutting Force to the Feed Cutting Force when using Distilled water as Cutting Fluid

b. A Small Ratio of the Tangential Cutting Force to the Feed Cutting Force when Chemical Additives added to Distilled Water

Figure 6.8: Effect of Chemical Additive on Forces during Machining

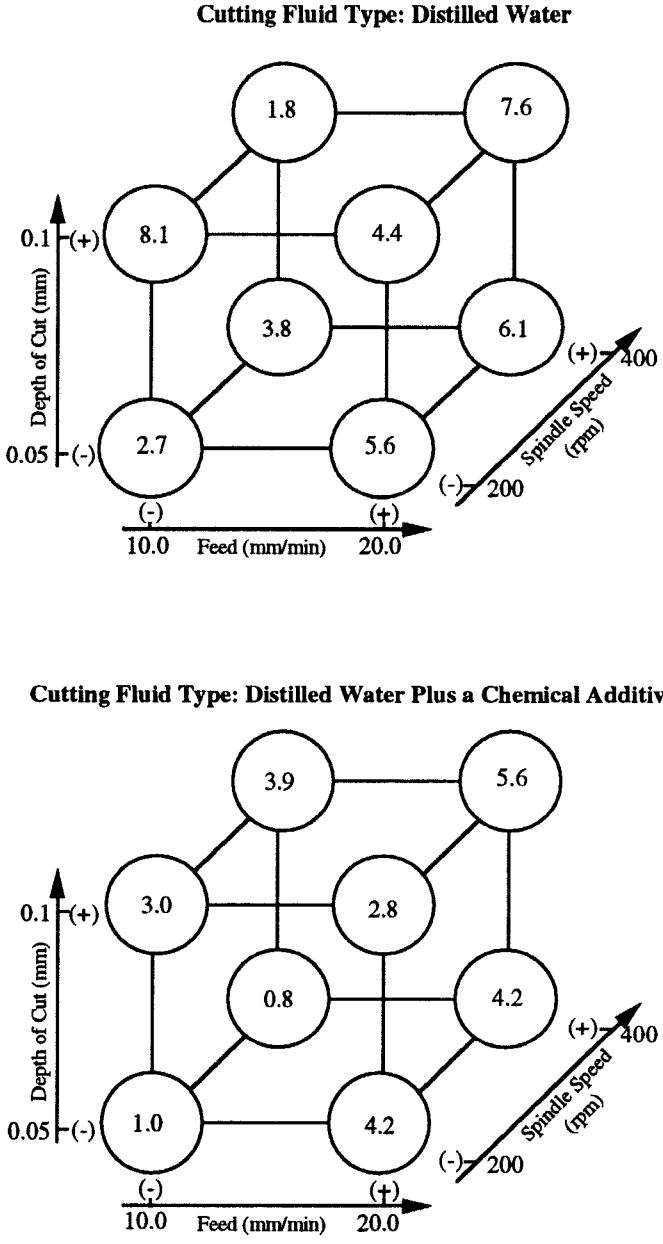

Figure 6.9: Roughness Average (μm) from Milling the DICOR

abrasive wear and adhesive wear are obvious. For controlling the abrasive wear, the surface finish quality of a coating is extremely important. We purchased the coated tools from two suppliers with roughness average values of 1.5 μm and 3.5 μm, respectively. A comparison was made by using the two types of tool under the identical machining conditions. The tool life of the coated tool with $R_a = 1.5\mu m$ is, at least, twice as long as the tool life of the tool with $R_a = 3.5\mu m$ in all cases. The explanation would be simple because of the chip flow over the rake face. A rougher surface increases abrasive wear significantly. Therefore, attention should be paid to controlling the diamond grain size for a smooth rake face.

For controlling adhesive wear, it is extremely important to control the temperature and an increase in the film bonding force will help significantly. It is well known that diamond is a thermodynamically unstable phase of carbon. At the machining region where temperature is highly elevated, the transformation of diamond to a more stable form, for example, carbon-graphite, is unavoidable [Ja. 89]. The hardness loss due to in-situ formation of graphite may cause the formation of crater wear on the rake face and wear land on the flank face. Under the high contact load exerted by the machining action, the bounding force may loose its control to hold the synthetic diamond coating on tool insert. The tool failure observed during machining is often a complete loss of the coating by stripping action.

Premature tool failure can easily occur if the three machining parameters are not set properly. To keep material removal rate below a certain limit in machining ceramics is critical because an excessive cutting force will cause malfunction of machine tool due to its power insufficiency and damage the

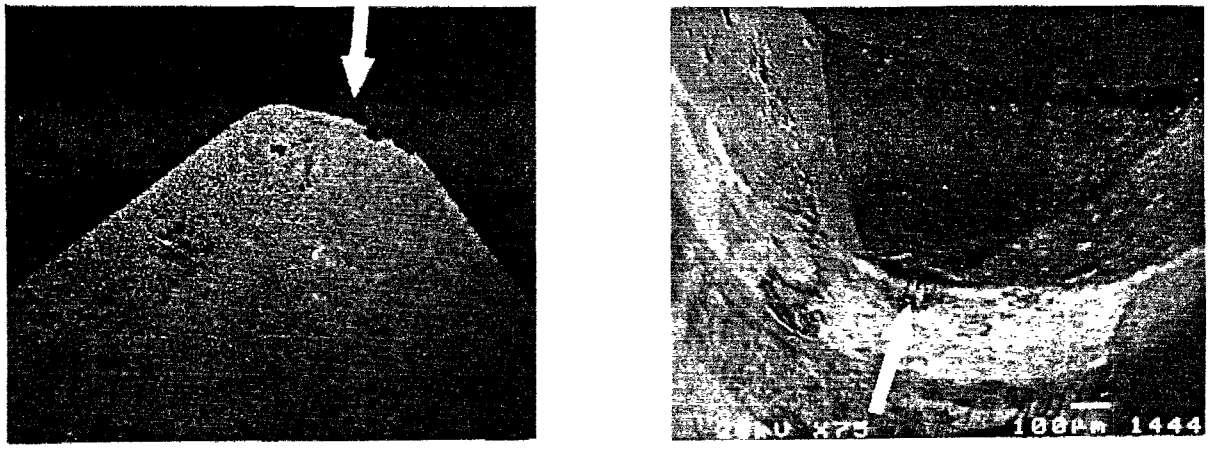

a. Tool Wear at the Initial Stage where the Arrows Show the Direction of Projection under Microscope

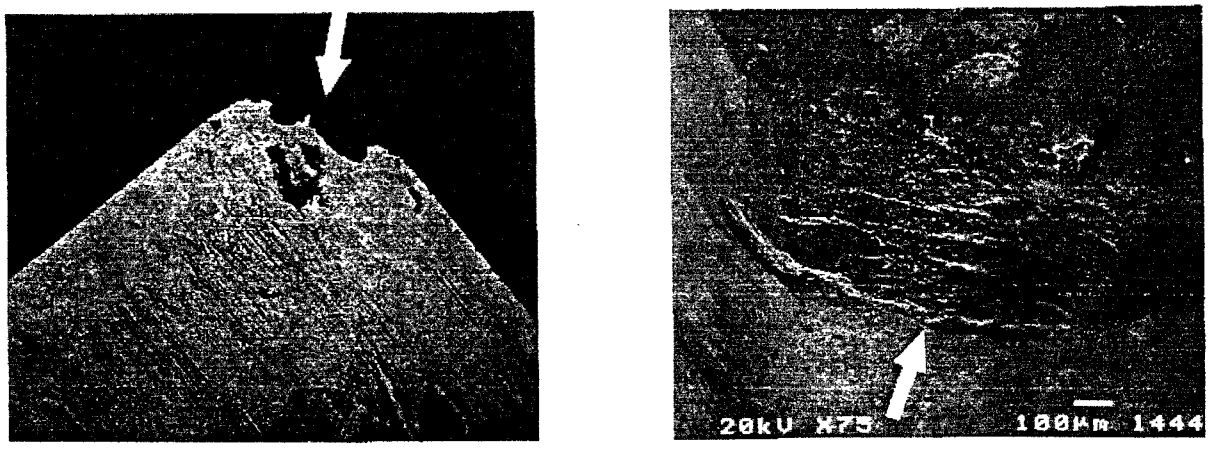

b. Tool Wear at the Severe Stage where the Arrows Show the Direction of Projection under Microscope

Figure 6.10: Evidence of Tool Wear in Two Different Stages

cutting tool easily. The concept of unit cutting force or minimum threshold load developed in this research provides a useful method to estimate the material removal rate per horse-power or the necessary bonding force to ensure that a synthetic diamond coated tool works properly.

6.5 Summary

In this research, a fundamental study related to the machining of engineering ceramic materials is conducted. Synthetic diamond coating tools are used to machine aluminum oxide and high-speed steel end mills are used to machine Dicor/MGC glass-ceramic material. This investigation involves cutting force measurement, a study of the chip formation process, assessment of surface finish quality, and a study of tool wear. The results are summarized as follows.

1. The results indicate that brittle fracture is the major mechanism during the material removal process. There exists a minimum threshold loading limit that distinguishes the fracture mechanism from the plastic flow mechanism. Such a limit is dependent on the material being machined, machining parameter selection, and the machining environment. The concept of unit cutting force is re-introduced to establish a quantitative relationship among these parameters involved in the machining system. The established formula has thrown deep insight into controlling the machining process for the purpose of improving machining quality and efficiency.

2. Criteria for tool material selection are proposed through experimentation. A design of experimentation approach is used to perform a systematic

study of effects of the three machining parameters on the machining performance. Specific attention has been paid to chemical-assisted machining. It has been observed that the feed cutting force increases while the tangential cutting force decreases when a selected chemical additive is used. This leads to a reduction of friction coefficient and improves machining efficiency significantly. The effectiveness of using chemical additives through possible tribological interaction(s) points out a new direction to develop innovative technologies for machining ceramic materials.

Chapter 7

Conclusions and Future Work

7.1 Conclusions

The main objective of this research has been focused on the analysis of surface quality in machining of metals and advanced ceramics. Through this research, a stochastic approach for modeling the random excitation sources such as the workpiece microstructures has been developed to characterize the random tool motion during machining. A three-dimensional finite element model has been used to analyze the effect of elastoplastic deformation and recovery processes on the machined surfaces. By integrating the analytical work of this research, a computer-based surface topography simulator is devloped for simulating the machined surface texture. It is a powerful tool which can provide essential information for the design engineer and process engineer to improve the surface quality of a machined part and to enhance the process capability of a machining operation. Experimental tests were performed to verify the validity of the developed models and simulator. Results from both theoretical and experimental work are well matched. Study of the fundamental material removal mechanisms

in the machining of advanced ceramics has provided rich information about the basic principles of preparing machining operations to achieve a meaningful and practical machining process for advanced ceramics.

Important conclusions drawn from this research are as follows:

1. In the stochastic modeling for the characterization of random tool motion during machining, a Markov-chain based stochastic approach is developed to model the random tool motion as the response of a machining system under random excitation. By introducing the *group distributions*, *segment model*, and *transition model*, a specific microstructural distribution pattern of the workpiece material can be modeled by the stochastic approach and quntitatively related to the cutting dynamics in machining. A method has also been developed to determine the states and state transition probabilities defined in the transition model. The significance of this research is that it provides a stochastic approach to quantify the random tool vibration during machining, a task which nowadays seems difficult but critical for developing sensor-based machining systems to improve the quality and productivity in the manufacturing industry.

2. The elastoplastic deformation observed on the machined surfaces has been examined through a non-linear finite element method. An updated Lagrangian approach is applied to solve the large strain elastoplastic deformation problem using a three-dimensional finite element model which simulates a single-point metal cutting process. The obtained results are in reasonable, quantitative agreement with the experimental results when the average slopes of surface profiles (dq's) are compared. It has been shown

that the dq's have linear relations with the feed rate as well as the depth of cut (with opposite trends). On the other hand, soft materials (such as aluminum alloy or brass) tend to have less effect of plastical recovery on machined surfaces; thus, the average slopes are smaller and closer to the ideal ones as opposed to the hard materials (such as carbon steel). This phenomenon is also observed from the results of finite element analysis. This enlightens the necessity of applying the results from the finite element analysis as a surface texture modification model to enhance the accuracy of a surface texture simulator. It has been shown that the predicted dq's, an important index for tribological performance of mating parts, from the surface texture simulator can be improved by as much as 50% after such a modification.

3. A computer-based surface topography simulator is developed by integrating the above-mentioned analytical work with machining dynamics and metrology science. The topography of a machined surface through computer visualization, confirmed by experimental verification, vividly depicts the dynamic process of surface texture formation during machining. As a strong hold of the computer-based simulator, it is capable of generating the data representing a machined surface in a three-dimensional space characterized by the three machining parameters; i.e., depth of cut, feed, and cutting speed. The uniqueness of this data base is that it clearly defines the spatial relationships as a whole, rather than as a set of parallel profiles. As demonstrated in this study, this information is very useful for pushing the control of finish quality as well as the geometric dimensions

and tolerances in the design stage. If an accurate calibration of the system parameters is made, the developed prototype system can be used as a comprehensive metrological system for industrial control and diagnostics of the surface quality. This prototype system may also become an important component of a quality assurance system to perform in-process inspection for the certification of the machining process.

4. In the study of the material removal mechanisms in machining of advanced ceramics, the cutting force measurement, study of the chip formation process, assessment of surface finish quality, and study of tool wear have been performed. Based on the observed results, it is concluded that

   (a) Brittle fracture is the major mechanism during the material removal process. There exists a minimum threshold loading limit that distinguishes the fracture mechanism from the plastic flow mechanism. Such a limit is dependent on the material being machined, machining parameter selection, and the machining environment. The concept of unit cutting force is re-introduced to establish a quantitative relationship among these parameters involved in the machining system.

   (b) Criteria for tool material selection are proposed through experimentation. A design of experimentation approach is used to perform a systematic study of effects of the three machining parameters on the machining performance. Specific attention has been paid to chemical-assisted machining. It has been observed that the feed cutting force increases while the tangential cutting force decreases if a selected chemical additive is used. This leads to a reduction of friction coef-

ficient and improves machining efficiency significantly. The effectiveness of using chemical additives through possible tribological interaction(s) points out a new direction to develop innovative technologies for machining ceramic materials.

7.2 Future Work

The following directions are suggested to extend the understanding of fundamentals in machining of metals and advanced ceramics.

1. An algorithm should be implemented into the evaluation of the transition probabilities of a given microstructure to guarantee that the basic Markov chain property as defined in Eq. 3.1 is satisfied. On the other hand, the Markov-chain based stochastic approach along with the sample variance theory could be further applied to the machining of materials which have certain specific trends in their microstructures; e.g., advanced composite materials where the orientations of fibers are important, and composite alloys where small "whisks" of fibers are added into alloys to strengthen the material.

2. In the three-dimensional finite element model, the effect of stress wave propagation on the workpiece material during high speed machining processes could become essential for further understanding of the elastoplastic deformation process observed on machined surfaces.

   On the other hand, the frictions between tool-work or tool-chip interface under low cutting speed, the effect of built-up edges and tool wear phe-

nomenon can also be considered in the model to account for more complex machining conditions.

3. Further improvement of the computer-based surface topography simulator could be done to make it a practical tool for design engineers and production engineers. Possible areas for improvement are:

   (a) adding features such as a more user-friendly interface,

   (b) improving the estimation of system parameters such as the machine tool structural dynamics,

   (c) integrating other machining processes such as drilling, milling, boring, and grinding to the simulator, and

   (d) creating a machining database system for process capability analysis.

4. In the research of machining of advanced ceramics, more effort can be paid to the following areas:

   (a) the study of fracture mechanics through finite element method,

   (b) the search of more efficient chemo-assisted machining processes, and

   (c) the creation of a ceramic machining database system for practical applications such as the machining of dental materials.

Appendix A

Derivation of b_i's

Equation 3.12 can be rewritten as

$$\underline{b}\Pi = \underline{\pi}\Gamma \tag{A.1}$$

where $\underline{b} = [b_1, b_2, ..., b_{N-2}]$, Π is a $(N-2) \times N$ matrix defined as

$$\Pi = \begin{bmatrix} \pi_2 & 0 & -\pi_2 & 0 & 0 & ... & 0 \\ 0 & \pi_3 & 0 & -\pi_3 & 0 & ... & 0 \\ 0 & 0 & \pi_4 & 0 & -\pi_4 & ... & 0 \\ ... & ... & ... & ... & ... & ... & ... \\ 0 & ... & ... & 0 & \pi_{N-1} & 0 & -\pi_{N-1} \end{bmatrix} \tag{A.2}$$

and Γ is a $N \times N$ matrix defined as

$$\Gamma = \begin{bmatrix} (1-p_{11}) & -(1-p_{11}) & 0 & \ldots & 0 \\ 0 & (1-p_{22}) & -(1-p_{22}) & \ldots & 0 \\ \ldots & \ldots & \ldots & \ldots & \ldots \\ 0 & \ldots & 0 & (1-p_{N-1\,N-1}) & -(1-p_{N-1\,N-1}) \\ 0 & \ldots & 0 & -(1-p_{NN}) & (1-p_{NN}) \end{bmatrix} \tag{A.3}$$

The matrices Π and Γ can be estimated based on the estimations of π_i's and p_{ii}'s as derived in the Eqs. 3.13, 3.10, and 3.9, respectively. In other words, $\hat{\Pi} = \Pi(\underline{\hat{\pi}})$ and $\hat{\Gamma} = \Gamma(\underline{\hat{p}_{ii}})$. Finally, the $\underline{b}$ can be estimated by minimizing the mean square error of $(\underline{b}\Pi - \underline{\pi}\Gamma)$; i.e., choose $\underline{b}$ such that

$$\| \underline{\hat{b}}\hat{\Pi} - \underline{\hat{\pi}}\hat{\Gamma} \| = \min (\| \underline{b}\hat{\Pi} - \underline{\hat{\pi}}\hat{\Gamma} \|)$$

where $\| \cdot \|$ stands for the mean-squared norm. Actually, the solution for $\underline{\hat{b}}$ is given by

$$\underline{\hat{b}} = \underline{\hat{\pi}}\hat{\Gamma}\hat{\Pi}^T(\hat{\Pi}\hat{\Pi}^T)^{-1}. \tag{A.4}$$

Appendix B

Microstructural Analysis Procedure

A procedure to perform the microstructural analysis of workpiece materials is discussed in this appendix. Tables and figures appeared in this report are based on the raw data of experiments or measurements.

Materials Preparation

The workpiece materials under investigation are 6061-T6 aluminum-ferrous-silicon alloy bar, AISI 1020 rolled steel bar, and Copper-Aluminum alloy bar (aluminum bronze, designation not available). All of these bars have the same diameter (76.2 mm) and length (304.8 mm). They were purchased from the physics shop at the University of Maryland at College Park.

Specimen Sectioning, Mounting, and Grinding

In order to perform the microstructural analysis of different workpiece materials, each of the samples taken from the materials should be well prepared. Listed below are the steps performed to prepare the samples:

1. A slice of 12.7 mm thick specimen is cut from each bar.

2. Sections are taken from each slice of the materials. The size of each section is about $8\,mm \times 8\,mm$.

3. Each section is oriented either along the cross-sectional or longitudinal direction of the original bar and is placed into a plastic mold cup. A mixture of epoxy and solidifier (4:1) is prepared and poured into the plastic mold cup which contains the section. The mixture is solidified after 24 hours. The sample which contains the section and solidified epoxy is taken out of the mold. Designation are marked on the 'back' of each sample to distinguish its material type and orientation from others. SiC papers (sandpapers) with grit numbers $240 \sim 600$ are used one after another to manually grind the surface of each sample. Cares should be taken during the process such that the surface of each sample is flat, and scratch marks on the surface should be minimized. For example, a) an extremely flat surface should be used as the platform for grinding, b) running water should be applied frequently during grinding to wash away the debris generated from grinding, and c) the direction of grinding should be kept the same when a new sandpaper with a specific grit number are used during the course of grinding.

Figure B.1 shows some of the samples prepared in this study.

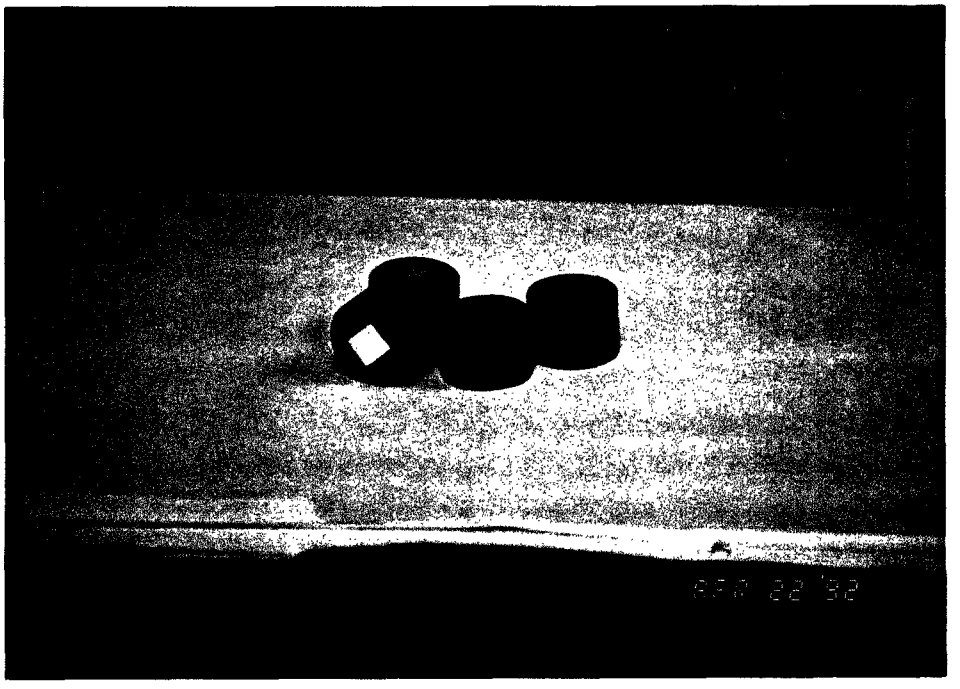

Figure B.1: Prepared Samples

Polishing and Etching

Both rough and fine polishing processes follow the grinding process. The purpose of polishing is to remove the scratch marks left on the sample surface produced from grinding and provide a very fine surface for further process. The ground surface of a sample is manually held in contact with a low-nap cloth which is attached to a wheel of the polishing machine. The rotational speed of the wheel as well as the polishing solution are selected depending on the conditions of sample surface. If the sample surface is rough, a 6 mm diamond paste diluted with acetone should be used as the polishing solution, and the speed of wheel should be selected to 'high' during polishing. A 1.0 or 0.3 μm alumina (Al_2O_3) powder solution can be applied if the sample surface is smooth after a rough polishing. The speed of the wheel, however, is selected to 'low'

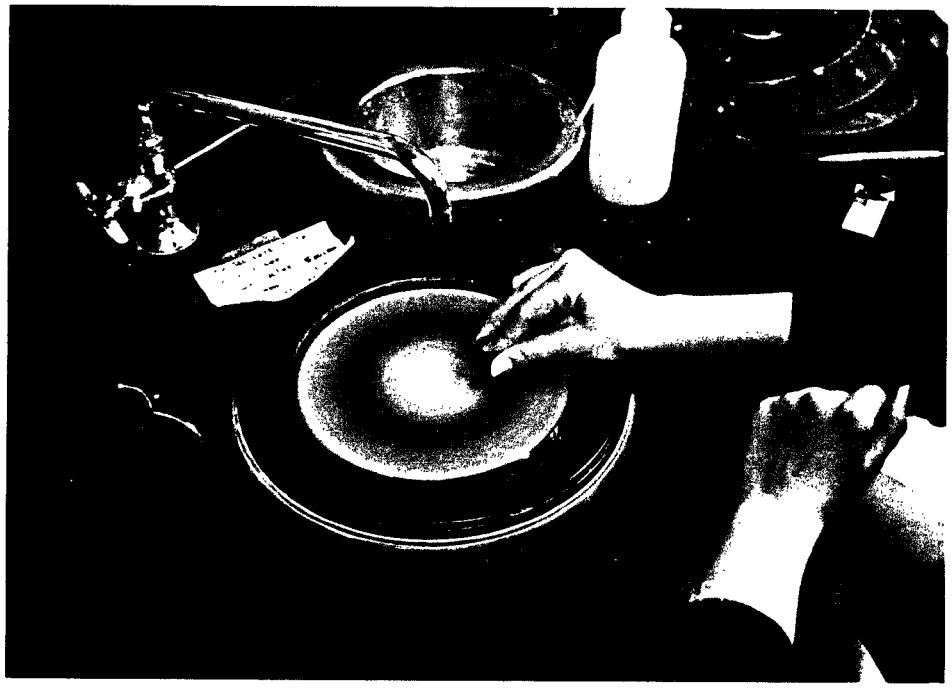

Figure B.2: Polishing a Sample

in this case to prevent 'over-polish' of the sample surface, a common problem encountered by a novice. Figure B.2 displays a polishing process.

After polishing, the sample surface is etched by an etchant to produce a very clear surface of the microstructures of the sample. There are a lot of different combinations of etchants can be used for a single material. It should be noted that other etchants might be more suitable for revealing different microstructures in the same material. A detailed reference of choosing etchants can be found in [Va 84]. Table B.1 is a list of the etchants applied in this research. When preparing the etchants, extreme care should be taken for handling the chemicals since most of them used as etchants are harmful to the animal, human, and environment. Gloves and special garments are also necessary when handling any of these chemicals. A well ventilated chamber covered with a hood is necessary to provide a proper location for preparing the etchants. The etched samples

should be kept in a cool and dry container (if vacuumed will be the best) to prevent oxidation on the surface.

Table B.1: List of Etchants Used for Etching Different Materials

Etchant Composition	Comments
Etchant for Iron and Steel: $1 \sim 10$ *ml* HNO_3 $90 \sim 99$ *ml* ethyl alcohol	*Nital*: Most common etchant for Fe, carbon and alloy steels, and cast iron. Reveals alpha grain boundaries and constituents. The 2% solution is most common, $5 \sim$ 10% used for high-alloy steels (use fresh). Use by immersion of sample for up to 60 sec (Boylston).
Etchant for Aluminum and Alloys: 2.5 *ml* HNO_3 1.5 *ml* HCl 1.0 *ml* HF 95 *ml* distilled water	*Keller's reagent*: A very popular general-purpose reagent for Al and Al alloy, except high-Si alloys. Immerse sample $10 \sim 20$ sec, wash in warm water. Can follow with a dip in conc. HNO_3. Outlines all common constituents, reveals grain boundaries in certain alloys.
Etchant for Copper and Alloys: 60 *ml* NH_4OH 30 *ml* H_2O_2 (3%) or 5 *g* $FeCl_3$ 15 *ml* HCl 60 *ml* ethyl alcohol	*General-purpose grain-contrast etch* for Cu and alloys (does not always produce grain contrast). Use fresh, add peroxide last. Swab sample $5 \sim 45$ sec. or Use by immersion or swabbing of sample. This special solution is for Al bronze.

Microstructural Image Processing

Photographing the Microstructures

At this stage of the microstructural analysis, the etched sample is placed either under an optical microscope or an electronic microscope depend on the type of information needed from the microstructures. For example, if a qualitative or quantitative element identification of a material or a very high magnification of the image is required, a scanning electronic microscope (SEM) might be the choice. A scanning electron microscope (JSM-5400) is used for this purpose. Figure B.3 shows the SEM used in this research.

Figure B.3: The JSM-5400 Scanning Electron Microscope

A Polaroid film is used when taking pictures from the image under microscope (optical or SEM). A high quality picture of the image under different magnification can be instantly taken if the brightness of the image, the exposure time,

as well as the development time are properly chosen. For example, when taking a 200x magnification picture, the optimal exposure time is 2 seconds, and the development time is about 25 seconds. In general, the higher the magnification, the longer exposure time (or higher brightness) is required to get a good picture. If more copies of the picture are needed, the negative attached with the film should be kept and immersed immediately in a 'Perma Wash' solution.

Picture Scanning and Image File Conversion

The pictures of each sample taken under the microscope are then scanned by a scanner. The purpose of the scanning is to digitize the images and convert the image files to binary ones for further analysis. The scanner is connected with a Macintosh II computer. A special software is required for running the scanner. In the software, several parameters can be set to control the resolution, brightness and contrast, image pattern, and size of the scanned images. For example, in this research, a 'line art' type of image is the best choice for the pictures of steel since most of the microstructures can be easily distinguished (either dark clusters of pearlite or bright clusters of ferrite) under this choice. The size of the scanned image should be reduced by 50% of the original picture size to maintain a smaller file size (without losing a good resolution of the picture) if the computer storage space as well as the CPU time for further analysis are restrained by the system.

When all the pictures are scanned and saved under the required format, namely, a so called 'TIFF' format, theses image files are then transferred (using the binary mode) through the network (TCP/IP) to a computer system which supports the software packages for further analysis. The Unix system on campus has such an environment. One of the image processing packages needed is called

'pbmplus'. This package has utilities which can convert files between the most popular image formats. The file format used in this analysis is called 'bitmap', which contains only 0's (white) and 1's (black) of the image. An example to perform the conversion is listed below for reference.

- *Example 1*: Image file conversion between TIFF and bitmap format. Suppose that an image file after scanning is called TEST.tiff and has been successfully transferred to the Unix system under the user's subdirectory (assuming that the directory which contains the image file is called /mydir). The following steps will convert the TIFF file format to a bitmap one:

  1. Find the location (path) where the 'pbmplus' package resides; e.g., /picasso/pbmplus).
  2. Change the current directory to that subdirectory type:

     ```
     cd /picasso/pbmplus
     ```

     and hit return.
  3. Type:

     ```
     tifftopgm  /mydir/TEST.tiff | pgmtopbm > /mydir/TEST.pbm
     ```

     and hit return.
  4. The output of the above command is the TEST.pbm file, which contains the 0's and 1's of the scanned image file, TEST.tiff.

Hardness Tests

The purpose of measuring the hardness values of different materials is to acquire both the macrohardness and microhardness values which are necessary for modeling the effects of microstructures of workpiece materials on the dynamic cutting force variation during machining.

Rockwell Hardness Tests

The hardness of different materials was measured under a Rockwell hardness testing machine. Table B.2 lists the measured hardness of different workpiece materials. The measured hardness will be applied as a reference for checking the microhardness, which will be discussed in the next section, of different microstructures within each material. Table B.2 gives the average hardness values of different materials. These numbers are then converted to the equivalent Brinell hardness numbers based on the information provided in the reference [Sm. 83].

Vickers Microhardness Tests

Microhardness of different microstructures within each material was measured under a Vickers microhardness tester. A Vickers diamond indenter was forced into the surface of the test piece with a load of 100 gram-force (gf). The microhardness tester should be calibrated carefully by checking the microhardness of a test block provided by the manufacturer of the tester. The calibration can correct the error about the load which will be applied during the test. It is important that the test should be performed under constant ambient temperature and atmospheric pressure (e.g., $25°C$, 1 atm), and any disturbance

Table B.2: Measured Rockwell Hardness Numbers of Different Materials

Steel Bar	Aluminum Alloy Bar	Copper Alloy Bar
Scale A2, Brale 60 kg (RHN)	Scale B, $\frac{1}{16}$" Ball 100 kg (RHN)	Scale B, $\frac{1}{16}$" Ball 100 kg (RHN)
53.00	43.60	25.80
54.00	43.20	15.90
53.50	44.70	20.40
53.30	45.80	11.90
49.30	46.50	14.20
52.00	48.10	18.50
53.50	48.50	21.50
52.70	48.80	21.40
53.90	46.90	16.10
51.20	46.40	8.90
52.60	49.00	13.00
52.30	49.20	22.10
54.00	49.10	19.60
52.90	49.30	21.30
52.20	49.20	15.20
52.30	47.30	20.20
51.40	47.00	18.50
51.60	48.20	23.80
53.00	43.00	16.40

due to vibration should be avoided. The following equation gives the Vickers hardness number from the test:

$$VHN = 1854.4\frac{P}{d^2} \tag{B.1}$$

where P is the applied load in gf, d is the mean length of the diagonals of the indentation in μm. Table B.3 shows part of the measured microhardness values of different microstructures in the AISI 1020 steel.

Table B.3: Measured Vicker's Hardness Numbers of an AISI 1020 Steel Sample

Type of Microstructure	d_1	d_2	d_{mean}	d_{mean} in μm†	VHN‡	BHN§
Ferrite	216	220	218.00	33.40	138.57	132
Ferrite	208	200	204.00	31.25	158.25	150
Ferrite	213	202	207.50	31.79	152.95	146
Ferrite	214	229	221.50	33.93	134.23	128
Ferrite	219	217	218.00	33.40	138.57	132
Ferrite	212	211	211.50	32.40	147.22	140
Ferrite	207	205	206.00	31.56	155.19	147
Pearlite	201	190	195.50	29.95	172.31	164
Pearlite	188	188	188.00	28.80	186.33	177
Pearlite	197	184	190.50	29.18	181.47	172

†They are converted based on the calibration factor of different magnification under the microscope; e.g., $d_{mean}(\mu m) = 0.1532 \times d_{mean}$ is used in this measurement.
‡The Vicker's hardness numbers are evaluated based on Eq. B.1, where the load was about 83.35 gf.
§The equivalent Brinell Hardness Numbers are converted based on the table from ASTM-E140 [Sm. 83].

Appendix C

Cutting Dynamics in Microscale

General View of Cutting Force Generation

Common sense dictates that the cutting force is generated immediately after the cutting tool digs into the workpiece material. Metal shearing theories have been well accepted to explain cutting mechanics. As an initial approximation, the magnitude of the nominal cutting force is taken to be proportional to the cutting area, A_c, or the nominal chip load (a product of feed, f, and depth of cut, d); i.e.,

$$F_{nominal} = K_s \times A_c = K_s(f \times d) \tag{C.1}$$

where the proportionality coefficient, K_s, is named as the unit cutting force. Results from empirical metal cutting research have already shown that the unit cutting force, K_s, is directly related to cutting conditions such as workpiece material, tool geometry, and the cutting parameters, feed (f), depth of cut (d), and cutting speed (v). For example, the unit cutting force for machining carbon steel ranges from 2000 MPa to 2600 MPa, while that for machining aluminum alloys ranges from only 700 MPa to 900 MPa. However, the unit cutting force

can be treated as a constant under a specific set of known cutting conditions. Consequently, the cutting force evaluated based on Eq. C.1 is called the nominal cutting force.

The cutting force generated during machining is a vector quantity and thus possesses its own distinct direction. This direction plays an important role in the determination of machining performance. As a typical example, one might utilize a negative rake angle to reduce, or even eliminate, tension in the tool surface, thereby reducing tool breakage. There has been substantial research, both analytical and experimental, on the determination of shear angle in the cutting zone [Shaw 84, Zo 65].

The evaluation of the generated cutting force in the previous research is in macroscale. It is a common practice to formulate the cutting force as a function of basic properties of the workpiece material (hardness and ductility), cutting parameters (f, d, v), and tool geometry. For overlapping cuttings, the surface modulation fed back through the regenerative mechanism to the cutting zone adds more dynamic variation to the cutting force. However, this variation is also dealt with in macroscale. The cutting dynamics in macroscale address stability of the machining system, the transient response of tool vibration, and the determination of the dynamic equilibrium position of the cutting tool. However, an inefficiency associated with the macroscale analysis of cutting dynamics is its failure to explain random tool motion observed during machining. This is due to the absence of analytical ground to support the establishment of a random excitation system capable of describing random tool vibration. As a result, there exists a pressing need to advance the study of cutting dynamics. One important aspect is to extend the cutting dynamics from the current macroscale study to

a microscale study, thus forming a scientific basis for the evaluation of random tool motion.

Basic Assumptions

Research of the cutting dynamics in microscale has been performed for many years [Kr 66, Shaw 84]. The photomicrograph of a partially formed chip confirmed the assumption that metal undergoes shearing strain in the cutting zone. Further study of cutting dynamics comes from the need for better control of machining accuracy. People have realized that a preheat-treatment, which alters characteristics of microstructures within the workpiece, may improve machinability of the workpiece material significantly. Additionally, proper selection of cutting data, such as feed, depth of cut, and cutting speed, seems to be an effective method to assure a high level of machining quality while maintaining high productivity. For quality control, on-line monitoring of the machining process, including tool life, has been proposed and implemented on some machine tools to reduce defects on a real-time basis. A key to the success of such a monitoring system is true detection of process deterioration and therefore elimination of false alarms. Since natural process variations are always present during machining, the separation of process deterioration, such as tool wear, from these natural variations is essential. This separation can be achieved by the integration of a quantitative prediction of the natural process variations and a statistical prediction of tool wear. The prediction of natural process variations can be based on a microscale analysis of the cutting process.

To evaluate the cutting force in microscale, the following two assumptions

are made.

1. The major cause of random variation of the cutting force during machining is the nonhomogeneous hardness distribution of the material being machined.

2. The random variation of the cutting force is mainly embodied in the variation of the magnitude of the cutting force. Thus, the direction of the cutting force remains unchanged or the directional changes due to the nonhomogeneous hardness distribution are too small to be of significance.

To validate the second assumption, the friction force between the chip and tool rake face in the second deformation zone is believed to dominate the determination of the direction of the cutting force. Factors related to the friction force are: chemical compositions of the workpiece and tool insert materials, cutting temperature, and tool geometry. The material hardness variation can hardly be related to the friction force variation. Consequently, the material hardness variation also may not be related to the variation of the cutting force direction.

Cutting Force Evaluation in Microscale

As presented in Fig. 3.1, the outside layer of the workpiece material will be removed after one revolution of the workpiece. In microscale, it may be imagined that the tool meets microstructures along its cutting edge instantaneously. The difference between the constituents of the microstructures removed at any two instants can be anticipated. A technique to take this measurement would be of great value since it would enable the evaluation of the instantaneous cutting

force.

Microstructural Analysis

In order to quantify the effects of basic material properties, such as microhardness variation on the cutting force generation, metallurgic identification of the microstructures present in the material is essential. After measuring the microhardness value for each identified microstructure, the three statistics, μ_a, σ_a^2, and $\rho(r)$ can be calculated as follows [Zh 86].

$$\mu_a = \frac{1}{N}\sum_{i=1}^{N} H_i \tag{C.2}$$

$$\sigma_a^2 = \frac{1}{N}\sum_{i=1}^{N}(H_i - \mu_a)^2 \tag{C.3}$$

$$\rho(r) = \frac{\sum_{i=1}^{N}\sum_{j=1}^{N}(H_{i,j} - \mu_a)[(H_{i,j+r} - \mu_a) + (H_{i+r,j} - \mu_a)]}{K\sigma_a^2} \tag{C.4}$$

where $H_{i,j}$ = microhardness value at the location (i, j); K = the total number of summation operations in the above equation, which depending on the r; N = number of locations taken on the chosen area of a sample; and r = the distance in space between two locations.

In general, μ_a represents the average hardness value of the machining material, σ_a^2 indicates the level of hardness variation within the material, and $\rho(r)$ is the correlation coefficient function which provides quantitative information on the size, shape, and segregation of the microstructures present in the material. The two microstructures shown in Fig. C.1a and C.1b are from the samples taken from the AISI 1020 steel and 6061-T6 aluminum alloy, respectively. The

two curves shown in Fig. C.1c are the correlation coefficient functions of the two microstructures. A sharp decrease shown in the dashed line curve indicates small sizes and spherical shapes of the microstructures of the aluminum alloy.

Random Excitation Model

Upon identifying the characteristics of the hardness variation in microscale, the second procedure is performed to relate this information to random tool motion. As illustrated in Fig. 3.1, the volume of the workpiece material removed during any time interval, Δt, may be considered to be equal to the volume of a parallelepiped. As indicated in Fig. 3.1, the cross-sectional area of this parallelepiped is equal to the product of feed and depth of cut. The height of this parallelepiped is given by

$$\frac{\pi D}{n_s} = \frac{\pi D}{T/\Delta t} = \frac{\pi D \Omega \Delta t}{60} \tag{C.5}$$

where D is the diameter of the workpiece, T is the time needed for one revolution of the workpiece, Ω is the rotational speed of workpiece in rpm, and n_s, equivalent to $T/\Delta t$, is the number of parallelepipeds assumed along the circumference of the workpiece. Due to the nonhomogeneous distribution of microstructures, the microstructural constituents within individual parallelepipeds are distinct. Averaging the microhardness values for each parallelepiped and taking this averaged value as an index to represent the parallelepiped hardness value, averaged hardness values of $\mu_1, \mu_2, \ldots \mu_{n_s}$ at time instants $\Delta t, 2\Delta t, \ldots n_s \Delta t$, respectively, may be obtained. For those μ_i's larger than $\overline{\mu}$ the mean value of $(\mu_1, \mu_2, \ldots \mu_{n_s})$, it is expected that the cutting force magnitudes at the corre-

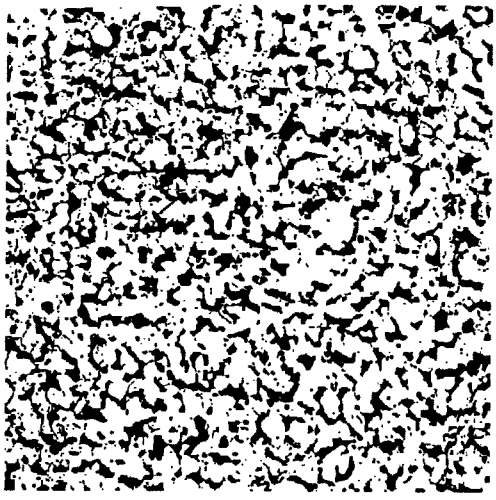

(a) AISI 1020 Carbon Steel

(b) 6061-T6 Aluminum Alloy

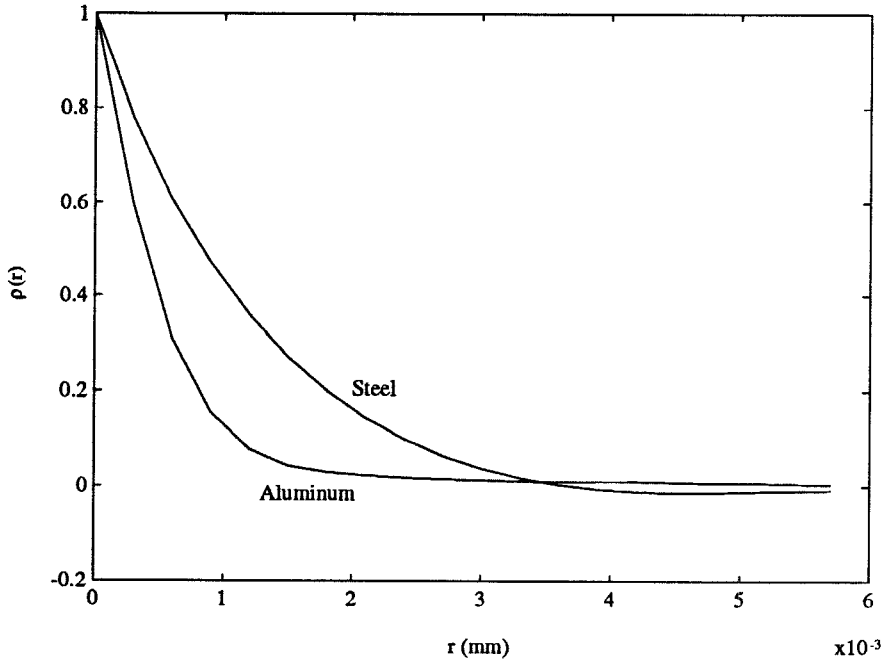

(c) Correlation Coefficient Functions

Figure C.1: Microstructures and Correlation Coefficient Functions of the AISI 1020 Carbon Steel and 6061-T6 Aluminum Alloy

sponding time instants are larger than the nominal cutting force, and vice versa. As a result of the introduction of the ratio term, $\mu_i/\overline{\mu}$, in Eq. C.1, the effect of the nonhomogeneous hardness distribution into the cutting force evaluation may be accounted for at time instants Δt, $2\Delta t$, ... $n_s\Delta t$, respectively.

The random variation of the cutting force can be described by an instantaneous fluctuation of the cutting force about its mean level. A quantitative representation of the random variation may be expressed as follows.

$$F_{random} = K_s A_c \left[\left(\frac{\mu_i}{\overline{\mu}} \right)^{hindex} - 1 \right], i = 1, 2, ,, , n_s \qquad (C.6)$$

where the exponent *hindex* explains the nonlinear relation between the instantaneous cutting force and the hardness ratio, $\mu_i/\overline{\mu}$. As a result, the Eq. 5.1 is given by combining the nominal cutting force (Eq. C.1) and the random cutting force.

$$\begin{aligned} F_{nominal} + F_{random} &= K_s A_c + K_s A_c \left[\left(\frac{\mu_i}{\overline{\mu}} \right)^{hindex} - 1 \right] \\ &= K_s A_c \left[\frac{\mu_i}{\overline{\mu}} \right]^{hindex}, i = 1, 2, ,, , n_s \end{aligned} \qquad (C.7)$$

Equation C.7 therefore simulates the magnitude variation of the cutting force. A large n_s value, corresponding to a small parallelepiped height value, is related to high frequency components of the cutting force. The highest frequency is given as below

$$f_{max} = \frac{T/\Delta t}{2} \frac{\Omega}{60} = \frac{n_s}{2} \frac{\Omega}{60} \, (Hz) \qquad (C.8)$$

The relation between the three cutting parameters and the random variation

of the cutting force can be sensed from the fact that a large parallelepiped volume reduces the variation of microstructural constituents within individual parallelepipeds. As illustrated in Fig. 3.1, it is evident that increasing feed and/or depth of cut adds additional volume to the parallelepiped. Consequently, the random variation of the cutting force is decreased due to the reduced variation of microstructural constituents within the parallelepipeds. Quantitative relations between the three cutting parameters and the random variation of the cutting force have been established by Zhang [Zh 86] and are equal to:

$$\sigma_s^2 = 4\pi\sigma_a^2 \frac{n_s}{fdv} \int_{r=0}^{\infty} \rho(r) w(r) r^2 dr \tag{C.9}$$

and

$$\sigma_a^2 = \frac{1}{N} \sum_{i=1}^{N} (\mu_i - \overline{\mu})^2 = \frac{1}{N} \sum_{i=1}^{N} (\mu_i - \mu_a^2) \tag{C.10}$$

where $w(r)$ is called the geometric parallelepiped shape function.

Interaction between the Cutting Mechanism and Machine Tool Structure

As shown in Fig. 3.1, tool vibration alters the nominal chip load instantaneously (the primary feedback path). The surface modulation produced behind will also alter the nominal chip load during the succeeding revolution of the workpiece under overlapping cutting (the regenerative feedback path). The two dynamic variations of the chip load inevitably lead to the dynamic variation of the cutting force, i.e.,

$$F_{primary} = -K_s w[a - y(t)], \tag{C.11}$$

and

$$F_{regenerative} = K_s w[\nu y(t-T)] \tag{C.12}$$

where w is the width of cut , a is the thickness of cut, ν is the overlapping factor, $y(t)$ is the instantaneous position of the tool or the system response, and y(t-T) is the thickness of the uncut part during the preceding revolution of the workpiece. From an analytical point of view, the cutting force generated during machining should consist of four components i.e.,

$$\begin{aligned} F_{resultant} &= F_{nominal} + F_{random} + F_{primary} + F_{regenerative} \\ &= K_s A_c \left[\frac{\mu_s}{\mu_a}\right]^{hindex} - K_s w[a - y(t)] + K_s w[\nu \Delta y(t-T)] \end{aligned} \tag{C.13}$$

In the case of nonoverlapping cutting, the fourth component diminishes. It is evident that the evaluation of $F_{primary}$ and $F_{regenerative}$ is heavily dependent upon the dynamic characteristics of the machine tool structure. This indicates the interaction between the cutting mechanism and the structural dynamics of the machine tool during machining. The Merritt block diagram shown in Fig. 5.2 explicitly illustrates the chain reaction. The input to and output from the cutting mechanism are the chip load and the cutting force, respectively. Additionally, the cutting force serves as the input to the structural dynamics of the machine tool for which the tool vibratory motion is the output. This vibratory motion in turn changes the chip load through the primary and regenerative feedback paths. Note the symbols of normal distributions displayed in Fig. 5.2. They represent the incorporation of the random excitation system in the cutting force evaluation through the use of the cutting dynamics in microscale.

Bibliography

[Alloy 75] Alloy Digest, Engineering Alloys Digest, Inc., Upper Montclair, New Jersey, 1975.

[ANSI 85] American National Standard, ASME/ANSI B46.1-1985, Surface Texture, ASME, N.Y., 1985.

[As 84] Askeland, D.R., The Science and Engineering of Materials, PWS Engineering, Boston, 1984.

[BePi 71] Bendat, J.S. and Piersol, A.G., Random Data: Analysis and Measurement Procedures, Wiley-Interscience, N. Y., 1971.

[Bi 85] Bielle, J., *Functional Needs, Machining Conditions, and Economics of Surface Finishing*, Precision Engineering, 7, pp. 31-37, 1985.

[BlRa 70] Black, J.T. and Ramalingam, S., *Fine Structure of Machined Surfaces*, Int. J. Mach. Tool Des. Res., vol. 10, pp. 439-463, 1970.

[BoTa 54] Bowden, F.P. and Tabor, D., Friction and Lubrication of Solids, Oxford University Press, 1954.

[Box. 78] Box, G., W. Hunter, and J. Hunter, Statistics for Experimenters, An Introduction to Design, Data Analysis, and Model Building. John Wiley & Sons, Inc., 1978.

[Boy 87] Boyer, H.E. (editor), Atlas of Stress-Strain Curve, American Society of Metals, 1987.

[Br. 86] Bradt, R.C., Evans, A.G., Hasselman, D.P.H. and Lange, F.F., Fracture Mechanics of Ceramics, Plenum Press, N. Y., 1986.

[Bri 88] Brigham, E. O., The Fast Fourier Transform and Its Applications, Prentice Hall, 1988.

bibitem[BS 72]BS:72BS 1134, Method for the Assessment of Surface Texture, Part 2, British Standards Institution, London, 1972.

[Bu. 74] Burke, J.J., Gorum, A.E. and Katz, R.N., Ceramics for High-Performance Application, Brook Hill, Massachusetts, 1974.

[Bur 67] Burgard, H.C. Jr., Physics and Non-Destructive Testing, Gordon & Breach Science Pub., N.Y., pp. 55-82, 1967.

[CaSt 88] Carroll, J.T. and Strenkowski, J.S., *Finite Element Models of Orthogonal Cutting with Application to Single Point Diamond Turning*, Int. J. Mech. Sci., vol. 30, no. 12, pp. 899-920, 1988.

[Ch. 86] Chryssolouris, G., Bredt, J., Kordas, S., and Wilson, E., *Theoretical Aspects of a Laser Machine Tool*, ASME Winter Annual Meeting Proceedings, PED 20, December 1986, pp. 177-190.

[Ch 67] Chung, Kai Lai, Markov Chains with Stationary Transition Probabilities, 2nd ed., Springer-Verlag, 1967.

[Da. 84] Dally, J.W., Riley, W.F., and McConnell, K.G., Instrumentation for Engineering Measurements, John Wiley & Sons, Inc., 1984.

[Dan 52] Danckwerts, P.V., *The Definition and Measurement of Some Characteristics of Mixtures*, Appli. Scient. Res., A3, pp. 279-296, 1952.

[De 79] Dewhurst, P., *The Effect of Chip Breaker Constraints on the Mechanics of the Machining Process*, CIRP Annalen , 28/1/1979, pp. 1-5.

[Do. 91] Dong, S., Jahanmir, S., and Hsu, S., *Tribological Characteristics of Alpha-Alumina at Elevated Temperature*, Transactions of American Ceramics Society, 1991.

[Dr 67] Drake, A.W., Fundamentals of Applied Probability Theory, McGraw-Hill, N.Y., 1967.

[El. 83] Elyasberg, M. E., et al., *A Method for the Structural Improvement of Machine Tool Vibration Stability during Cutting*, Soviet Engineering Research, Vol. 3, No. 4, pp. 59-64, 1983.

[ErMe 41] Ernst, H. and Merchant, M.E., *Chip Formation, Friction, and Finish*, Cincinnati Milling Machine Company, Cincinnati, Ohio, 1941.

[EvMa 80] Evan, A.G., and Marchall, D. B., *Wear Mechanisms in Ceramics*, In Fundamentals of Friction and Wear, Ed. D. A. Rigney, Metals Park, Ohio, American Society of Metals, pp. 439-452, 1980.

[Ga. 89] Gates, R.S., Hsu, S.M. and Klaus E.E., *Tribochemical Mechanism of Alumina with Water*, Journal of Society of Tribologists and Lubrication Engineers, vol. 32, no. 3, pp. 357-363, 1989.

[Gr 91] Grossman, D., *Structure and Physical Properties of Dicor/MGC Glass-Ceramic*, Proceedings of the 1991 International Symposium on Computer Restorations, Regensdort-Zurich, Switzerland, pp. 103-115, 1991.

[Ha 84] Hatch, J.E. (editor), Aluminum : Properties and Physical Metallurgy, American Society for Metals, 1984.

[Hu 73] Hutchinson, J.W., *Finite Strain Analysis of Elastic-Plastic Solids and Structures*, Numerical Solution of Nonlinear Structural Problems, vol. 17, ASME, New York, pp. 17-29, 1973.

[HwZh 92] Hwang, T.W. and Zhang, G.M., *A Stochastic Modeling for the Characterization of Random Tool Motion during Machining*, submitted for publication in the ASME Journal of Dynamic Systems, Measurement and Control, also appears at the 1992 ASME Winter Annaul Meeting, Anaheim, CA, Nov. 8 - 13, 1992.

[ISO 84] ISO Standard, ISO 4287/1, Surface Roughness - Terminology - Part 1: Surface and Its Parameters, International Organization for Standardization, 1984.

[Iw. 84] Iwata, K., Osakada, k. and Terasaka, Y., *Process Modeling of Orthogonal Cutting by the Rigid-Plastic Finite Element Method*, ASME Journal of Engineering Materials and Technology, vol. 106, pp. 132-138, 1984.

[Ja. 89] Jahanmir, S., Deckman, D. E., Ives, L. K., Feldman, A., and Farabaugh, *Tribological Characteristics of Synthesized Diamond Films on Silicon Carbide*, Wear, 133, pp. 73-81, 1989.

[Ka. 83] Kaneeda, T., Ikawa, N., Kawabe, H. and Tsuwa, H., *Microscopical Separation Process at a Tool Tip in Metal Cutting*, Bull. Japan Soc. of Prec. Engg., vol. 17, no. 1, pp. 25-30, 1983.

[KiWh 66] King, A.G. and Wheildon, W.M., Ceramic in Machining Process, Academic Press, N. Y., 1966.

[Kl 73] Klamecki, B.E., *Incipient Chip Formation in Metal Cutting-A Three Dimensional Finite Element Analysis*, Ph.D. dissertation, University of Illinois at Urbana Champaign, 1973.

[Ko. 91] Komvopoulos, K. and Erpenbeck, S.A., *Finite element Modeling of Orthogonal Metal Cutting*, ASME Journal of Engineering for Industry, vol. 113, pp. 253-267, 1991.

[Kr 66] Kronenberg, M, Machining Science and Application - Theory and Practice for Operation and Development of Machining Processes, Pergamon Press, Inc., 1966.

[KwAl 68] Kwaitkowski, A.W. and Al Samarai, H.M., *Process in the Application of Random Signal Analysis Methods to the Identification of Machine Tool Structures*, Advances MTDR, 1968.

[Lin 91] Lin, Zone-Ching, Lin, Yau-Yi and Liu, C.R., *Effect of Thermal Load and Mechanical Load on the Residual Stress of Machined Workpiece*, Int. J. Mech. Sci., vol. 22, no. 4, pp. 263-278, 1991.

[Lo. 89] Lovett, C.D. et al., *Progress Report of the Quality in Automation Project for FY88*, NISTIR 89-4045, National Institute of Standards and Technology, April 1989.

[Ma 41] Martellotti, M.E., Trans. ASME, 63, 8, 677, 1941.

[MARC 91] MARC K.4 Users Manual, Vol. A, MARC Analysis Research Corp., Palo Alto, California, 1991.

[Mash 88] Mashinostroeniya, V., *Technological Basis of the Surface Roughness Parameters of Machined Parts Produced by Tools with Cutting Edges*, Machine Building Technology, vol. 68, issue 1, pp. 40-42, 1988.

[Maz 91] Mazurkiewicz, M., *Understanding Abrasive Waterjet Performance*, Machining Technology, Vol. 2, No.1, pp. 1-3, 1991.

[Me 65] Merritt, H.E., *Theory of Self-Excited Machine Tool Chatter*, Journal of Engineering for Industry, Trans. ASME, vol. 87, pp. 447-454, 1965.

[Na 71] Nayak, P.R., *Random Process Model of Rough Surfaces*, Trans. ASME, Journal of Lubrication Technology, 93, pp. 398-407, 1971.

[Na. 81] Nagtegaal, J.C. and de Jong, J.E., *Some Computational Aspects of Elastic-Plastic Large Strain Analysis*, Int. J. Num. Meth. Engng., vol. 17, pp. 15-41, 1981.

[Nak. 85] Nakagawa, T., Suzuki, K., and Uematsu, T., *Three Dimensional Creep Feed Grinding of Ceramics by Machining Center*, Report in Machining of Ceramic Materials and Components: Eds. K. Subramanian, Norton Company and R. Komanduri, General Electric Company, New York, NY, ASME, pp. 1-7, 1985.

[NaIn 56] Nakayama, K. and Inokuchi, K., J. Soc. Prec. Mech., Japan, 22, p. 169, 1956.

[NaWu 77] Nassipour, F. and Wu, S.M., *Statistical Evaluation of Surface finish and Its Relationship to Cutting Parameters in Turning*, Int. J. Mach. Tool Des. Res. vol. 17, pp. 197-204, 1977.

[Ni 85] Nikitin, B. V., *Determining Optimum Cutting Process Parameters*, Soviet Engineering Research, Vol. 5, No. 12, pp. 65-69, 1985.

[Ox 89] Oxley, P.L.B., Mechanics of Machining - an analytical approach to assessing machinability, John Wiley & Sons, 1989.

[Pa. 80] Pandit, S.M., Suzaki, H., and Khang, C.H., *Application of Data Dependent System to Diagnostic Vibration Analysis*, ASME Journal of Mechanical Design, Vol. 102, No. 2, pp. 223-241, April 1980.

[PaRe 81] Pandit, S.M. and Revach, S., *A Data Dependent System Approach to Dynamics of Surface Generation in Turning*, Journal of Engineering for Industry, Trans. ASME, vol. 103b, pp. 437-445, 1981.

[Pe 60] Pekelharing, A.J., *Finish Turning*, Microtecnic, vol. 14, no. 2, pp. 61-69, 1960.

[RabJu 86] Rabiner, L.R., and Juang, B.H., *An Introduction to Hidden Markov Models*, IEEE ASSP Magazine, January 1986, pp. 4-16.

[Ro 83] Ross, S.M., Stochastic Processes, John Wiley, N. Y., 1983.

[Sa 63] Sata, T., *Surface Finish in Metal Cutting*, CIRP Annalen, XII, 1963, pp. 190-197.

[ScBr 74] Scott, A.M. and Bridgwater, J., *The Characterization of Patchy Mixtures*, J. of Chem. Engng. Sci., pp. 1789-1800, 1974.

[SeBa 77] Selvam, M.S. and Balakrishnan, K., *The Study of Machined Surface Roughness by Random Analysis*, Wear, 41, pp. 287-293, 1977.

[Shaw 84] Shaw, Milton C., Metal Cutting Principles, Oxford University Press, N. Y., 1984.

[Sm. 83] Smithells, et al., Metals Reference Book, 6th ed., pp. 21-1 - 21-7, 1983.

[So 59] Solaja, V., *Wear of Carbide Tools and Surface Finish Generated in Finish Turning of Steel*, Wear, vol. 2, no. 1, 40, 1959.

[St. 83] Stevenson, M.G., Wright, P.K. and Chow, J.G., *Further Developments in Applying the Finite Element Method to the Calculation of Temperature Distributions in Machining and Comparisons with Experiment*, ASME Journal of Engineering for Industry, vol. 105, pp.149-154, 1983.

[StDa 84] Stout, K. J. and Davis, E. J., *Surface Topography of Cylinder Bores: the Relationship between Manufacture Characterization and Function*, Wear, Volume 95, 1984, pp. 111-125.

[StCa 85] Strenkowski, J.S. and Carroll, J.T., *A Finite Element Model of Orthogonal Metal Cutting*, ASME Journal of Engineering for Industry, vol. 107, pp. 349-354, 1985.

[Ta. 74] Tay, A.O., Stevenson, M.G. and Davis, G.D.V., *Using the Finite Element Method to Determine Temperature Distributions in Orthogonal Machining*, Proc. Inst. Mech. Engrs., 188, pp. 627-638, 1974.

[Th 82] Thomas, T.R., Rough Surfaces, Longman House, U. K., 1982.

[Tl 78] Tlusty, J., *Analysis of the State of Research in Cutting Dynamics*, CIRP Annalen, 27/2/1978, pp. 583-589, 1978.

[TlAn 83] Tlusty, J., and Andrews, G.C., *A Critical Review of Sensors for Unmanned Machining*, Annals of the CIRP, vol.32/2/1983, pp. 563-572.

[Tr 91] Trent, E.M., Metal Cutting, 3rd ed., Butterworth Heinemann, Oxford, 1991.

[Tu 81] Tucker III, C.L., *Sample Variance Measurement of Mixing*, Chemical Engineering Science, vol. 36, No. 11, pp. 1829-1839, 1981.

[UsSh 82] Usui, E. and Shirakashi, T., *Mechanics of Machining - From "Descriptive" to "Predictive" Theory*, On the Art of Cutting Metals-75 Years Later, ASME PED vol.7, pp. 13-35, 1982.

[Va 84] vander Voort, G.F., Metallography - Principles and Practice, McGraw-Hill, N.Y., 1984.

[WaBu 78] Wang, N.M. and Budiansky, B., *Analysis of Sheet Metal Stamping by a Finite-Element Method*, ASME J. Appl. Mech., vol. 45, pp. 73-82, 1978.

[Wh. 74] Whitehouse, D. J., Vanherck, P., deBruin, W., and van Luttrervelt, C. A., *Assessment of Surface Typology Analysis Techniques in Turning*, Annals of the CIRP, Vol. 23/2, pp. 265-282, 1974.

[Zh. 89] Zhang, G.M., Hwang, T.W. and Harhalakis, G., *Control of Surface Topographies formed during Machining*, Proceedings of 2nd International Conference on Computer Integrated Manufacturing, Troy, N.Y., IEEE Comput. Soc. Press, pp. 339-345, 1989.

[ZhKa 90] Zhang, G.M., and Kapoor, S.G., *Dynamic Generation of Machined Surfaces, Part 1: Description of a Random Excitation System, and Part 2: Construction of Surface Topography*, Journal of Engineering for Industry, Vol. 113, May 1990, pp. 135-153.

[ZhHw 90a] Zhang, G.M., and Hwang, T.W., *Analysis of the Cutting Dynamics in Microscale*, PED-Vol. 43, 1990 ASME Winter Annual Meeting, pp. 25-37.

[ZhHw 90b] Zhang, G.M., and Hwang, T.W., *Analysis and Control of Dimensioning and Geometric Tolerancing through Surface Topography Generation*, DSC-Vol. 22, 1990 ASME Winter Annual Meeting, pp. 31-38.

[Zh 86] Zhang, G.M., Dynamic Modeling and Dynamic Analysis of the Boring Machining System, Ph.D. Thesis, University of Illinois at Urbana-Champaign, January, 1986.

[Zh. 92] Zhang, G., Hwang, T., Anand, D., and Jahanmir, S., *Tribological Interaction in Machining Aluminum Oxide Ceramics*, Proceedings of the Navy Tribology Workshop, Annapolis, Maryland, May 11-13, 1992, pp. 9-13.

[ZiGo 74] Zienkiewicz, O.C. and Godbole, P.N., *Flow of Plastic and Visco-Plastic Solids with Special Reference to Extrusion and Forming Processes*, Int. J. Num. Meth. Engng., vol. 8, pp. 3-16, 1974.

[Zo 65] Zorev, N. N., Metal Cutting Mechanics, Pergamon Press, Oxford, 1965.